WRDC-TR-90-3050

ELEVATED TEMPERATURE CRACK GROWTH IN TITANIUM ALUMINIDES

An-Yu Kuo, and Kuan-Luen Chen

Structural Integrity Associates, Inc.
3150 Almaden Expressway, Suite 226
San Jose, CA 95118-1250

Ashok Saxena

Mechanical Properties Research Laboratory
Georgia Institute of Technology
Atlanta, Georgia 30332

K. Khobaib
and
Joseph P. Gallagher

University of Dayton Research Institute
Dayton, Ohio 45469

May 1990

Final Report For Period October 1989 - April 1990

FLIGHT DYNAMICS LABORATORY
WRIGHT RESEARCH AND DEVELOPMENT CENTER
AIR FORCE SYSTEMS COMMAND
WRIGHT-PATTERSON AIR FORCE BASE, OHIO 45433-653

NOTICE

WHEN GOVERNMENT DRAWINGS, SPECIFICATIONS, OR OTHER DATA ARE USED FOR ANY PURPOSE OTHER THAN IN CONNECTION WITH A DEFINITELY GOVERNMENT-RELATED PROCUREMENT, THE UNITED STATES GOVERNMENT INCURS NO RESPONSIBILITY OR ANY OBLIGATION WHATSOEVER. THE FACT THAT THE GOVERNMENT MAY HAVE FORMULATED OR IN ANY WAY SUPPLIED THE SAID DRAWINGS, SPECIFICATIONS, OR OTHER DATA, IS NOT TO BE REGARDED BY IMPLICATION, OR OTHERWISE IN ANY MANNER CONSTRUED, AS LICENSING THE HOLDER, OR ANY OTHER PERSON OR CORPORATION; OR AS CONVEYING ANY RIGHTS OR PERMISSION TO MANUFACTURE, USE, OR SELL ANY PATENTED INVENTION THAT MAY IN ANY WAY BE RELATED THERETO.

THIS REPORT HAS BEEN REVIEWED BY THE OFFICE OF PUBLIC AFFAIRS (ASD/PA) AND IS RELEASABLE TO THE NATIONAL TECHNICAL INFORMATION SERVICE (NTIS). AT NTIS IT WILL BE AVAILABLE TO THE GENERAL PUBLIC INCLUDING FOREIGN NATIONS.

THIS TECHNICAL REPORT HAS BEEN REVIEWED AND IS APPROVED FOR PUBLICATION.

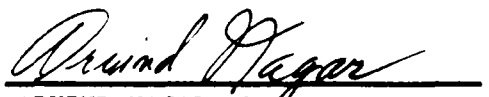

ARVIND NAGAR, Project Engineer
Fatigue, Fracture & Reliability Gp
Structural Integrity Branch

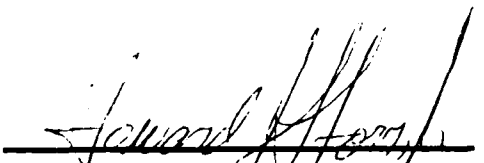

1st Lt Howard J. Storr, Tech Mgr
Fatigue, Fracture & Reliability Gp
Structural Integrity Branch

FOR THE COMMANDER

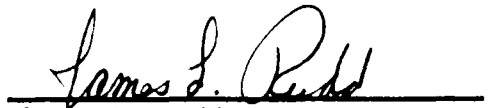

James L. Rudd, Chief
Structural Integrity Branch
Structures Division

IF YOUR ADDRESS HAS CHANGED, IF YOU WISH TO BE REMOVED FROM OUR MAILING LIST, OR IF THE ADDRESSEE IS NO LONGER EMPLOYED BY YOUR ORGANIZATION PLEASE NOTIFY WRDC/FIBE , WRIGHT-PATTERSON AFB, OH 45433-6553 TO HELP MAINTAIN A CURRENT MAILING LIST.

COPIES OF THIS REPORT SHOULD NOT BE RETURNED UNLESS RETURN IS REQUIRED BY SECURITY CONSIDERATIONS, CONTRACTUAL OBLIGATIONS, OR NOTICE ON A SPECIFIC DOCUMENT.

Unclassified
SECURITY CLASSIFICATION OF THIS PAGE

REPORT DOCUMENTATION PAGE

Form Approved
OMB No. 0704-0188

1a. REPORT SECURITY CLASSIFICATION	1b. RESTRICTIVE MARKINGS
2a. SECURITY CLASSIFICATION AUTHORITY	3 DISTRIBUTION/AVAILABILITY OF REPORT Approved for public release; distribution is unlimited
2b. DECLASSIFICATION/DOWNGRADING SCHEDULE	
4. PERFORMING ORGANIZATION REPORT NUMBER(S) SIR-90-017	5. MONITORING ORGANIZATION REPORT NUMBER(S) WRDC-TR-90-3050
6a. NAME OF PERFORMING ORGANIZATION Structural Integrity Associates, Inc. 6b. OFFICE SYMBOL (If applicable)	7a. NAME OF MONITORING ORGANIZATION Flight Dynamics Laboratory (FIBEC) Wright Research & Development Center
6c. ADDRESS (City, State, and ZIP Code) 3150 Almaden Expressway, Suite 226 San Jose CA 95118-1250	7b. ADDRESS (City, State, and ZIP Code) Wright-Patterson AFB OH 45433-6553
8a. NAME OF FUNDING/SPONSORING ORGANIZATION SBIR Program Office 8b. OFFICE SYMBOL (If applicable)	9 PROCUREMENT INSTRUMENT IDENTIFICATION NUMBER F33615-89-C-3213
8c. ADDRESS (City, State, and ZIP Code) Washington DC 20301-0001	10 SOURCE OF FUNDING NUMBERS PROGRAM ELEMENT NO: 65502F; PROJECT NO: 3005; TASK NO: 40; WORK UNIT ACCESSION NO: 66

11. TITLE (Include Security Classification)
Elevated Temperature Crack Growth in Titanium Aluminides

12. PERSONAL AUTHOR(S)
An-Yu Kuo, K. L. Chen, Ashok Saxena, M. Khobaib, and J. P. Gallagher

13a. TYPE OF REPORT	13b. TIME COVERED	14. DATE OF REPORT (Year, Month, Day)	15. PAGE COUNT
Final	FROM 89 TO 0 90	1990 May	109

16. SUPPLEMENTARY NOTATION
This is a Small Business Innovative Research Program, Phase I Final Report

17. COSATI CODES			18. SUBJECT TERMS (Continue on reverse if necessary and identify by block number)
FIELD	GROUP	SUB-GROUP	Titanium Aluminides, Creep, Fracture Mechanics, Crack Growth, High Temperature
010	312		

19. ABSTRACT (Continue on reverse if necessary and identify by block number)

Crack growth of Titanium intermetallics at elevated temperatures has been studied. Based on limited amount of test data available in the literature, it is concluded that, for Titanium aluminides at temperatures over 700°C, C_t correlates better with da/dt than the LEFM parameter K. An alternative definition of C_t has also been derived in this study. The new C_t definition is based on a line integral along the outer boundary of the whole structure. Such an alternative definition has made it easier to calculate C_t for structural components.

20 DISTRIBUTION/AVAILABILITY OF ABSTRACT	21. ABSTRACT SECURITY CLASSIFICATION
☒ UNCLASSIFIED/UNLIMITED ☐ SAME AS RPT ☐ DTIC USERS	Unclassified
22a NAME OF RESPONSIBLE INDIVIDUAL Dr Arvind Nagar	22b TELEPHONE (Include Area Code) (513) 255-6104
	22c OFFICE SYMBOL WRDC/FIBEC

DD Form 1473, JUN 86 *Previous editions are obsolete.*

SECURITY CLASSIFICATION OF THIS PAGE
Unclassified

ACKNOWLEDGEMENT

The authors wish to acknowledge the support and participation of Dr. Arvind Nagar of the Flight Dynamics Laboratory, Wright Research and Development Center.

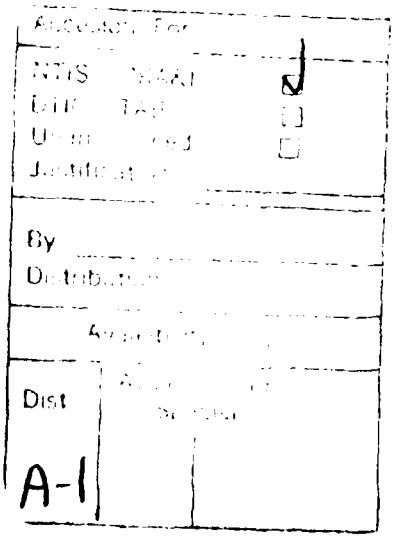

TABLE OF CONTENTS

LIST OF TABLES

LIST OF FIGURES

LIST OF FIGURES (continued)

LIST OF FIGURES (concluded)

1.0 INTRODUCTION

For aircraft structures under constant amplitude cyclic loads, the relationship between fatigue crack growth rate, da/dN, and cyclic stress intensity factor, ΔK, can usually be characterized by one of the laws proposed by Paris, Walker [1], Collipriest [2], Hop-Rau [3], or Forman [4,5]. However, in many aerospace problems, the stress can vary significantly from cycle to cycle. Such variation in loading, or spectrum loading can have significant effects on fatigue crack growth rate [6]. The overloads generally retard crack growth below the levels predicted from constant amplitude conditions using the crack growth laws referenced above. If load interaction effects are ignored, the predicted life is generally conservative, but more realistic crack growth prediction can be achieved by the use of retardation models.

For pure mechanical loads at relatively low temperatures, the retardation models proposed by Wheeler [7] or Willenborg [8] have been widely used. However, the load spectra in aircraft structures often consist not only of sustained mechanical stresses but may also include high amplitude transient thermal stresses. The transient thermal stresses, at elevated temperatures, can cause increased plastic deformation and crack surface closure at crack tips, and thus may significantly influence the subsequent fatigue crack growth behavior. During the sustained load period which often follows the transient thermal stresses, time-dependent creep may also occur locally in the crack tip region, which will also influence the subsequent crack growth behavior.

Recent developments in processing technology has led to the emergence of a series of high temperature titanium alloys and intermetallics. Some of these materials are being considered for structural components of advanced aircraft and hypervelocity vehicles. Intelligent use of these materials requires the

ability to predict the life of the component under service conditions. The current push to use these materials at elevated temperature over a long period of time has drawn attention to the time-dependent (creep) elevated temperature response of high temperature titanium alloys and intermetallics.

A technique for fatigue crack growth modeling with retardation and acceleration effects in a thermal-mechanical environment is needed but does not exist. The objective of this proposed research (Phases I and II) is to develop and demonstrate a new technique for modeling fatigue crack growth with retardation/ acceleration effects in combined mechanical thermal stress applications at elevated temperatures.

In this Phase I study, experimental data on crack growth of titanium alloys and intermetallics were first compiled. In all of the data collected in this literature survey, the crack growth rates, da/dt, were correlated with the stress intensity factor K, which is a valid parameter in lower temperature range but may not be appropriate for the high temperature applications when creep deformation occurs. Several crack tip parameters, including K, C^*, C(t), and C_t, were then evaluated for their applicability and practicality for titanium alloys and intermetallics in the high temperature environments. It is identified under this task that C_t may be the best parameter for characterizing creep crack growth of titanium alloys. Application of C_t to creep-fatigue crack growth modeling of titanium intermetallics is also discussed briefly in this report even though there is not enough data to substantiate it. In the last task of this phase I study, C_t was reexamined and alternative ways of calculating C_t were derived. C_t can be calculated more easily for components using this method.

It is concluded after this Phase I study that research in both the analytical and the experimental areas, on creep crack growth

of titanium alloys and intermetallics in high temperature environments is far from complete. Recommendations for future research work in these areas are made.

2.0 CREEP CRACK GROWTH DATA COLLECTION

Extensive studies have been conducted in the past for predicting the crack growth behavior of Ni-base superalloys and stainless steels at elevated temperatures. The crack growth in a number of nickel base superalloys has been successfully characterized with Linear Elastic Fracture Mechanics (LEFM) parameters. However, since different materials can behave differently in high temperature environments, the use of LEFM parameters, cannot be universally justified. For example the preliminary studies on the high temperature crack growth behaviors of titanium aluminides have shown that da/dt may noy uniquely correlate with K. The crack growth at elevated temperatures has been shown to be very complex and depends on load cycles, time and environmental conditions. Further, special attention is required to deal with the situation of complex loading at elevated temperatures such as a flight spectrum involving hold time, overload, etc.

The amount of elevated temperature crack growth data in titanium alloys is limited. Specifically, creep crack growth data on titanium alloys are scarce. The crack growth data, available in the literature, under different hold times and overloads are limited to relatively lower temperatures. Since these alloys are designed for applications at elevated temperatures with long hold periods, information regarding the time-dependent response as well as the means of implementing this information into a life prediction model is essential.

The technical community currently has no standard for evaluating creep crack growth behavior at elevated temperatures. A number of parameters (other than K) such as the nonlinear elastic parameter, J^*-integral, or the creep crack growth parameters, the C^*-integral, and reference stress, etc., have been identified which could be used to correlate the crack growth behavior at

elevated temperatures. Saxena, et al, [9] have successfully demonstrated the advantages of C_t over K for creeping solids.

The titanium alloys for the most part have not attracted much application in industry at temperatures greater than 500°C due to their limited oxidation resistance above this temperature. At temperatures less than 500°C, the creep process in these alloys is not important. Therefore, it is not surprising that hardly any data are available on creep crack growth of titanium alloys. It is anticipated that the new elevated temperature titanium alloys such as Ti-1100, IMI 834, etc., will see application at temperatures above 500°C in aerospace components; also titanium aluminides are expected to sustain complex loading at temperatures up to 700°C. As indicated earlier, these alloys might sustain measurable creep damage at operating temperatures under flight spectrum loadings, involving overload, hold time, etc. Hence, a strong need exists for a reasonable parameter which could uniquely account for damage caused by complex load excursions at high temperatures.

In an attempt to demonstrate the feasibility of use of C^*, C(t), C_t, and K to describe the damage evolution during crack growth in high temperature titanium alloys and intermetallics, an extensive literature survey was conducted to obtain elevated temperature crack growth data. During this survey, only limited data on time dependent crack growth were available on titanium alloys; therefore, the study focused on intermetallics. The limited data on the creep deformation [10,11], creep crack growth [10-12], hold time, creep fatigue interaction [10], and thermal fatigue [13] of titanium aluminide which were available were used to demonstrate a better correlation of crack growth rates with time-dependent fracture mechanics parameters. The original data were correlated with the stress intensity factor K. These results are summarized in Figures 2-1 through 2-12. In Figures 2-1 and 2-2, creep behavior of Ti-24Al-11Nb at several different

load levels are illustrated for temperatures at 700°C amd 750°C, respectively. Rupture time and final failure strain for the above two tests are shown in Figures 2-3 and 2-4. Crack growth curves for Titanium aluminides at 750°C by [13] are shown in Figures 2-5 to 2-7 in terms of K. It is noted from these three figures that crack growth rate of Titanium aluminides at 750°C does not correlate well with K. Recent test data by Khobaib [12] for Ti-24Al-11Nb are plotted in Figures 2-8 to 2-11. Again, it is concluded from these figures that crack growth rate of Ti-24Al-11Nb does not correlate well with K. These data will be reploted in terms of C_t in section 3 of this report. Balsone et al [27] have studied the frequency effects on crack growth and their data is shown in Figure 2-12.

The fatigue crack growth rate (FCGR) behavior of titanium alloys at elevated temperature has been extensively studied [14-19]. Most of the studies, however, describe either the correlation of microstructures with FCGR or the effect of composition on FCGR. The effect of environment has also been investigated [20,21] and an inert environment seems to improve FCGR resistance at higher temperatures. The effect of frequency and stress ratio has been mainly studied at room temperature, where the main interests have been the role of hydrogen. The issue of hold time effect also have been extensively studied [22-26]. However, these studies are limited in scope, because the temperatures of interest are relatively low, and the main interest in these studies also centers around the effect of hydrogen. Currently, Balsone, et al [27], are investigating the effect of frequency on the elevated temperature FCGR of Ti-24Al-11Nb. Reportedly, the crack growth increases at lower frequencies, but a clear time dependent model as in the case of Ni-base superalloy [28] has not been reported. The inert environment, of course, slows down the FCGR, but more work is needed to define the creep contribution on the crack growth behavior at these elevated temperatures.

The crack growth rate retardation due to single or multiple overload cycles on FCGR have been studied by numerous workers [29-49]. Almost all investigations were conducted at room temperature where no creep effect is involved. The retardation effects have been explained by (1) compressive residual stresses ahead of the crack tip, (2) crack closure, and (3) the strain hardening effect in the overloaded plastic zone.

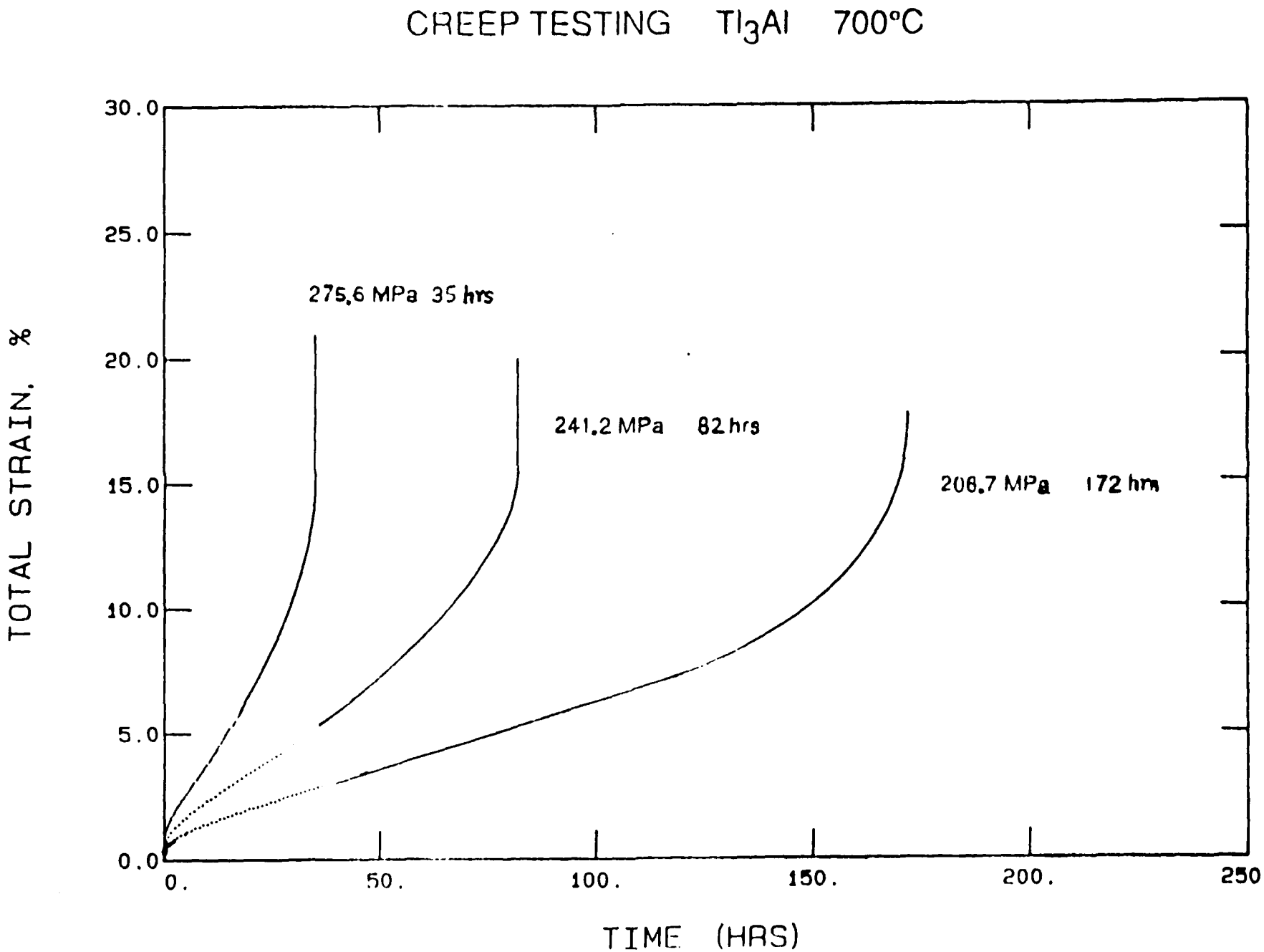

Figure 2-1. Creep Behavior of Ti-24Al-11Nb at Stress Levels of 275.6 MPa, 241.2 MPa and 206.7 MPa and Temp. of 700°C (Rev. 11)

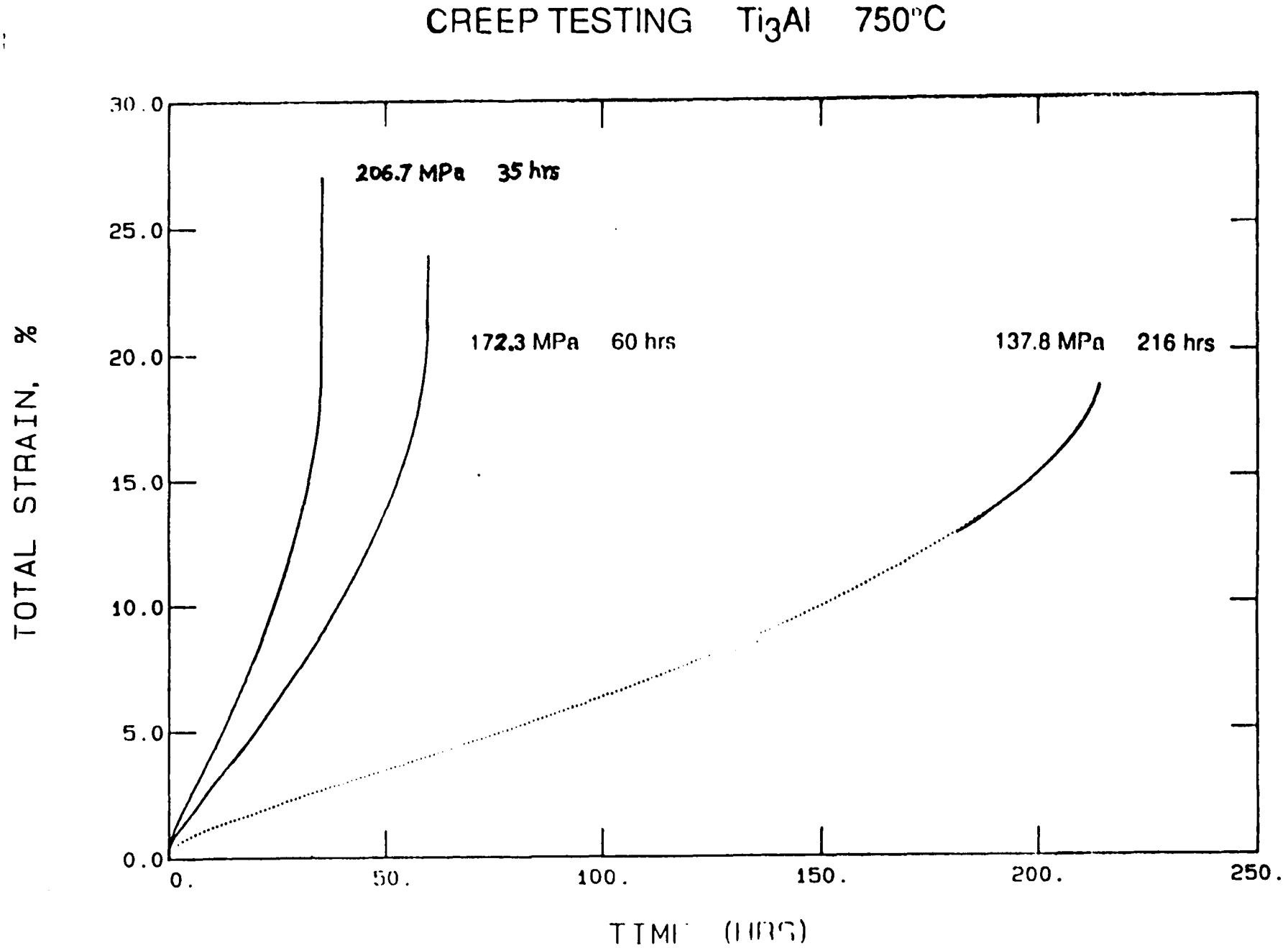

Figure 2-2. Creep Behavior of Ti-24Al-11Nb at Stress Levels of 137.8 MPa, 172.3 MPa and 206.7 MPa and Temp. of 750°C (Ref. 11)

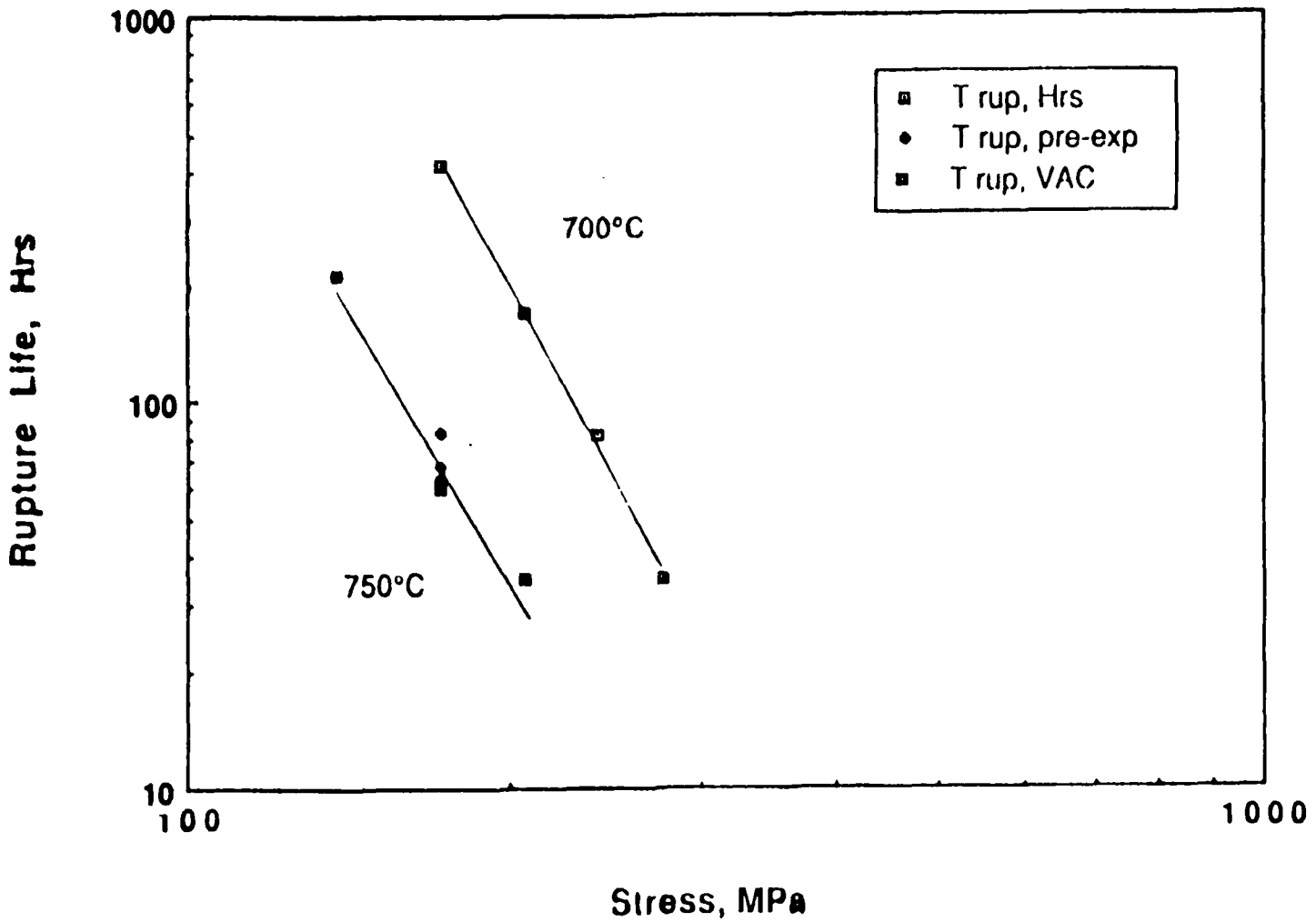

Figure 2-3. Plot of Stress vs. Rupture Life for Creep Rupture of Ti-24Al-11Nb (Ref. 11)

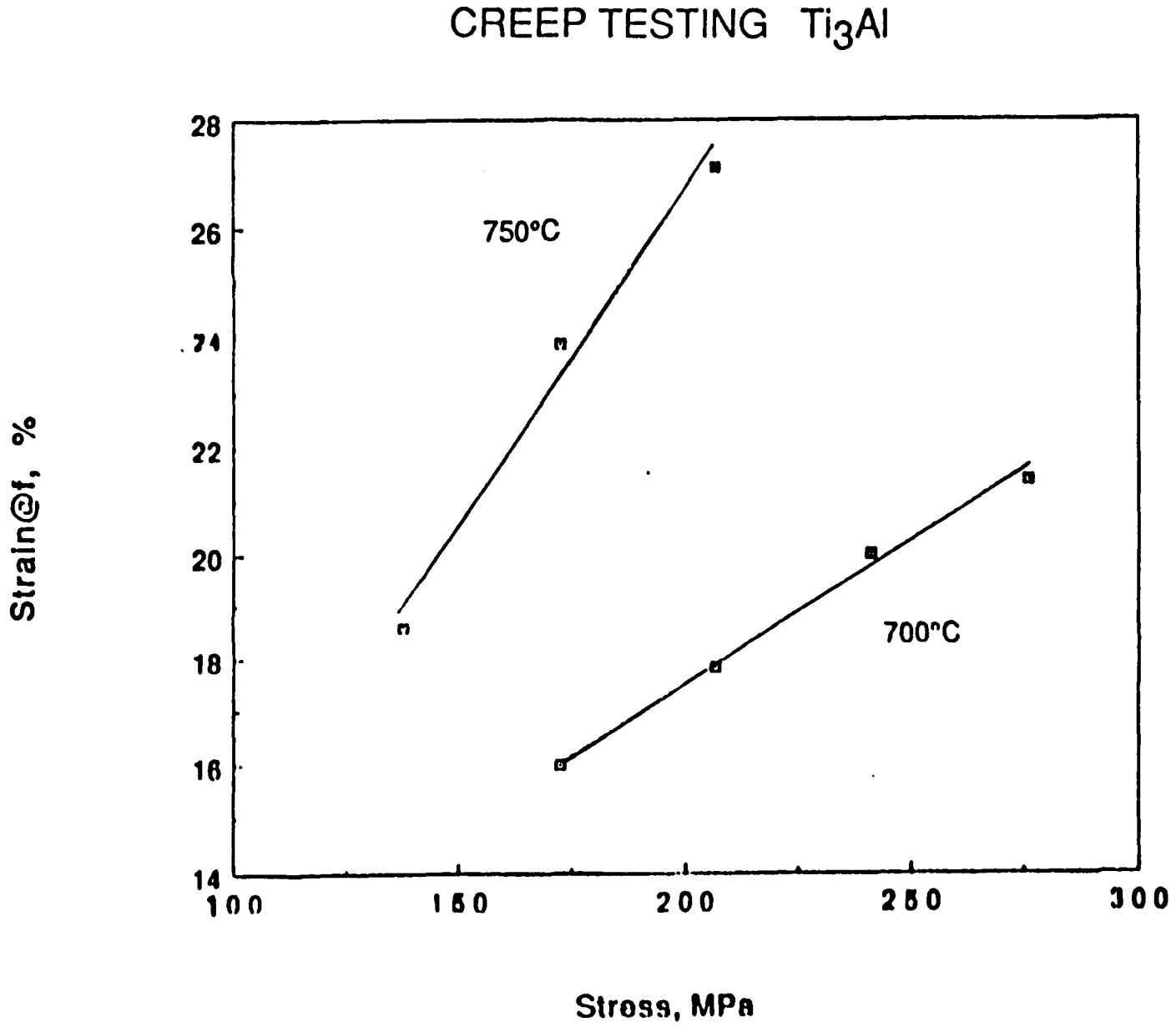

Figure 2-4. Steady Strain Rate vs Stresses at 700°C for Ti-24Al-11Nb (Ref. 11)

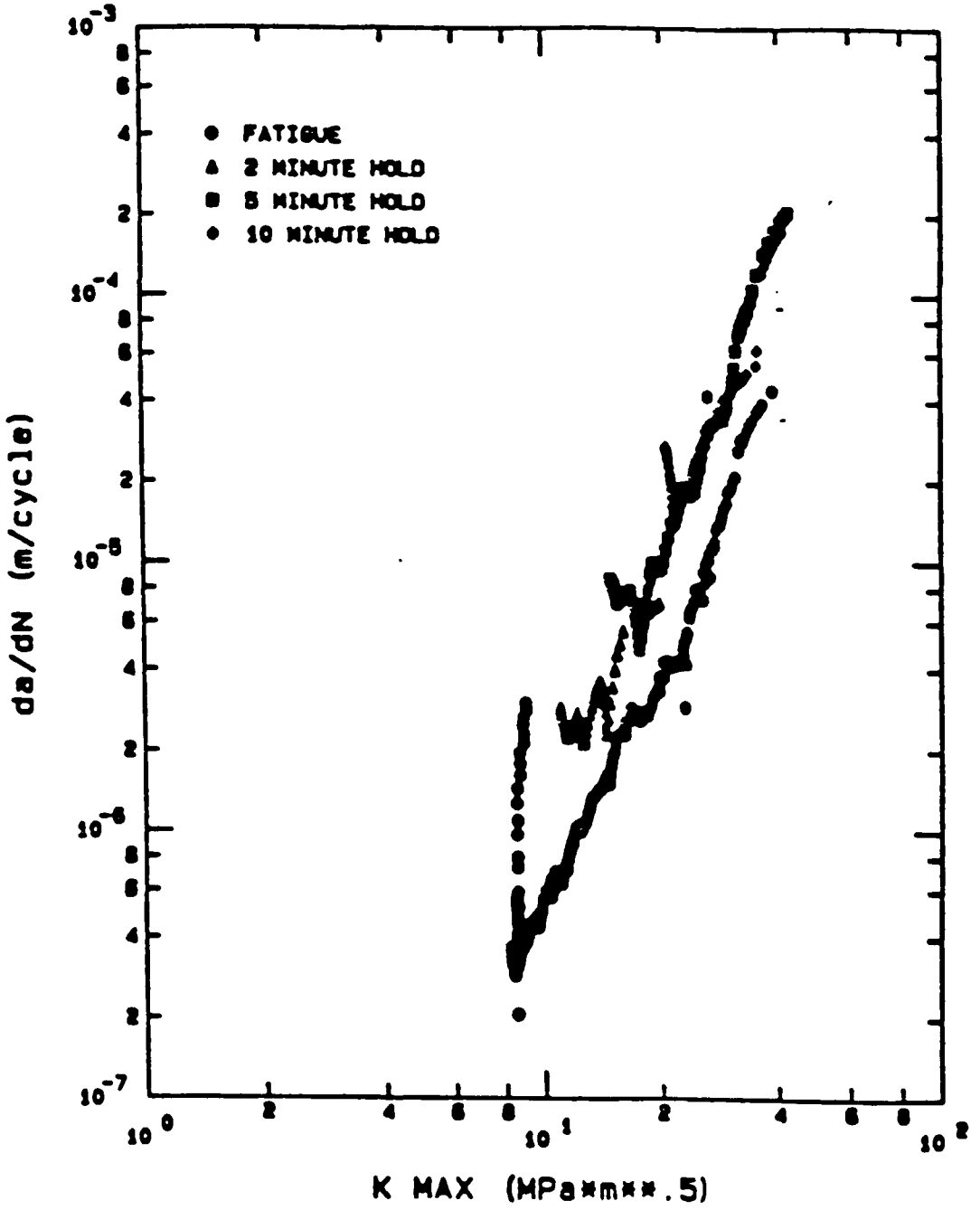

Figure 2-5. Crack Growth Per Cycle Curves for 750°C (Ref. 13)

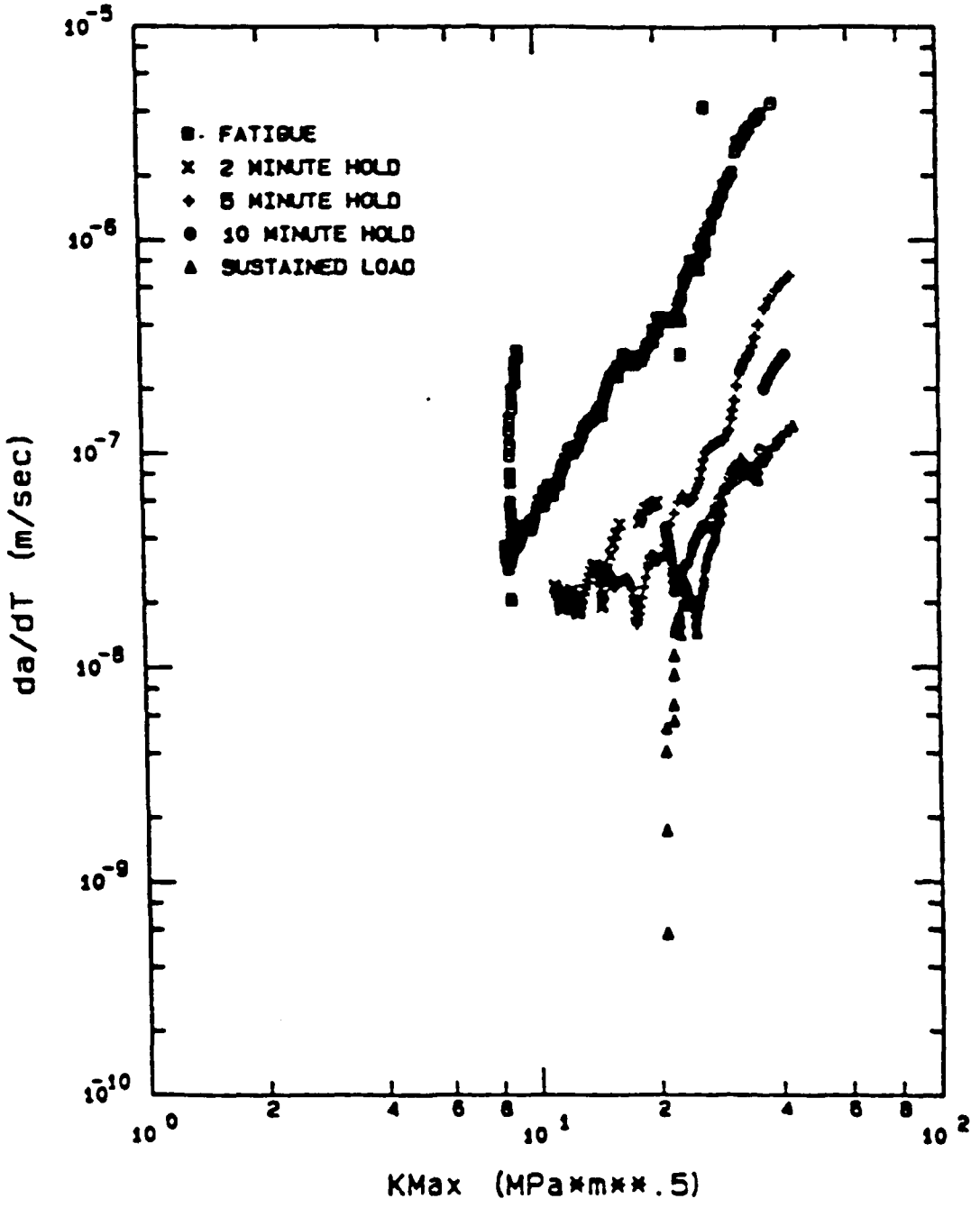

Figure 2-6. Crack Growth Rate Curves for 750°C (Rev. 13)

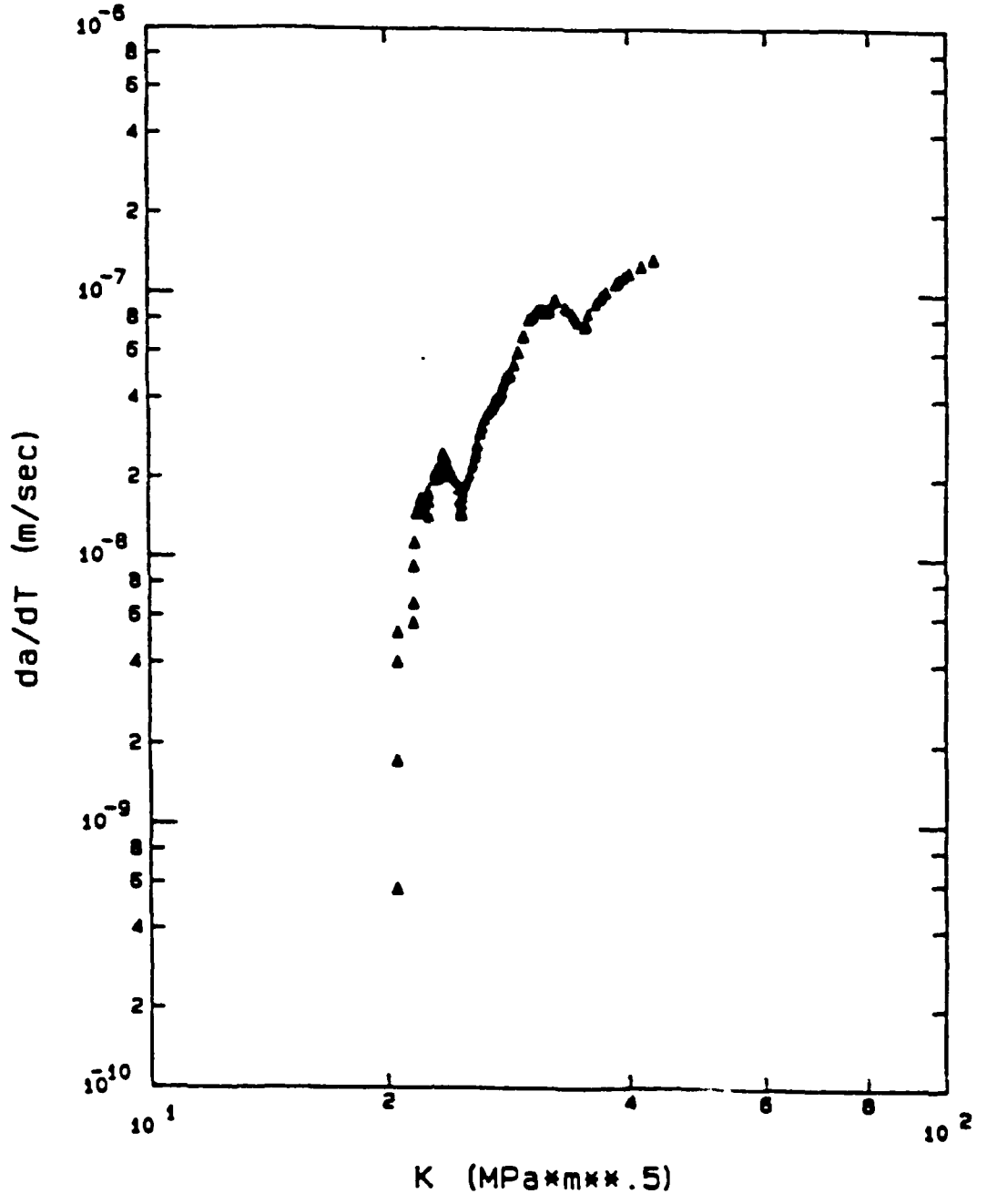

Figure 2-7. Sustained Load Crack Growth Rate for 750°C (Ref. 13)

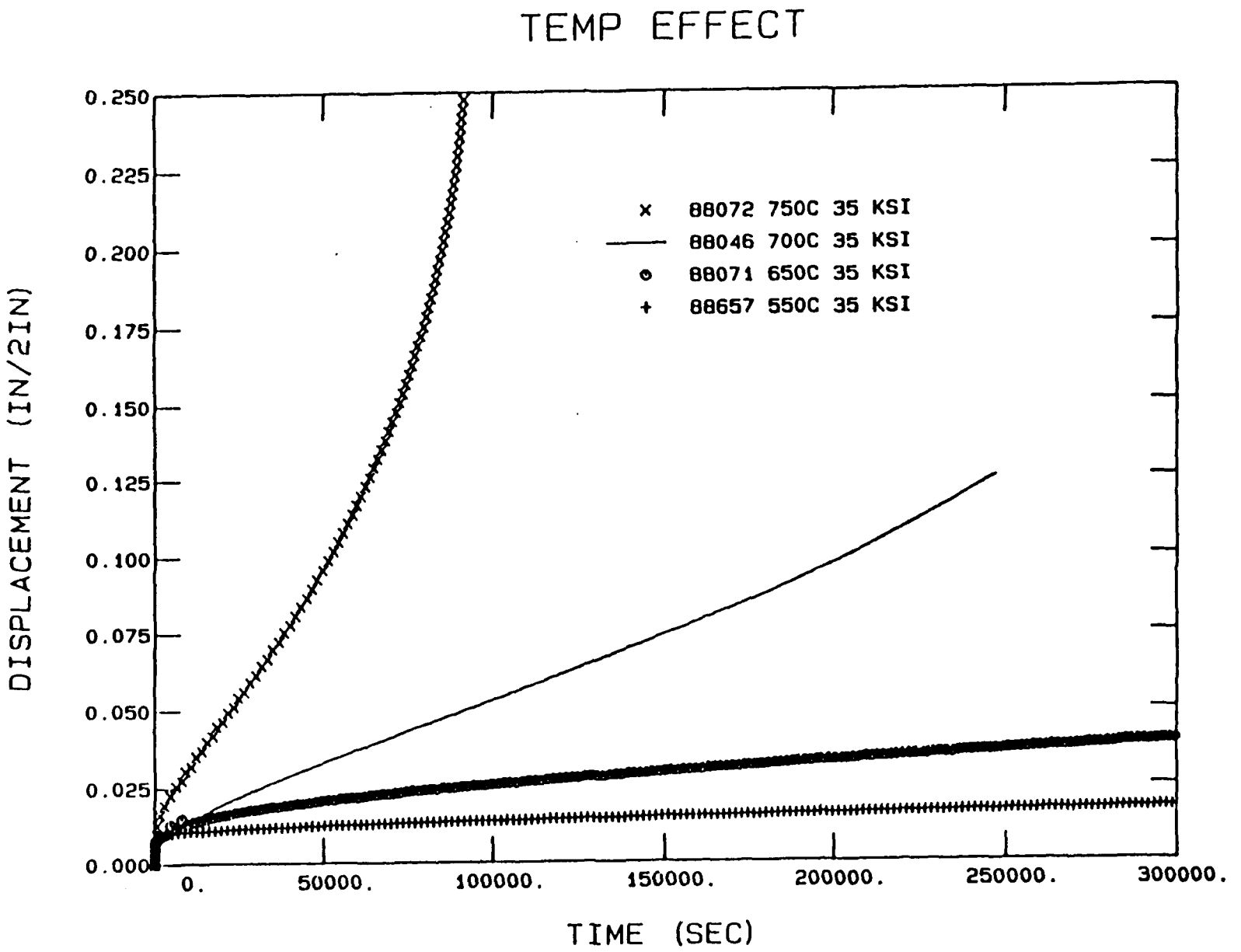

Figure 2-8. Effect of Temperature on Creep Behavior of Ti-24Al-11Nb (Ref. 12)

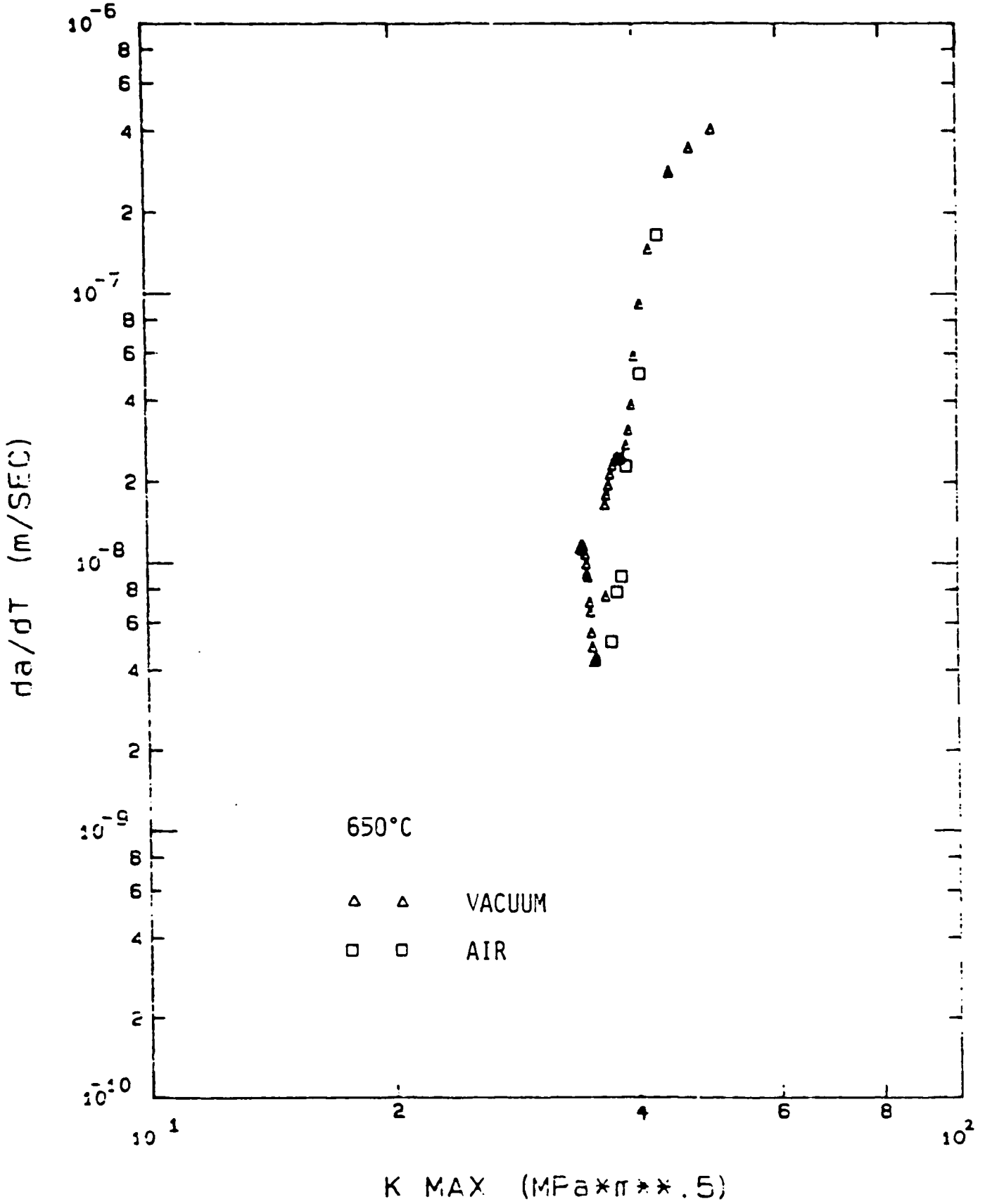

Figure 2-9. Creep Crack Growth Behavior of Ti-24Al-11Nb (Ref. 12)

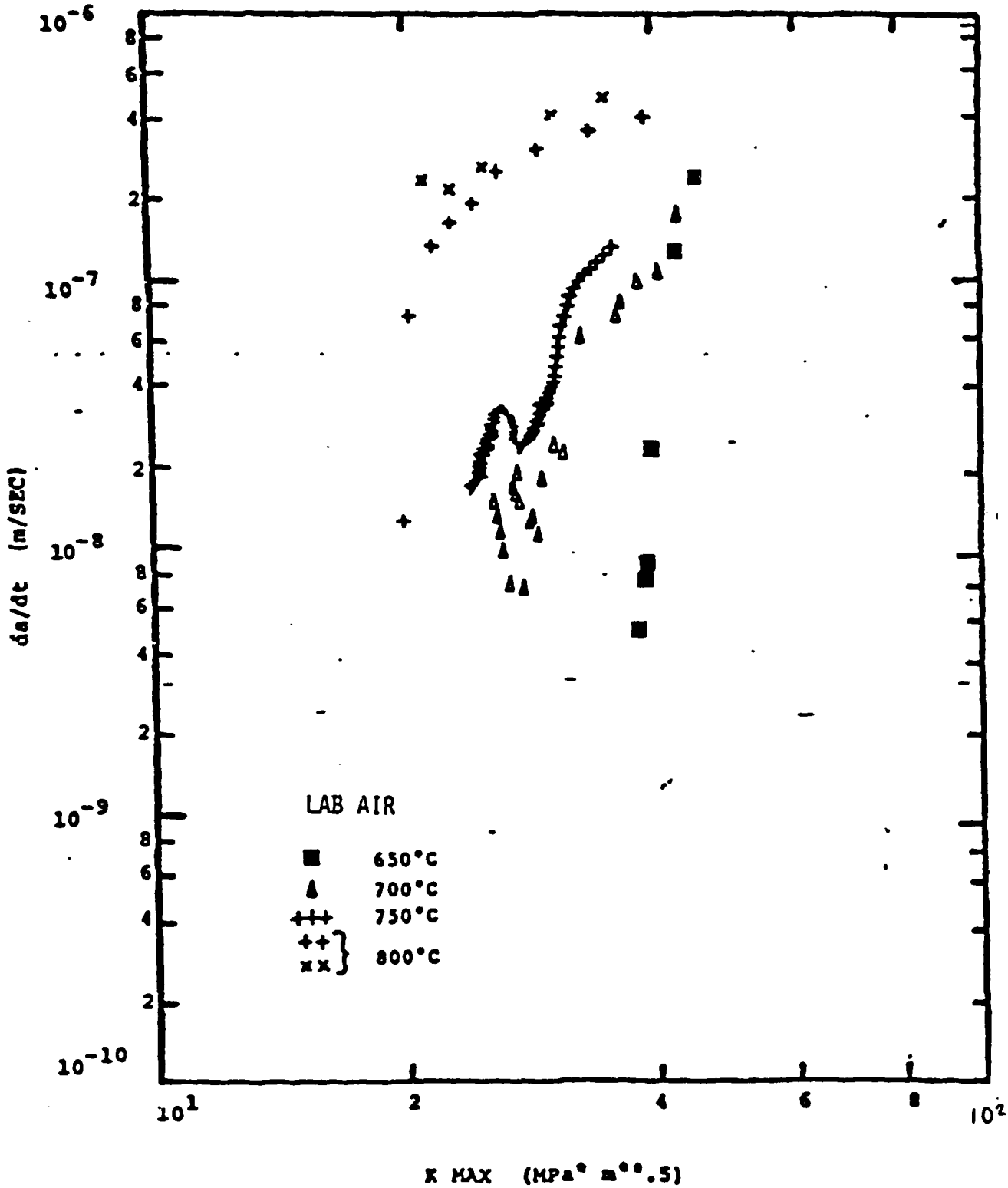

Figure 2-10. Creep Crack Growth Rate Behavior of Ti-24Al-11Nb (Ref. 12)

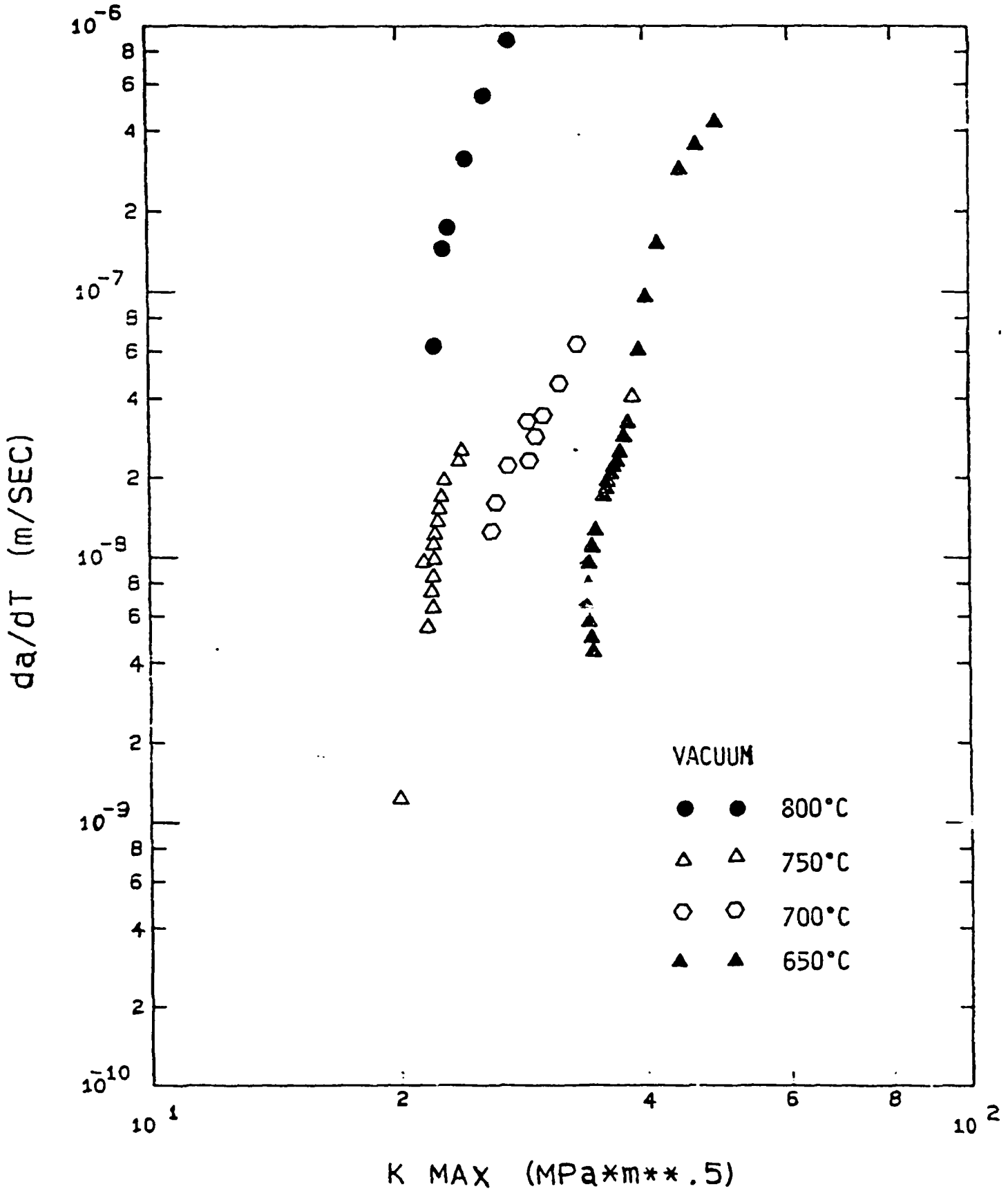

Figure 2-11. Creep Crack Growth Behavior of Ti-24Al-11Nb (Ref. 12)

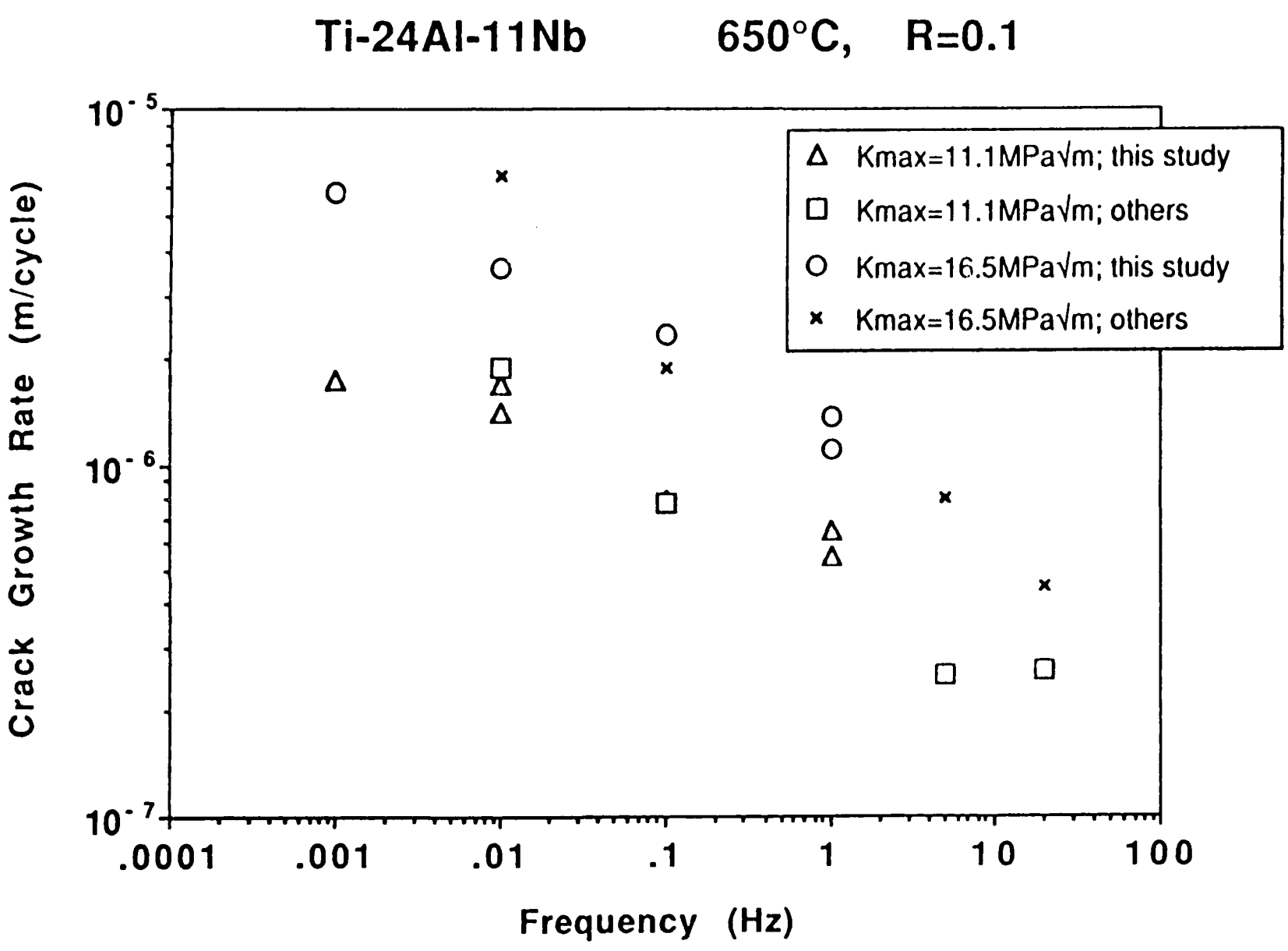

Figure 2-12. Effect of Frequency on Fatigue Crack Growth of Ti-24Al-11Nb at 650°C (Ref. 27)

3.0 CREEP CRACK GROWTH PARAMETERS

Titanium aluminides are an important class of candidate materials for application in the manned hypersonic vehicle program. In the temperature regime of 600 to 900°C, these materials have high specific strength properties and possess good environmental and creep resistance [12]. However, before they can be used in the aerospace structures, it is necessary to develop accurate models for predicting their crack growth behavior in the intended service environment.

Recently, some studies have been performed for characterizing the creep and creep-fatigue crack growth behavior in a titanium aluminide intermetallic [12,13]. These studies were planned with the objective of correlating the crack growth data using the linear elastic fracture mechanics (LEFM) parameters. However, after completion of these tests it was recognized that the crack growth was accompanied by considerable creep deformation. Thus, the crack growth rate correlations presented in terms of the LEFM parameters are not as good as those in the low temperature applications.

In this section, the results from the creep crack growth tests for which all raw data were available, are reanalyzed using time-dependent fracture mechanics (TDFM) concepts and crack tip parameters. Analytically estimated values of load-line deflection rates were obtained by considering the creep deformation rates of these materials and were subsequently used to estimate the TDFM parameters. In the subsequent discussion, the TDFM concepts are first briefly reviewed and subsequently, the results of the analysis of the creep crack growth data are presented and discussed. Unfortunately, the raw data for the creep-fatigue tests were not available and could not be reanalyzed in the same way as the creep crack growth data. However, some discussion on the applicability of TDFM concepts to creep-fatigue crack growth is presented in this section.

3.1 Crack Tip Parameters in TDFM

Figures 2-1 and 2-2 show the creep deformation behavior of Ti-24Al-11Nb at 700 and 750°C, respectively. At both temperatures, the strain versus time behavior shows the classical three region behavior consisting of primary, secondary and tertiary creep. At a constant temperature, such creep behavior can be represented by an equation of the type given below:

$$\dot{\epsilon}_c = A_1 \epsilon_c^{-p} \sigma^{n_1 (1+p)} + A\sigma^n + A_3 (\epsilon_t)^{p_3} \sigma^{n_3 (1-p_3)} \qquad (3\text{-}1)$$

where, $\epsilon_c = \epsilon_p + \epsilon_s + \epsilon_t$

ϵ_p, ϵ_s, ϵ_t are primary, senondary and tertiary components, respectively, of the total creep strain, ϵ_c, σ is applied stress, and A_1, p, n_1, A, n, A_3, p_3, n_3 are regression constants which describe the creep deformation trend in their various regimes.

In Figures 2-1 and 2-2 it is observed that the creep ductilities are in excess of twenty percent at all stress levels and at both temperatures. Also, the primary creep behavior is limited to short periods following loading. In cracked bodies of ductile materials, tertiary creep is expected to be restricted to the process zone near the crack tip and is not anticipated to contribute significantly to the remote load-point deflection. Thus, the most significant contribution to the load-line deflection rate in titanium aluminide specimens will be from the second term (secondary creep rate) on the right hand side of Equation (3-1). However, initially upon loading, the crack tip stress field will redistribute and an elastic strain rate term must be added to the creep strain rate to determine the overall strain rate, $\dot{\epsilon}$ which can be written as:

$$\dot{\epsilon} = \dot{\sigma}/E + A\sigma^n \qquad (3\text{-}2)$$

where, $\dot{\sigma}$ is the rate of change of stress with time. Figure 3-1 shows the plot of $\dot{\epsilon}_s$ versus σ at both test temperatures for Ti-24Al-11Nb. The following equation represents the steady-state creep rate at both temperatures.

$$\dot{\epsilon}_s = 9.5 \times 10^{-17} \exp\left[-\frac{87,700}{R}\left(\frac{1}{T} - 1.0277 \times 10^{-3}\right)\right]\sigma^{5.5} \qquad (3\text{-}3)$$

where, R is the universal gas constant and T is the absolute temperature in Kelvin.

The crack tip parameters discussed in this section will be formulated for elastic, power-law creep materials which deform according to Equation (3-2). However, if necessary, these parameters can be generalized to include the contributions from the primary and tertiary creep [51,52]. It may be necessary to include contributions from primary creep at low stresses and low temperatures. However, sufficient data are not available at the present time to proceed with such an analysis.

There are three crack tip parameters in TDFM. These are the C^*-Integral [54-56], C(t)-Integral [57] and the C_t parameter [57]. In order to completely understand the regions of validity of these parameters, it is necessary to consider the size of the region of creep deformation as shown in Figure 3-2. During the small-scale-creep regime, the creep deformation is localized and the creep zone size is small in comparison to the remaining ligament size. This is analogous to the small-scale-yielding (SSY) regime in linear elastic fracture mechanics [57,58]. During the transition regime, the creep zone is no longer small compared to crack size or the remaining ligament size. This is analogous to the elastic-plastic regime. The third region is the extensive creep regime in which the creep deformation has spread through the entire ligament. This regime is analogous to the

fully-plastic regime and is also referred to the steady-state regime because the creep deformation behavior is dominated by steady-state creep.

The C^*-Integral was proposed as a creep analog to the J-Integral and is defined as follows [53]:

$$C^* = \int_\Gamma W^* dy - T_i \frac{\partial \dot{u}_i}{\partial x} ds \qquad (3\text{-}4)$$

where, W^* is determined by the following equation:

$$W^* = \int_0^{\dot{\epsilon}_{ij}} \sigma_{kl} \, d\dot{\epsilon}_{kl} \qquad (3\text{-}5)$$

T_i is the traction vector along a path Γ (considering the region enclosed by the path as a free body) which originates at a point along the lower crack surface, and goes around counter-clockwise, and ends at a point on the upper crack surface. Thus, the contour encloses the crack tip. σ_{ij} and $\dot{\epsilon}_{ij}$ are the stress and strain rate tensors and $\dot{u}_i$ is the deflection rate vector along the direction of the traction. ds is an arc length element along Γ. C^* has also been interpreted as the difference between the energy rates (or power) provided to two bodies with incrementally differing crack lengths which are otherwise identical.

Thus, C^* is given by:

$$C^* = - \frac{1}{B} \frac{dU^*}{da} \qquad (3\text{-}6)$$

where, B is thickness and U^* is the stress-power ($\sigma_{ij}\dot{\epsilon}_{ij}$) times [n/(n+1)] and is obtained by calculating the area under the load versus load-point deflection rate plot. C^* also uniquely

characterizes the crack tip stress and strain rate fields [59,60]:

$$\sigma_{ij} = \left(\frac{C^*}{AI_n r}\right)^{1/1+n} \tilde{\sigma}_{ij}(\theta) \qquad (3\text{-}7)$$

$$\dot{\epsilon}_{ij} = A \left(\frac{C^*}{AI_n r}\right)^{n/n+1} \tilde{\epsilon}_{ij}(\theta) \qquad (3\text{-}8)$$

where, I_n is a constant dependent on the n value, r is the radial direction from the crack tip and $\tilde{\sigma}_{ij}(\theta)$ and $\tilde{\epsilon}_{ij}(\theta)$ are dimensionless angular functions.

In the small-scale and the transition creep regimes in which components often lie, the elastic strain rate term in Equation (3-2) cannot be ignored. Thus, C^* is no longer path-independent (because strain rate is not just a function of stress alone due to the $\dot{\sigma}$ term) and it also does not uniquely characterize the crack tip stress fields. Thus, additional crack tip parameters need to be defined to characterize creep crack growth behavior. The C(t)-Integral and the C_t parameter have been introduced to generalize C^* to include the small-scale and the transition creep regions.

The C(t)-Integral of Bassani and McClintock [56] is the same as C^* in eq. (3-4) except it is determined along a path very near the crack tip ($r \to 0$). C(t) uniquely characterizes the amplitude of the crack tip stress fields at all times ranging from small-scale creep to extensive creep conditions. Under extensive creep conditions, it reduces to C^*. The value of the C(t)-Integral can be approximated by the following equation [61]:

$$C(t) = \left(\frac{t_T}{t} + 1\right) C^* \qquad (3\text{-}9)$$

where, t is the elapsed time and t_T is the transition-time for extensive creep conditions to develop. Under constant load conditions, t_T has been given by [58,62]:

$$t_T = \frac{K^2(1-\nu^2)}{E(n+1)C^*} \qquad (3\text{-}10)$$

where, K is the stress intensity parameter, ν is Poisson's ratio and E is elastic modulus. As can be seen clearly from Equation (3-4) that, $C(t) \rightarrow C^*$ as $t \rightarrow \infty$. The major drawback of using C(t) is that in the small-scale and transition creep regions it can not be measured at the load-point. It can only be calculated.

The C_t parameter defined by Saxena [57] is also a generalization of C^* but is different from the C(t)-Integral. C_t generalizes upon the energy rate interpretation of C^* as follows. Consider several identical pairs of cracked specimens. Within each pair, one specimen has a crack length a and the other has an incrementally larger crack length a + Δa. The specimen of each pair are loaded to various constant load levels P_1, P_2, P_3, ... P_i, etc. at elevated temperatures, and the load-line deflection as a function of time is recorded (Figure 3-3a). The load-line deflection due to creep is V_c. It is assumed that no crack extension occurs in any of the specimens and the instantaneous response is linear elastic. At a fixed time, the load versus deflection rate, $\dot{V}_c$, behavior is plotted for all specimens. A schematic of the expected behavior is shown in Figure 15b. Several such plots can be generated from these tests by varying time.

The area between the P-$\dot{V}_c$ curves for specimens with crack length a and a + Δa, is called ΔU_t^* (the subscript denotes that this

value is at a fixed time, t). The C_t parameter is given by the following equation,

$$C_t = - \frac{1}{B} \frac{\partial U_t^*}{\partial a} \qquad (3\text{-}11)$$

where, B is specimen thickness. As $t \to \infty$, $C_t = C^*$ by definition because $\partial U_t^* / \partial a = dU^*/da$ under steady-state conditions.

C_t can be measured at the loading pins and can also be calculated as will be discussed later. It has also been shown to be directly related to the rate of expansion of the creep zone size in the small scale creep region [63] and it may then be argued that the rate of crack tip damage accumulation must scale with the rate of creep zone expansion. Thus, C_t can be expected to characterize the creep crack growth rate in the small-scale creep and the transition creep region. This has been borne out by a considerable amount of data [64].

In summary, there are three crack tip parameters in TDFM; C^*, C(t) and C_t. C^* is a subset of both C(t) and C_t because the latter parameters reduce to C^* under extensive creep conditions. In the small-scale and the transition creep regions, C^* loses its significance but C(t) and C_t continue to retain their significance. Also, in these regimes, $C(t) \neq C_t$. Since C_t can also be measured always at the load point, it has an advantage over C(t) which can only be calculated. Both parameters can be generalized to include primary and tertiary creep [51,65]. Recent studies have shown that C_t can successfully characterize creep crack growth rate data over a wide range of creep deformation conditions. Therefore, we have used C_t exclusively for correlating creep crack growth data in Ti-24Al-11Nb.

Since C(t), C_t, and C^* are defined only for stationary cracks, their applicability for growing cracks becomes increasingly more important in the lower temperature ranges of the creep regime. Several analytical and experimental studies have addressed this issue [66-70] and it is now well established that these parameters may be used for slowly growing cracks. One approach to assure the validity of C_t is to compare the overall deflection rate at the load-point, $\dot{V}$, (which includes the deflection rate associated with the growing crack) with the deflection rate due to creep deformation only ($\dot{V}_c$). For constant load conditions used during creep crack growth testing, the two are related in the following way [69]:

$$\dot{V}_c = \dot{V} - \frac{B(da/dt)}{P}\left[\frac{2K^2}{E} + (m+1)J_p\right] \qquad (3\text{-}12)$$

where, P is load, B is specimen thickness, J_p is plastic contribution to J-Integral and m is the Ramberg-Osgood exponent relating plastic strain to applied stress. For the tests conducted in the dominantly elastic regime, $J_p \simeq 0$. When $\dot{V}_c/\dot{V} < 0.8$, the validity of C_t as a crack tip parameter becomes suspect. As can be seen from Equation (3-12), this condition is more likely to be violated at high values of da/dt. Low temperatures will cause $\dot{V}_c$ to be smaller. Thus, in an extreme case of the subcreep temperature regime, $\dot{V}_c=0$ and C_t can no longer be expected to be a viable crack tip parameter.

3.2 Creep Crack Growth Behavior in Ti-24Al-11Nb

All the data reported in this section is from the work of Khobaib, et al, [12] generated as a part of an Air Force sponsored program at the University of Dayton Research Institute (UDRI). Table 3-1 shows the summary of all tests conducted and

the loading conditions used. All specimens were compact tension (CT) type. The test temperatures were 650, 700, 750 and 800°C. Tests were conducted in an air environment as well as in vacuum at each temperature. The nominal width of the specimens tested in air was 40 mm (1.58 in.) with one exception. Specimen 88-258 was tested in air but was only 20 mm (.79 in.) wide. These tests were conducted under constant load conditions and the crack length was continuously monitored. No measurement of the load-line deflection was made during these tests. The test durations ranged from less than 2 hours to 70 hours which yielded data in the crack growth rate range of 2.54×10^{-2} to 2.54 mm/hr (.001 to .1 in/hr). These data were analyzed as a part of this project and the da/dt were correlated with C_t. For comparison, plots of da/dt versus K were also generated. The data analysis method is described next and the results are discussed subsequently.

3.2.1 Data Analyses Methods

Since the load-line displacements were not available, C_t could only be calculated. Equation (3-3) was used to estimate the value of A in Equation (3-2) at the four test temperatures (see Table 3-2). The value of A for 650 and 800°C are extrapolations of the actual data at 700 and 750°C. Estimated values of the .2% yield strength and the elastic modulus [71] at these temperatures are listed in Table 3-3.

The crack size versus time (a vs. t) data were used to calculate da/dt by the secant method. The corresponding values of the average crack size and time for the same interval were also calculated. The minimum crack extension between successive data points was taken to be 0.25 mm (0.01 in.). A computer program was developed to reduce this data into the da/dt versus C_t format. Various other parameters such as K, transition time, predicted load-line deflection rate, $\dot{V}$, and the predicted

load-line deflection rate due to creep, $\dot{V}_c$, were also calculated for each data point. The listing of the computer code is given in Appendix A and the equations used to calculate the various parameters are given below.

C_t was calculated using the following equation [63,72]:

$$C_t = \frac{4\alpha(1-\nu^2)\beta\tilde{r}_c(\theta)}{E(n-1)} \frac{K^4}{W} (EA)^{2/n-1}(F'/F)t^{-(n-3)(n-1)} + C^* \quad (3\text{-}13)$$

where, $\alpha = (1/2\pi)\ [(n+1)^2/1.38n]^{2/(n-1)}$ for $3 < n < 13$, $\beta = .33$ and $\tilde{r}_c(\theta) = .4$ which were estimated from finite element analysis [63]. F = K-calibration factor = $(K/P)BW^{1/2}$ and F' = dF/d(a/w). C^* can be calculated from the following equation for CT specimens [73]:

$$C^* = \frac{h_1 WA}{(1-a/W)^n} \left[\frac{P}{1.455\ BW\eta}\right]^{n+1} \quad (3\text{-}14)$$

where, h_1 is a function of a/W and n given in Reference 73. The values of h_1 for n = 5 and 7 were linearly interpolated to obtain the values for 5.5. η is given as follows:

$$\eta = (\phi^2 + 2\phi + 2)^{1/2} - (\phi + 1) \quad (3\text{-}15)$$

where, $\phi = \frac{2a}{W-a}$.

The stress intensity parameter, K, is calculated using the standard expression for CT specimens [74]. The transition time (t_T) is then calculated from Equation (3-10). The load-line deflection rate, $\dot{V}$, and the load-line deflection rate due to creep deformation, $\dot{V}_c$, are also calculated using equations given in Appendix B. The ratio $\dot{V}_c/\dot{V}$ is important in assuring that

creep deformation dominates the behavior of the specimen. If ductile tearing or environmental attack causes the crack to grow out of the creep deformation zone, the above ratio will approach a value of zero. If the above ratio exceeds 0.8, the crack growth rate data are expected to correlate well with C_t [69].

3.2.2 Results and Discussion

The tabular results from the analyses of all specimens are given in Appendix C. In the following discussion, the primary goal will be to examine the applicability of TDFM concepts to titanium aluminides. The influence of temperature and environment will also be considered.

One of the ways to experimentally validate a crack tip parameter is to test specimens of different size, geometry, starting crack lengths and applied load levels and to determine whether the data fall on a unique trend. At 750°C in air, the test matrix (see Table 3-1) includes one test each on specimens with widths of 40 and 20 mm (specimens 88-094 and 88-258). Since all other test conditions were identical, the results of these tests are plotted in Figure 3-4 on a da/dt versus C_t plot and in Figure 3-5 on a da/dt versus K plot. The data for specimen 88-094 show a dip which may have occurred due to transient conditions during testing. The ratio $\dot{V}_c/\dot{V}$ was also somewhat less than 0.8 for specimen 88-258 and the test lasted for slightly more than six hours. It appears that the load level for this test was on the high side for generating slow subcritical crack growth data. Thus, these data are not sufficient to make any definite conclusions about the applicability of TDFM crack tip parameters. Nevertheless, there appears to be a better correlation between da/dt than that between da/dt and K in the data from these tests.

Figure 3-6 shows the da/dt versus C_t behavior for crack growth tests conducted at 650°C in air and in vacuum. At equal C_t values, the crack growth rates in air appear to be much higher than those in vacuum. Comparing the values of $\dot{V}$ and $\dot{V}_c$ for these tests (see Appendix C), it appears that for the test conducted in air (88-111), $\dot{V}_c << \dot{V}$ throughout the test. Hence, a unique correlation between da/dt and C_t is not expected. Even for the specimen tested in vacuum (88-269), $\dot{V}_c/\dot{V} < 0.8$ except for the first two data points. Thus, even though the data trend for air and vacuum are in the right direction, no definite conclusions can be made from these data. In Figure 3-7, the crack growth data from the same two specimens are plotted as a function of the stress intensity parameter, K. At equal K values, the da/dt is higher for tests conducted in vacuum. This result cannot be rationalized except by assuming that da/dt does not correlate with K under these conditions. It appears that these data are in the transition regime between C_t and the K controlled regimes for which no suitable parameters are yet available.

Figure 3-8 shows the crack growth data from all tests conducted in air and Figure 3-9 shows all the data from the tests conducted in vacuum. The air data show temperature effects. In other words, da/dt is dependent on temperature. However, the crack growth rates are the highest for 650°C and the lowest for 800°C which is opposite to the expected trend. This is attributed to the problems in correlating the low temperature data with C_t because of the high applied loads resulting in very high crack growth rates causing problems discussed earlier. This is further confirmed by comparing the data in vacuum generated at different temperatures (Figure 3-9). With the exception of the test at 650°C for which the condition $\dot{V}_c/\dot{V} < 0.8$ was not met for most of the test, the temperature effects are normalized when da/dt is

expressed as a function of C_t. This result is consistent with other similar data in stainless steels [70] and in Cr-Mo-V steels [57].

In summary, creep crack growth data in a titanium aluminide appears to correlate well with C_t in the temperature range of 700 to 800°C. There are strong indications that TDFM concepts are necessary for characterizing the high temperature crack growth rates in this material. At 650°C, these correlations are suspect. It is recommended that a systematic investigation involving specimens of different geometries, sizes and load-levels be undertaken to examine this issue in much more detail. It is also recommended that load levels be selected such that the resultant test durations are at least one week and some tests last for several weeks. Load-line deflection should be monitored continuously during these tests. These data can then be used for definitely establishing the role of TDFM in predicting the elevated temperature crack growth behavior of these materials.

3.3 Creep-Fatigue Crack Growth Behavior

It has been recently shown [75] that the average crack growth rate, $(da/dt)_{avg}$, during a hold time can be characterized by the average value of C_t parameter $(C_t)_{avg}$ during the hold time. $(da/dt)_{avg}$ and $(C_t)_{avg}$ are defined as follows:

$$(da/dt)_{avg} = \frac{1}{t_h}\left[(da/dN) - (da/dN)_o\right] \qquad (3\text{-}16)$$

where, t_h is hold time, da/dN is crack growth rate per cycle and $(da/dN)_o$ is the crack growth rate for a loading waveform with zero hold time but with loading and unloading times which are the

same as for the waveform with hold time of t_h.

$$(C_t)_{avg} = \frac{1}{t_h} \int_o^{t_h} C_t \, dt \qquad (3\text{-}17)$$

If $t_h << t_T$, $(C_t)_{avg}$ can be estimated by integrating the small-scale-creep term in Equation (3-13), which is the first term on the right hand side of the equation.

Thus, $(C_t)_{avg}$ can be analytically estimated by the following equation:

$$\frac{2\alpha(1-\nu^2)\beta\tilde{r}_c(\theta)}{E(n-1)} \frac{K^4}{W} (EA)^{2/n-1} (F'/F) t^{-(n-3)(n-1)} \qquad (3\text{-}18)$$

If load-line deflections are measured during the hold time, $(C_t)_{avg}$ can also be measured. Figure 3-10 shows the $(da/dt)_{avg}$ versus $(C_t)_{avg}$ behavior for a 1Cr-1Mo-.25V steel for hold times ranging from 50 seconds to 24 hours at 538°C. Figure 3-11 shows the same data plus the additional creep-fatigue crack growth data at 427°C and creep crack growth data at various temperatures. Several observations can be made from these data.

The $(da/dt)_{avg}$ appears to uniquely correlate with $(C_t)_{avg}$ for different hold times and also for two quite different temperatures. It also shows that the creep-fatigue crack growth rates are somewhat lower than the creep crack growth rates at equal C_t. However, this does not imply that the component lives will be enhanced by periodic unloading. In fact, the result is quite the opposite. Periodic unloading does decrease the crack growth rates at the same C_t but it also increases the magnitude of C_t itself for the same applied load and crack size. Figures

3-12 and 3-13 schematically show C_t as a function of time for wave forms involving periodic unloading. The unloading interrupts the crack tip stress relaxation and during reloading a stress peak is regenerated every cycle [76] followed by stress relaxation during hold time. This can also be envisioned as resharpening of the crack tip due to periodic loading and unloading.

The behavior of Cr-Mo-V steels is similar to that of titanium aluminide under elevated temperature creep conditions. Therefore, the TDFM framework described above is expected to apply to titanium aluminides. This should, of course, be established by conducting an appropriate experimental program.

Table 3-1

UDRI Test Matrix for Creep Crack Growth Tests
on Ti-24Al-11Nb [12]

Spec. No.	Temp(°C)	Environment	P(Kips)	W(in.)	B(in.)
88-11	650	Air	2.142	1.578	0.3942
88-269	650	Vac	0.558	0.800	0.181
88-093	700	Air	1.986	1.578	0.3912
88-268	700	Vac	0.435	0.804	0.1827
88-094	750	Air	1.875	1.575	0.391
88-258	750	Air	0.418	0.804	0.190
88-260	750	Vac	0.359	0.802	0.180
88-266	750	Vac	0.323	0.803	0.1758
88-270	750	Vac	0.321	0.801	0.1758
88-254	800	Air	0.252	0.798	0.178
88-267	800	Vac	0.310	0.805	0.1796

B = thickness
W = width
P = load

1 in. = 25.4 mm
1 kip = 4.45 kilo-Newtons

Table 3-2

Values of the Creep Constant "A"
at Various Test Temperatures

Test Temp (°C)	A	
	$(ksi)^{-n}hr^{-1}$	$(MPa)^{-n}hr^{-1}$
650	3.29×10^{-13}	8.05×10^{-18}
700	3.88×10^{-12}	9.5×10^{-17}
750	3.61×10^{-11}	8.83×10^{-16}
800	2.70×10^{-10}	6.60×10^{-15}

Note: n = 5.5

Table 3-3

Tensile and Elastic Modulus
at Various Temperatures

Test Temp (°C)	σ_{ys}		E	
	ksi	MPa	Ksi	MPA
650	41	282.6	12.7×10^3	8.75×10^4
700	39	268.9	12.4×10^3	8.55×10^4
750	37	255.0	12.0×10^3	8.27×10^4
800	35	241.3	11.7×10^3	8.06×10^4

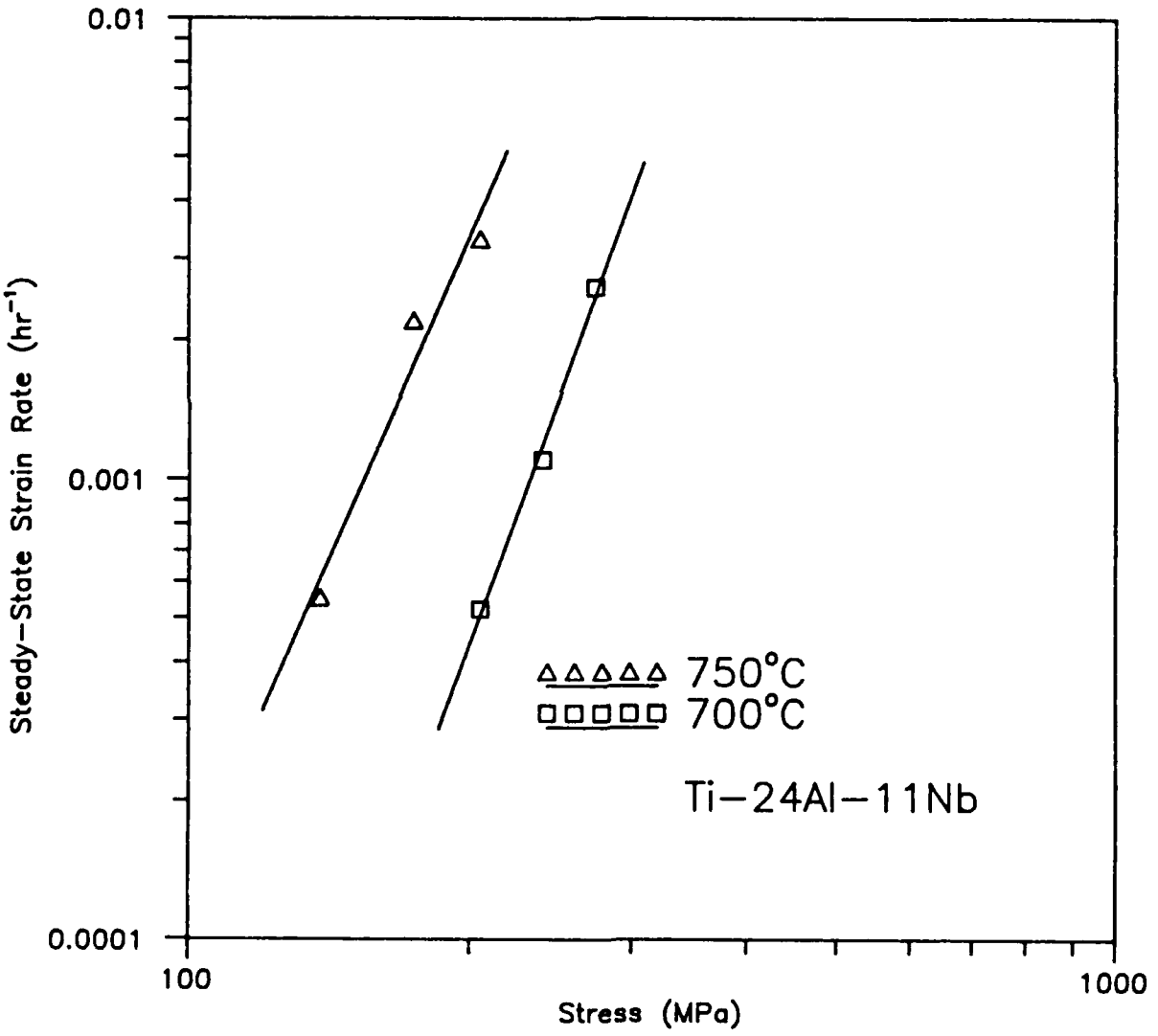

Figure 3-1. Creep Deformation Behavior of Ti-24Al-11Nb

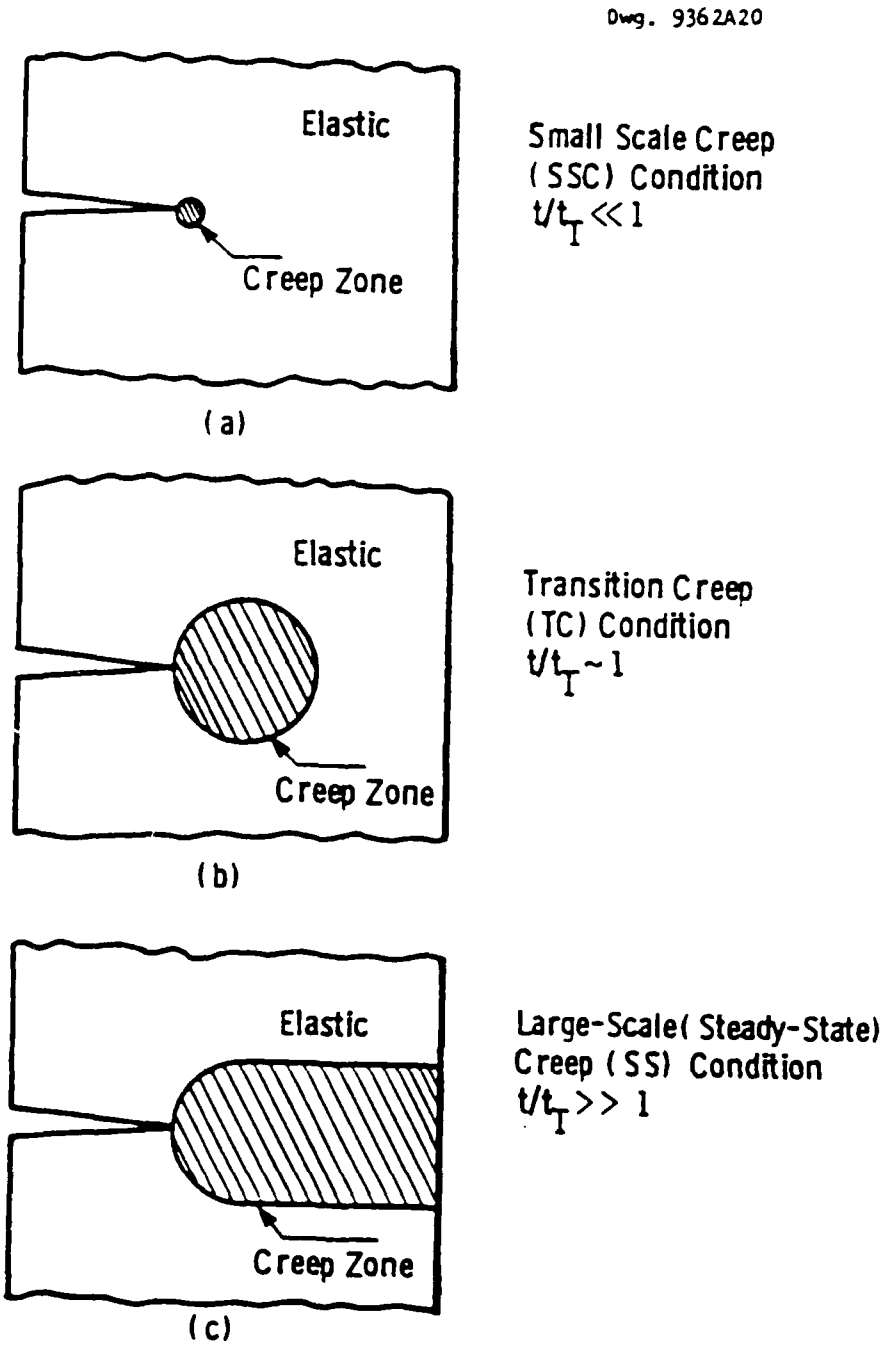

Figure 3-2. Schematic Representation of the Levels of Creep Deformation Under Which Creep Crack Growth Can Occur

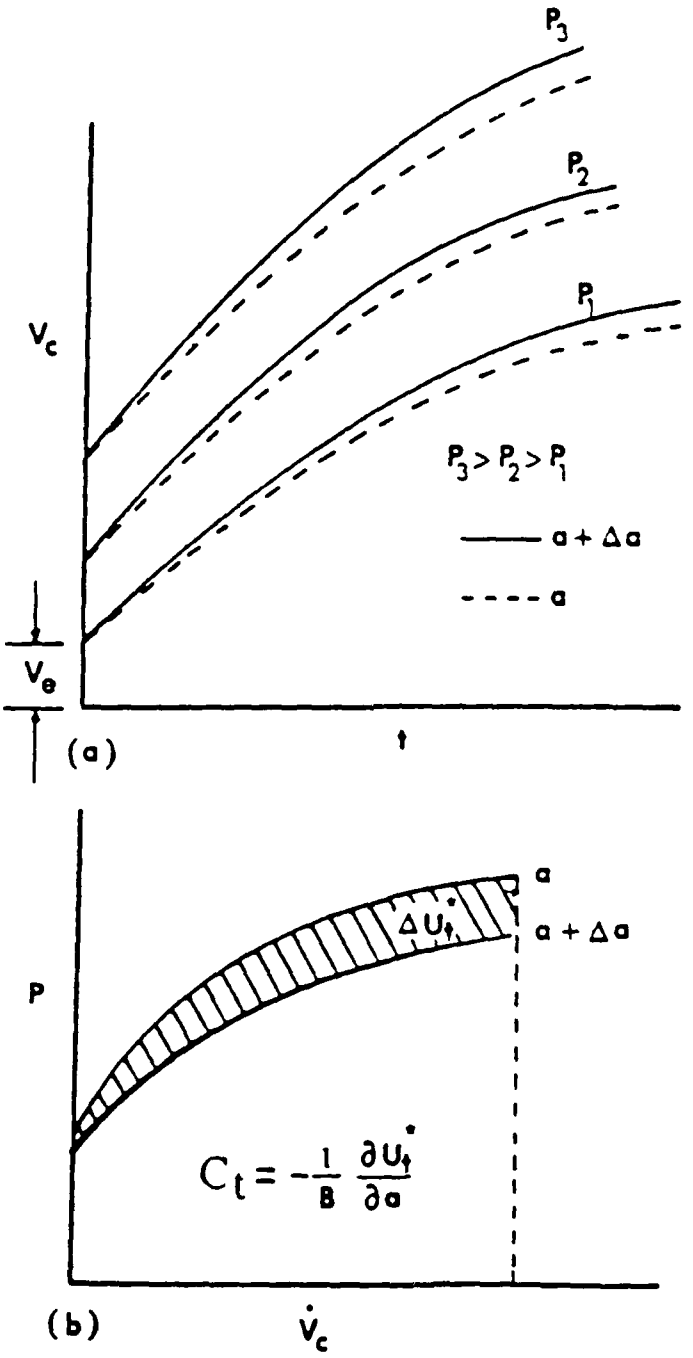

Figure 3-3. (a) Load Line Deflection, V_c, as a Function of Time for Bodies of Crack Lengths a and a+Δa at Various Load Levels, and (b) the Definition of the C_t Parameter

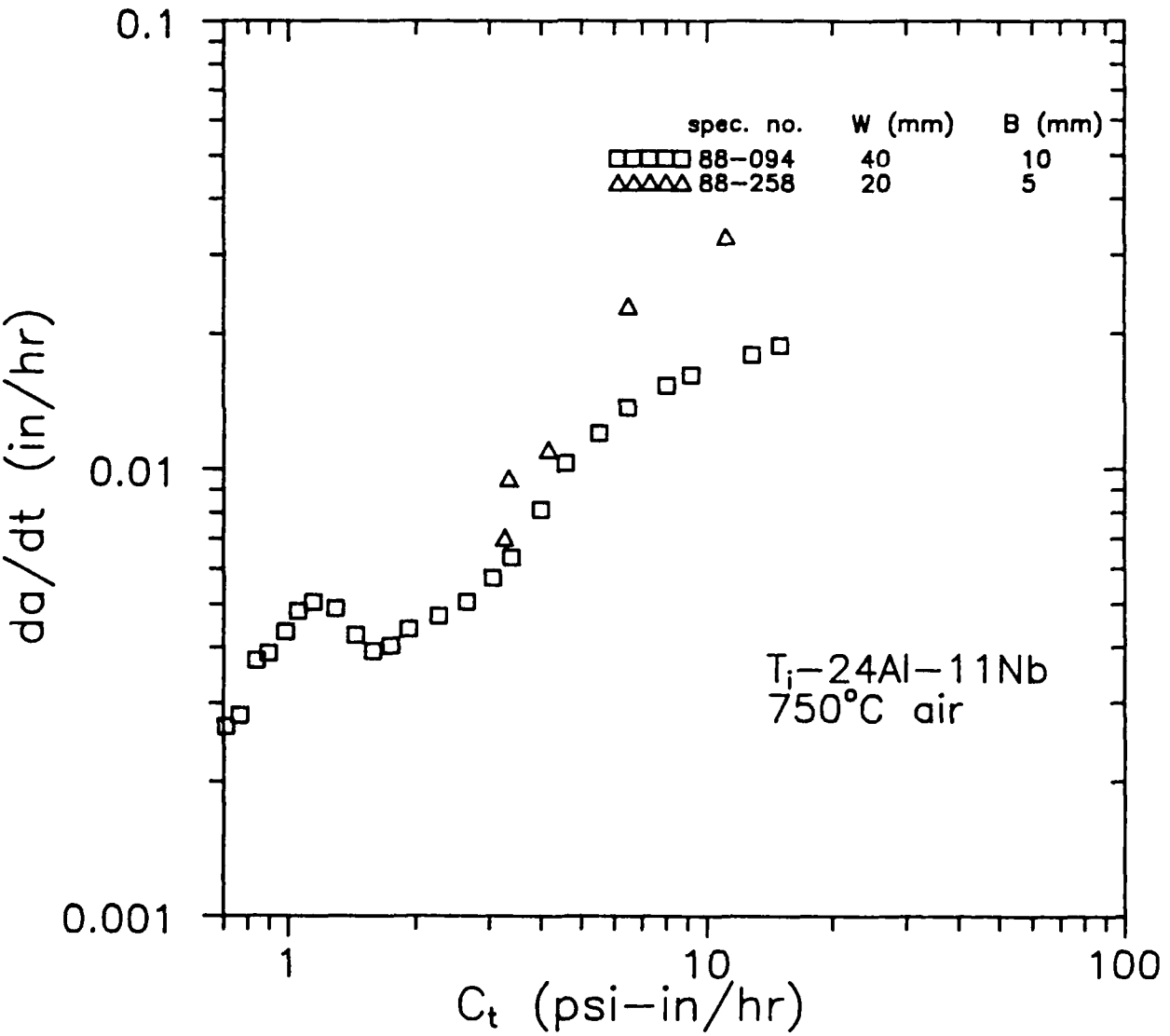

Figure 3-4. da/dt Versus C_t Data for Ti-24Al-11Nb Obtained From Specimens of Two Sizes

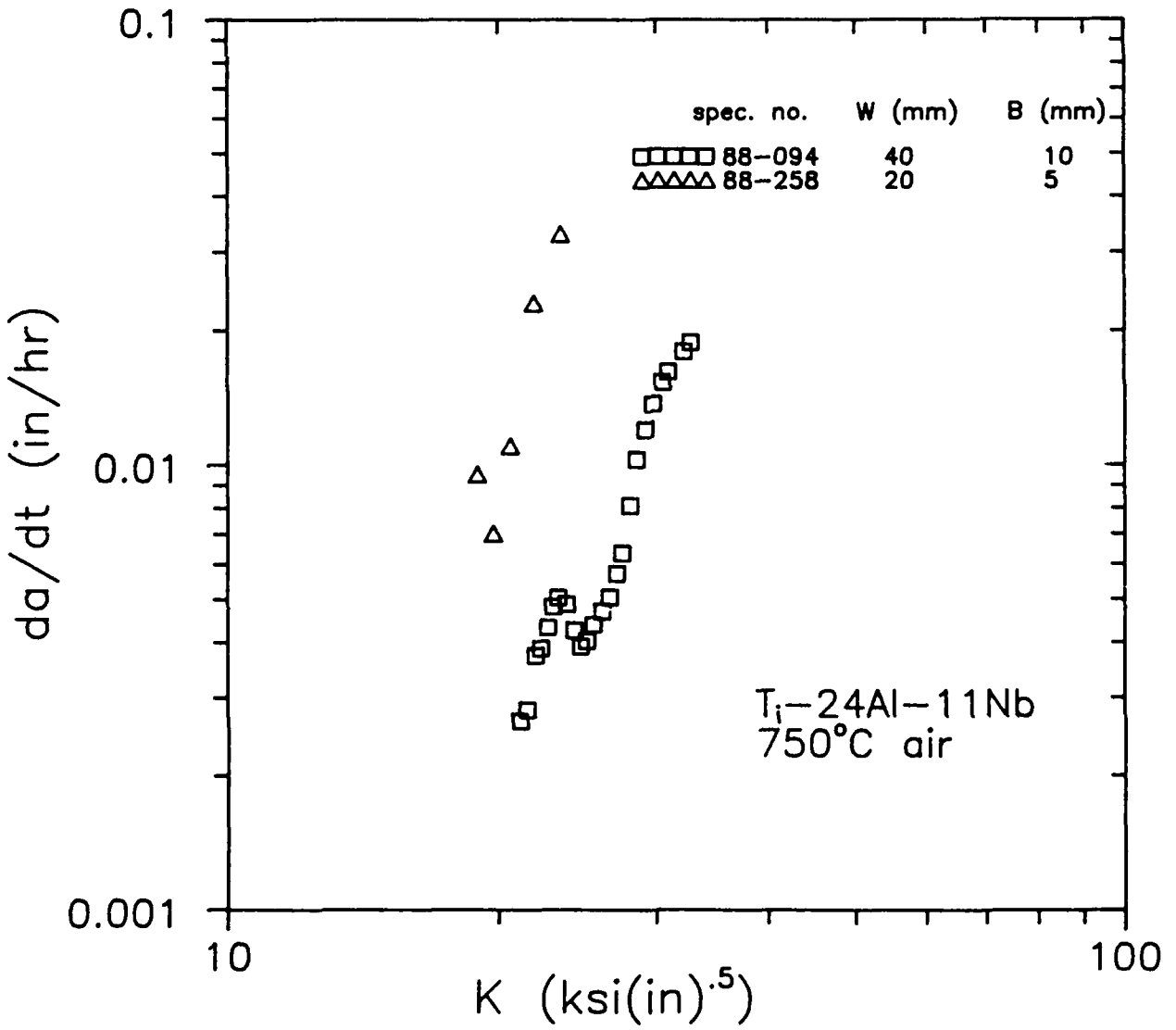

Figure 3-5. da/dt Versus K Data for the Ti-24Al-11Nb Obtained from Specimens of Two Sizes

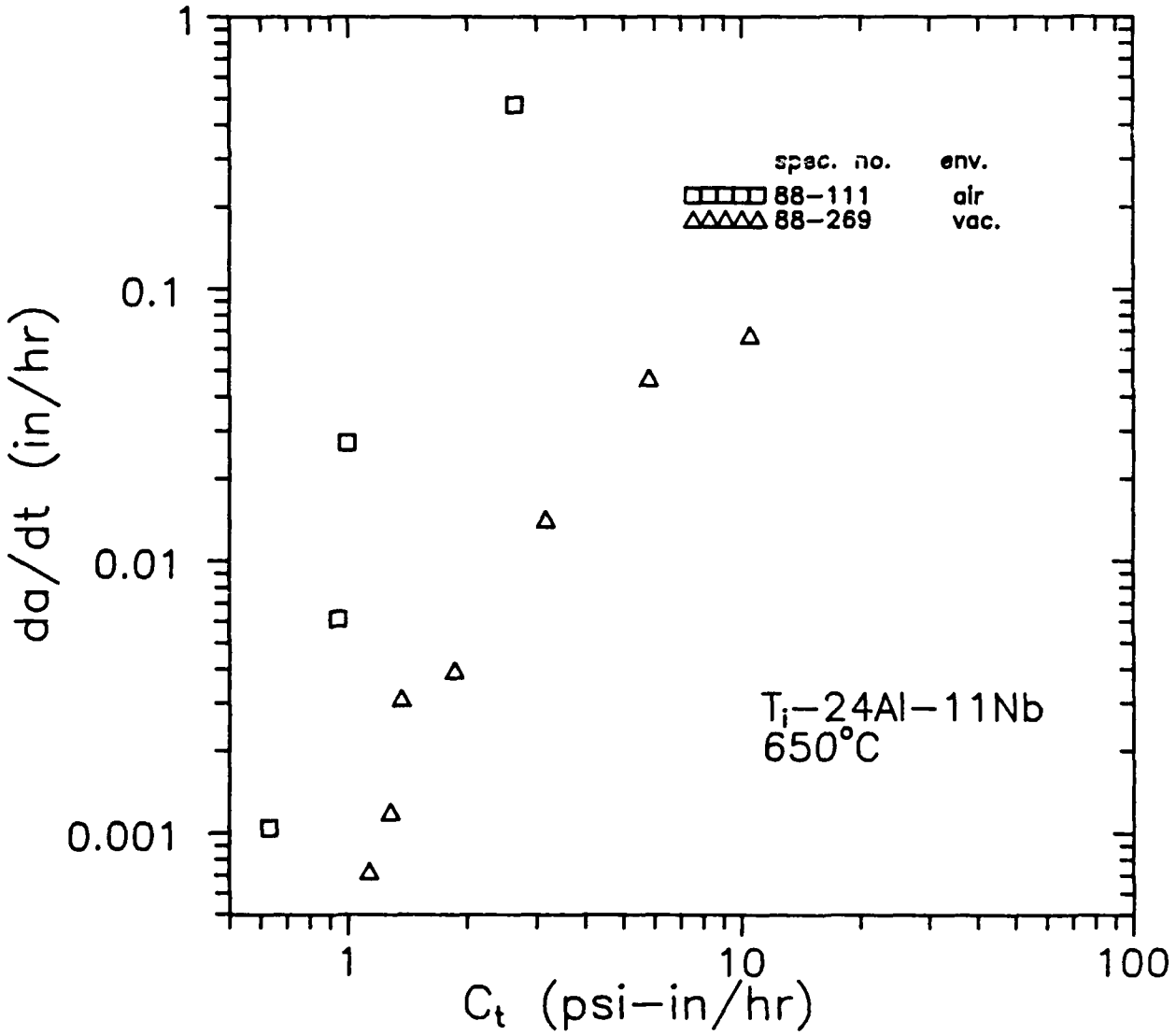

Figure 3-6. da/dt Versus C_t Data for Ti-24Al-11Nb Obtained at 650°C in Air and Vacuum Environments

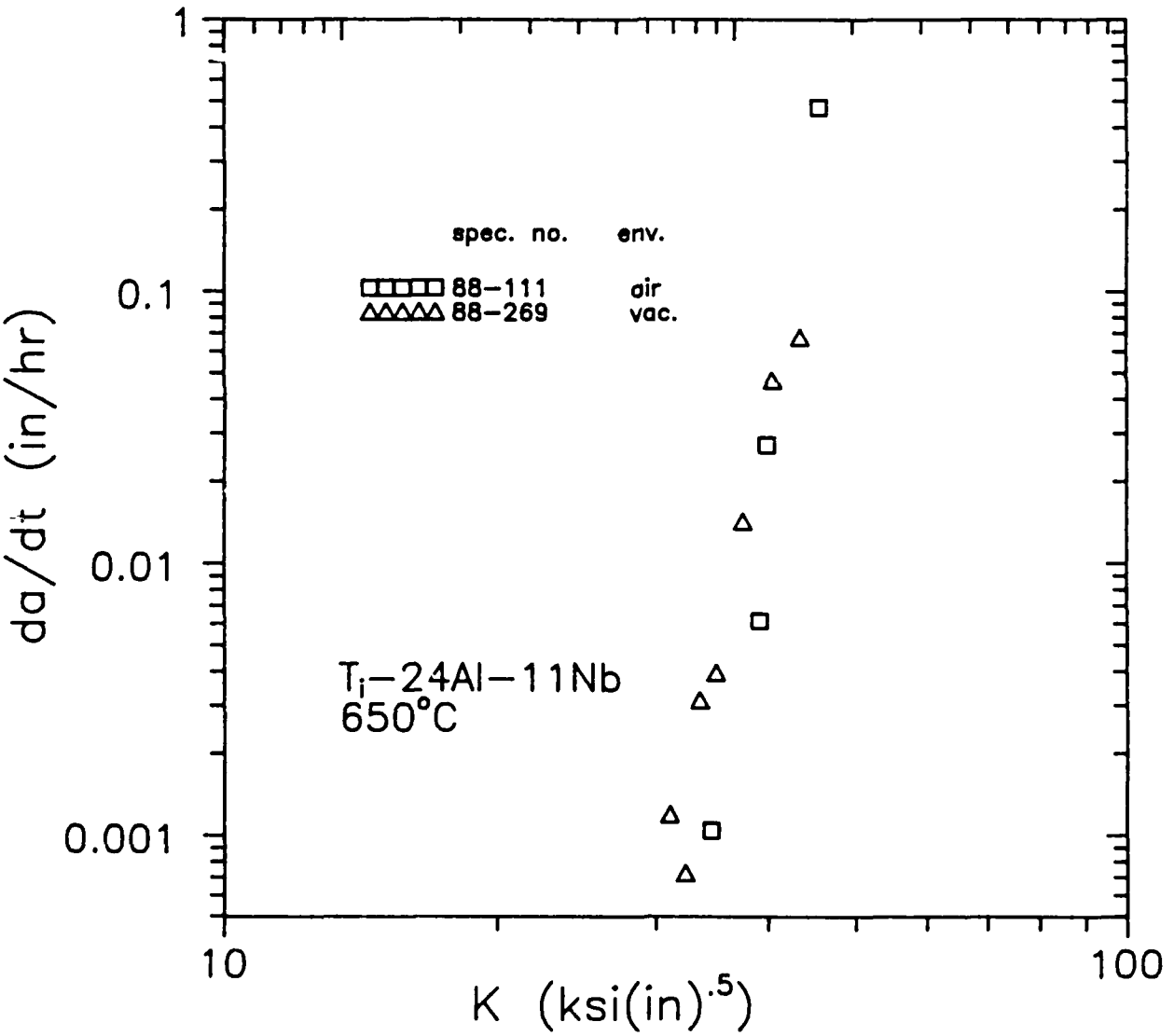

Figure 3-7. da/dt Versus K Data for Ti-24Al-11Nb Obtained at 650°C in Air and Vacuum Environments

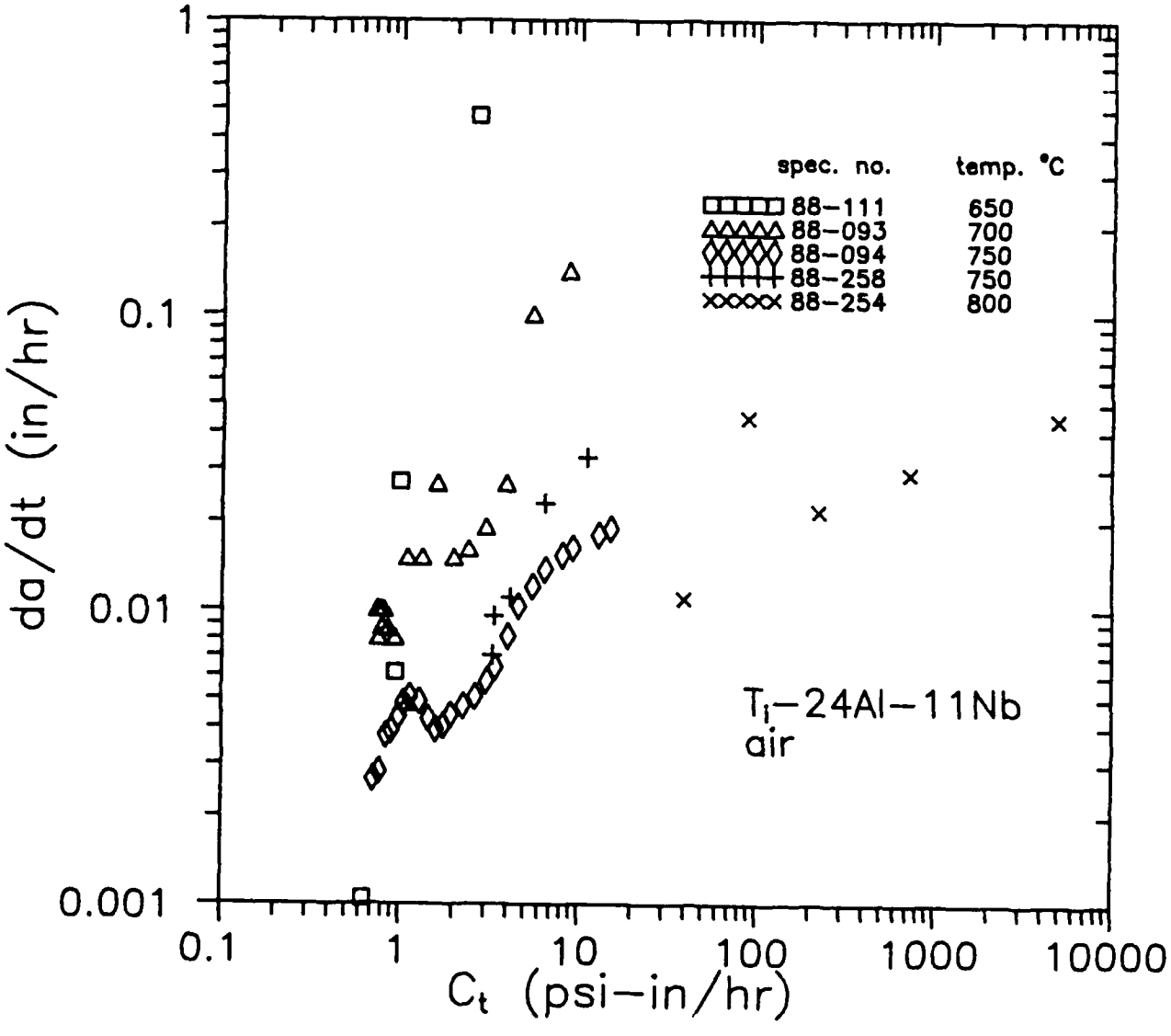

Figure 3-8. Creep Crack Growth Behavior of Ti-24Al-11Nb in Air at Various Temperatures

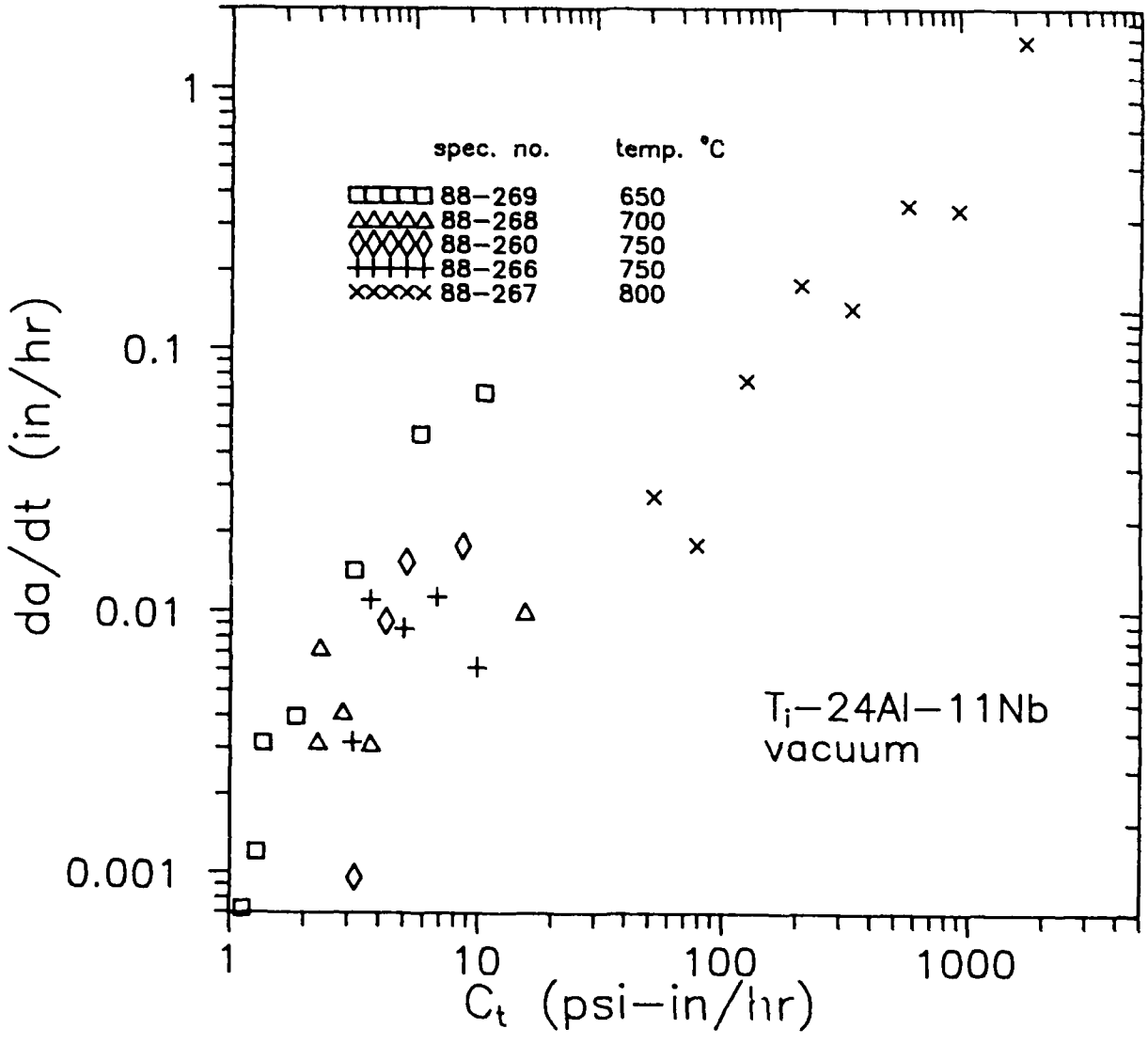

Figure 3-9. Creep Crack Growth Behavior of Ti-24Al-11Nb in Vacuum at Various Temperatures

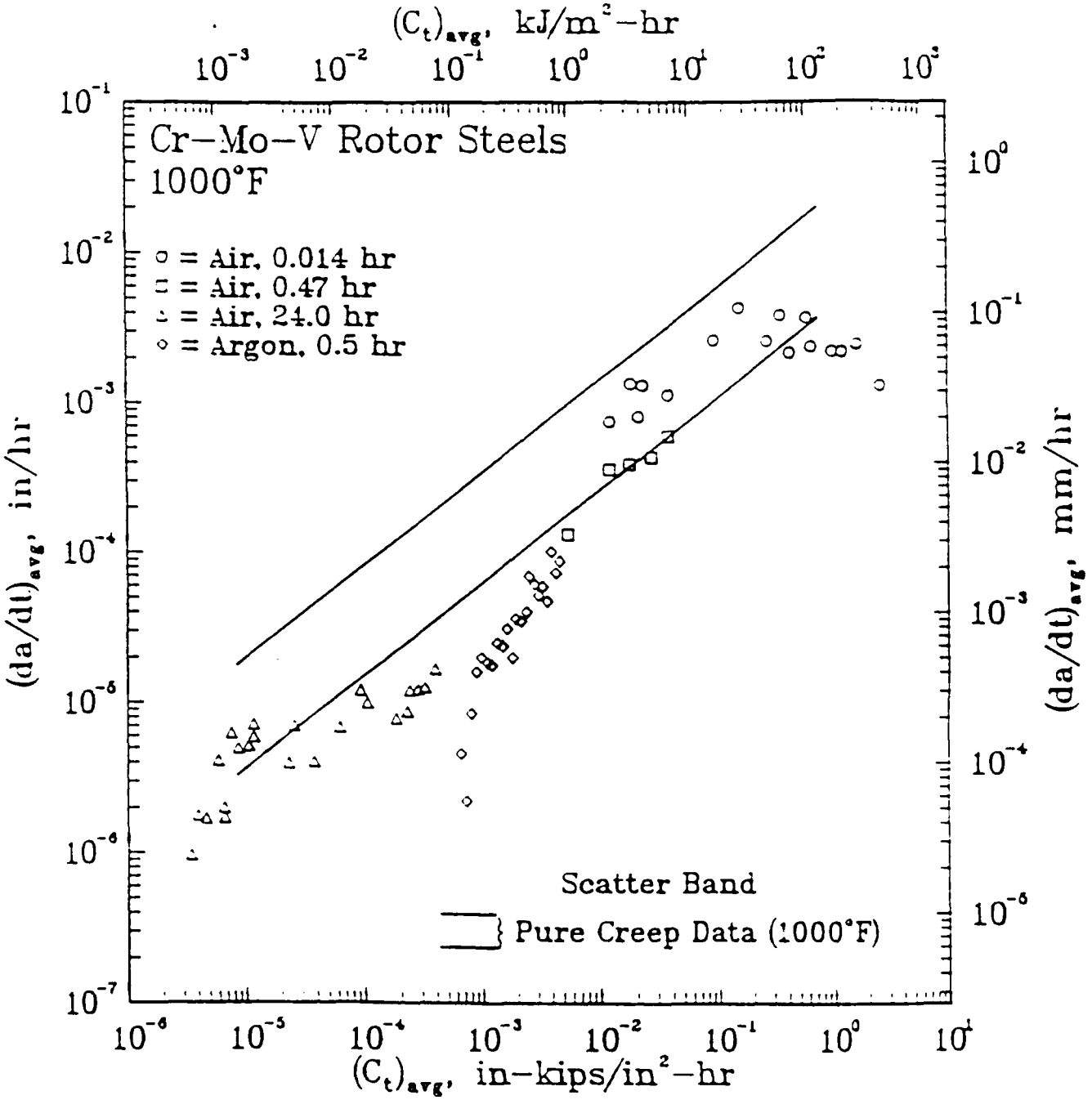

Figure 3-10. Representation of Creep-Fatigue Crack Growth Behavior in Terms of the $(C_t)_{avg}$ Parameter for New Cr-Mo-V Steels Tested at 1000°F (538°C) in Air and Argon (Ref. 75)

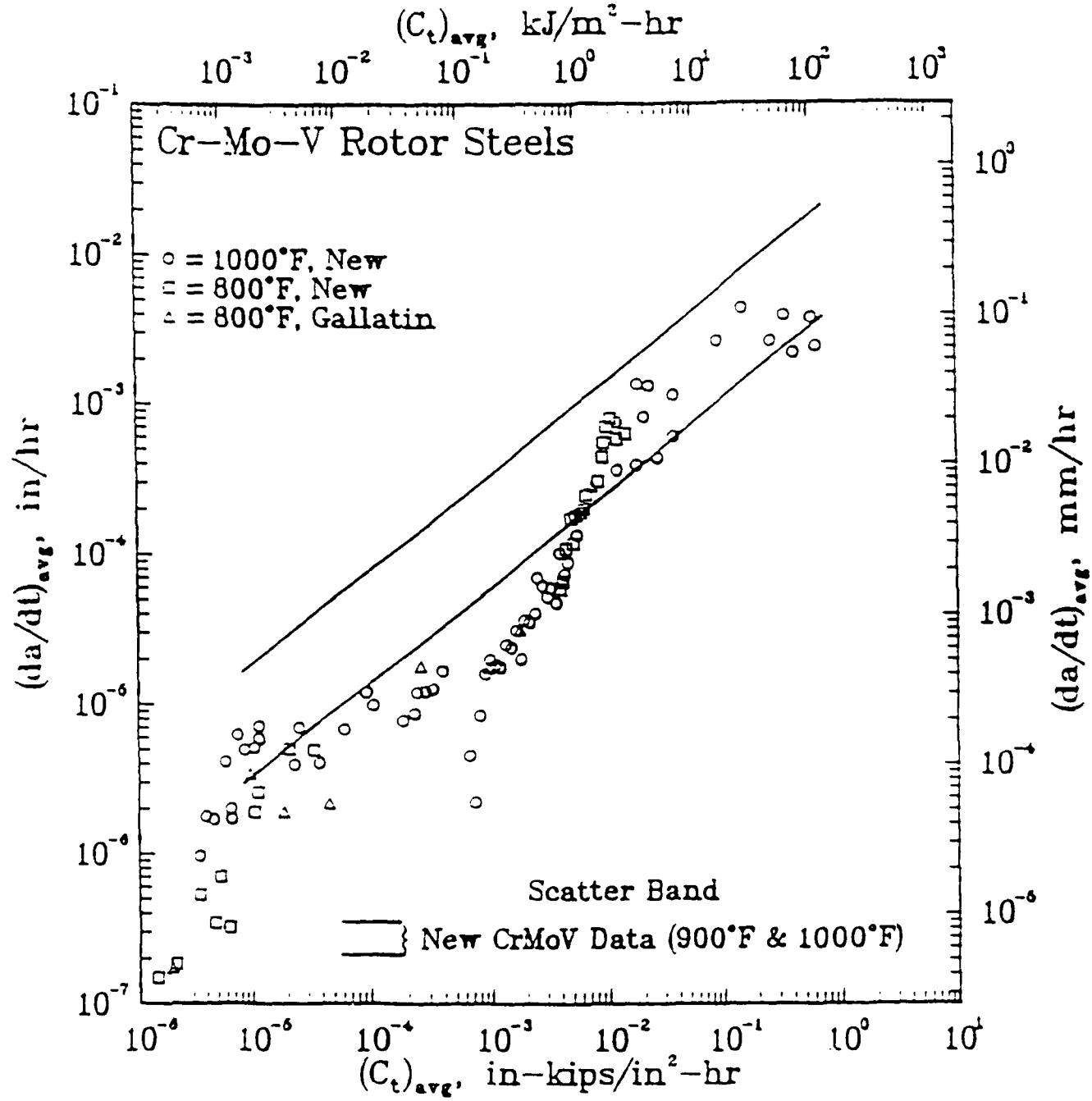

Figure 3-11. Superimposition of Creep-Fatigue Crack Growth Data According to the $(C_t)_{avg}$ Parameter Concept for New and Ex-Service Cr-Mo-V Steels Tested at 1000°F (538°C) and 800°F (427°C) (Ref. 75)

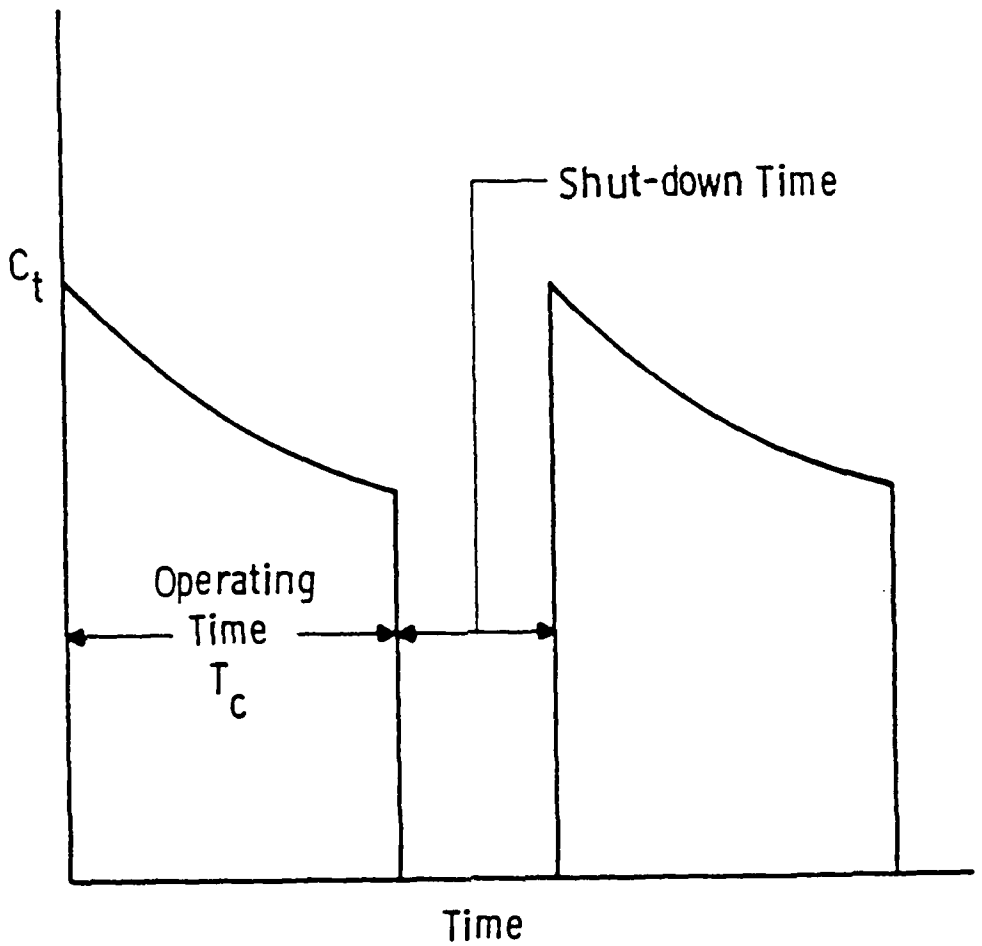

Figure 3-12. Schematic of C_t as a Function of Time for Cyclic Operation

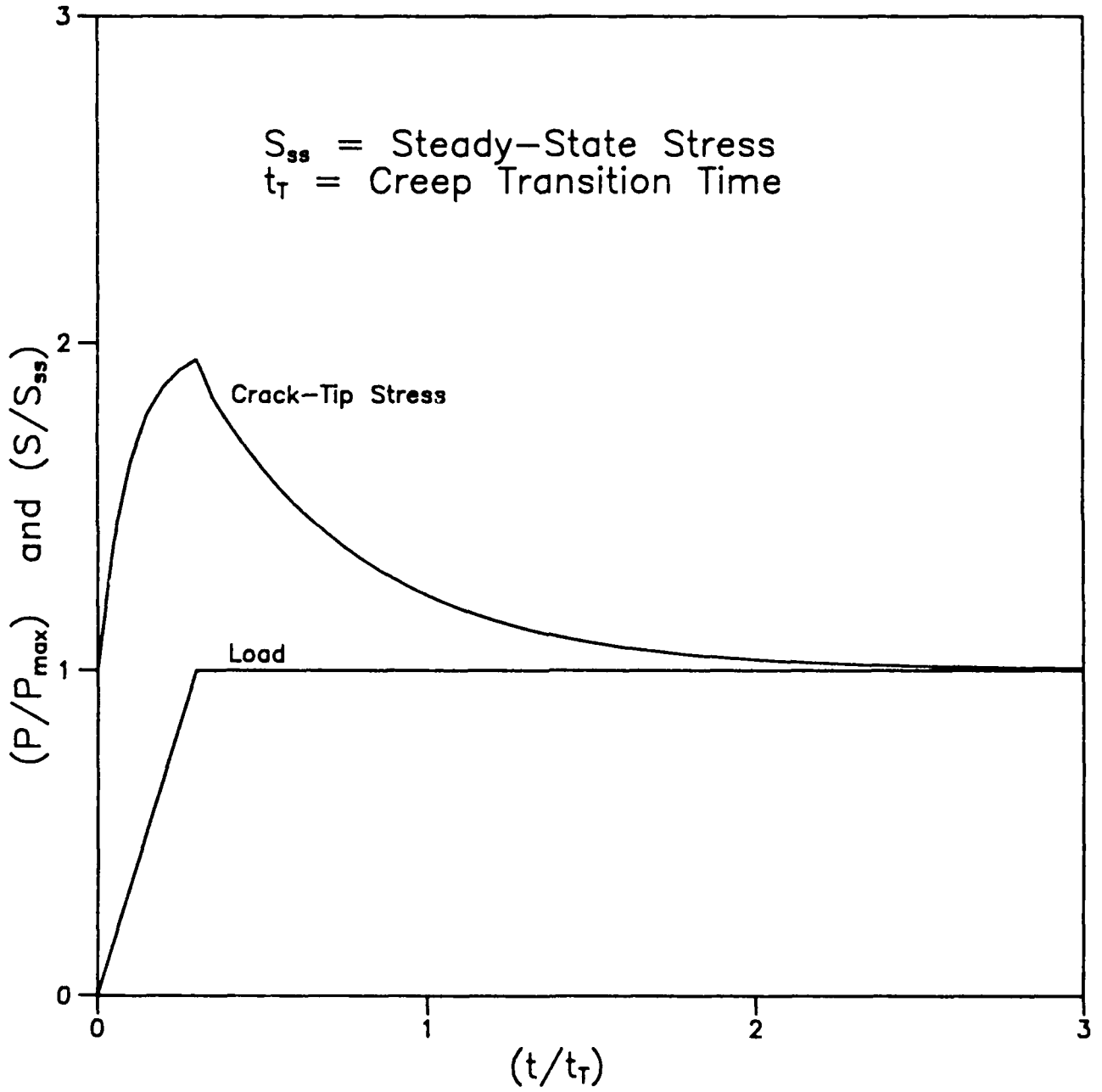

Figure 3-13. Normalized Crack Tip Stress as a Function of Normalized Time at a Fixed Distance Ahead of the Crack Tip for Fast Loading Followed by a Sustained Load

4.0 Reexamination and Application of C_t

As discussed in section 3 of this report, C_t appears to be the best parameter, among C_t, C(t), K and C^*, for characterizing creep crack growth of titanium intermetallics under transient as well as steady-state creep. The same behavior for steel has been reported by Saxena and his co-workers (see e.g. [63]) in their experimental results. The good correlation between C_t and creep crack growth can be attributed to the fact that C_t is proportional to the rate of expansion of the creep zone [63], which characterizes the damage zone at the crack tip region under creep conditions.

Although both C_t and C(t) are related to the crack tip damage (or stress) under creep conditions, C_t can be readily measured from load line deflection curves in a test while C(t) can only be computed. On the other hand, C(t) is easier to compute than C_t for structural components. This section reexamines the definition of C_t and provides alternative ways of computing C_t.

4.1 Pseudo-Potential P^* and C_o

For a two-dimensional structure, we define pseudo-potential P^* as

$$P^* = \int_{\partial A_t} T_i \dot{u}_i \, ds - \int_A W^* \, dA \qquad (4\text{-}1)$$

where A is the entire body, ∂A_t is the boundary of A on which traction is specified, and W^* is defined by

$$W^* = \int_0^{\dot{\epsilon}_{ij}} \sigma_{kl} \, d\dot{\epsilon}_{kl} \qquad (4\text{-}2)$$

It is worth noting that, even though the expression of W^* in eq. (4-2) looks simple and somewhat familiar, W^* does not bear any physical meaning. The first term in eq. (4-1), which is the total power which flows into the body at a given instant, depends only on the current state (stresses, strains, and strain rates) of the body. On the contrary, the second term in eq. (4-1) is history dependent. In other words, for a structure body A, the first part of P^* is a function of its current state while the second part of P^* depends on the loading path from time zero.

For a stationary crack, we then define another quantity $C_o(t)$ as

$$C_o(t) = \frac{dP^*}{da} = \frac{d}{da}\left[\int_{\partial A_t} T_i \dot{u}_i ds - \int_A W^* dA\right] \tag{4-3}$$

where a is the crack length. It will be shown later in this report that C_o and C_t are uniquely related in small scale creep and steady-state creep conditions. It should be noted that A in eq. (4-3) is the entire body and eq. (4-3) is defined for two stationary cracks at length of a and a+Δa under the same loading conditions. The subscript "o" of C_o stands for the outer boundary. By following the same procedure as that used by Rice [77] in deriving the well-known J-integral, it can be shown that eq. (4-3) can be reduced to

$$C_o(t) = \int_{\partial A}(W^* n_1 - T_i \dot{u}_{i,1})ds - \int_A (W^*_{,a} - \sigma_{ij}\dot{\epsilon}_{ij,a})dA$$

$$= C(t)\big|_{\partial A} - \int_A (W^*_{,a} - \sigma_{ij}\dot{\epsilon}_{ij,a})dA \tag{4-4}$$

where A is the entire structure body and ∂A is the entire outer boundary of the body. Thus, the new parameter C_o defined in eq. (4-3) is nothing but an area integral plus the C(t) integral [56] computed along the entire outer boundary of the body. The area

integral in eq. (4-4), however, is not always zero since, in general, W^* is a function of $\dot{\epsilon}_{ij}$, $\dot{\sigma}_{ij}$, ..., implying $W^*_{,a} \neq \sigma_{ij}\dot{\epsilon}_{ij}$. The inequality of C_o and $C(t)$ has also been observed numerically by Bassani, et al, [63] and Leung, et al, [78]. Further, like C_t and $C(t)$, $C_o(t)$, in general, is not path independent.

4.2 Steady-State Creep

From eq. (4-4), it can be easily deduced that, at long times $t \to \infty$,

$$C_o(t) = C_t(t) = C(t) = C^* = \int_\Gamma (W^* n_1 - T_i \dot{u}_{i,1}) ds \qquad (4\text{-}5)$$

where Γ is any integration contour which encompasses the crack tip counterclockwise, because

$$W^* = W^*(\dot{\epsilon}_{ij}) \qquad (4\text{-}6)$$

$$W^*_{,a} = (\partial W^* / \partial \dot{\epsilon}_{ij}) \dot{\epsilon}_{ij,a} = \sigma_{ij} \dot{\epsilon}_{ij,a} \qquad (4\text{-}7)$$

is true under steady-state creep conditions. Therefore, for steady-state creep, C_o and C_t represent the same physical quantity.

4.3 Small Scale Creep

We next examine the behavior of C_o at the other end of the time spectrum, very small times $t \to 0$. As illustrated in Figure 4-1, when the elapsed time t is much less than the transition-time t_T defined by eq. (3-10), the creep dominant zone A'_c is much smaller than the surrounding elastic zone A_e. The creep dominant zone A'_c has the same shape as the creep zone A_c defined by Riedel and

Rice [58] but is larger in size. The latter is the locus of points where the equivalent creep strain equals to the equivalent elastic strain. As will be shown later in this report in an example problem, it is found that good agreements can be achieved consistently for a wide range of creep exponents n when A_c' is set to be six times the size of A_c defined by Riedel and Rice [58]. For small scale creep, it can be argued that

$$\int_A W^* dA = \int_{A_c'} W^* dA + \int_{A_e} W^* dA \cong \int_{A_c'} W^* dA \tag{4-8}$$

since integration of W^* over the elastic region A_e is negligible compared with the contribution from the creep dominant region A_c'. From eq. (4-8), it can be seen that A_c' has to be larger than A_c because at the boundary of A_c, total creep strains equal to total elastic strains and the W^* values at the boundary of A_c are still not negligible. Also, the net power dissipated in the elastic region is near zero, i. e.,

$$\int_{\partial A} T_i \dot{u}_i \, ds \cong \int_{\partial A_c'} T_i \dot{u}_i \, ds \tag{4-9}$$

With eqs. (4-8) and (4-9), $C_o(t)$ defined in eq. (4-3) now reduces to

$$C_o(t) = \frac{d}{da} \left[z \int_{\partial A_c'} T_i \dot{u}_i \, ds - \int_{A_c'} W^* \, dA \right] \tag{4-10}$$

where z=1 under load-control conditions and z=0 under displacement-control conditions. It is worth noting that C^* was defined [53] originally under displacement-control conditions while C_t was defined [57] originally under load-control conditions. That is, the P-$\dot{V}$ curves should be constructed by running constant displacement rate tests when measuring C^* but

constant load tests when measuring C_t. However, at steady-state creep conditions, both constant load tests and constant displacement rates will lead to the same P-$\dot{V}$ curve due to the fact that P and $\dot{V}$ at steady-state creep conditions are uniquely related. The same conclusion can not be drawn for C_t at small scale creep or transition creep conditions, because, under these conditions, the P-$\dot{V}$ relation [72]

$$\dot{V}_c = \frac{4\alpha(1-\nu^2)}{E(n-1)} \left(\frac{P}{B}\right)^3 \left(\frac{F^4}{W^2}\right)(EA)^{2/(n-1)} t^{-(n-3)/(n-1)} \tag{4-11}$$

is true only for constant loads.

Inside the creep dominant zone A_c' the overall strain rate is determined by the power law relationship given in eq. (3-1). Thus, in A_c'

$$W^* = \frac{n}{(n+1)} \sigma_{ij} \dot{\epsilon}_{ij} \tag{4-12}$$

and the stresses, strain rates, and displacements behave asymptotically like the HRR field [58-60]:

$$\sigma_{ij} = \sigma_o \left[\frac{C(t)}{\dot{\epsilon}_o \sigma_o I_n r}\right]^{1/(n+1)} \tilde{\sigma}_{ij}(\theta) \tag{4-13}$$

$$\dot{\epsilon}_{ij} = \dot{\epsilon}_o \left[\frac{C(t)}{\dot{\epsilon}_o \sigma_o I_n r}\right]^{n/(n+1)} \tilde{\epsilon}_{ij}(\theta) \tag{4-14}$$

$$\dot{u}_i = r\dot{\epsilon}_o \left[\frac{C(t)}{\dot{\epsilon}_o \sigma_o I_n r}\right]^{n/(n+1)} \tilde{u}_i(\theta) \tag{4-15}$$

where dimensionless functions $\tilde{I}_n$, $\tilde{\sigma}_{ij}$, $\tilde{\epsilon}_{ij}$, and $\tilde{u}_i$ have been tabulated by Shih [79] and Symington and Shih [80] for various n values, σ_o is yield strength, and $\dot{\epsilon}_o$ is strain rate at σ_o.

In eq. (4-10), the creep dominant zone A_c' is not fixed in space but is moving and changing in size with different crack lengths, implying that the differentiation procedure used by Rice [77] in deriving J is not applicable here.

We further assumed that the creep zone for the stationary crack of lengths a and a+Δa are self similar. That is, it is assumed that

$$r_c(\theta,t) = F(t)\ F_{cr}(\theta) \tag{4-16}$$

where r_c is radial distance measured from the crack tip of the boundary ∂A_c of the creep zone A_c. This assumption is valid as long as the body is under small scale creep. In fact, Riedel and Rice [58] have shown that, under constant loads,

$$r_c(\theta,t) = r_c^o(t)\ F_{cr}(\theta) \tag{4-17a}$$

$$r_c^o(t) = \frac{1}{2\pi}\left(\frac{K}{E}\right)^2 \left[\frac{(n+1)\dot{\epsilon}_o I_n E^n t}{2\pi(1-\nu^2)\sigma_o^n}\right]^{2/(n-1)} \tag{4-17b}$$

where K is stress intensity factor and $F_{cr}(\theta)$ is a non-dimensional function.

Substituting eqs. (4-12) to (4-15) and applying the differentiation technique described in Appendix D, equation (4-10) can be reduced to

$$C_{os}(t) = \frac{6}{n+1} F_{cr}\left(\frac{\pi}{2}\right) \left[L_n\ r_c^o \frac{\partial C(t)}{\partial a} + M_n\ C(t)\ \frac{\partial}{\partial a} r_c^o\right] \tag{4-18}$$

where the additional subscript "s" on C stands for small scale creep, the factor 6 comes from the assumption that A_c' is six times the size of A_c, and

$$L_n = \frac{1}{I_n} \int_{\partial A_c} \tilde{\sigma}_{ij} \tilde{u}_i n_j \, d[s/r_c(\tfrac{\pi}{2},t))] \tag{4-19}$$

$$M_n = \frac{1}{I_n} \int_{\partial A_c} \tilde{\sigma}_{ij} \tilde{\epsilon}_{ij} \, d[s/r_c(\tfrac{\pi}{2},t))] \tag{4-20}$$

are dimensionless constants which depend on the creep constant n and shape function $F_{cr}(\theta)$ of the creep zone A_c. Creep zone shapes under mode I loading for different n values have been computed analytically by Riedel and Rice [58]. For the creep zone shapes computed by Riedel and Rice [58], L_n, and M_n for n= 5, 7, 10, 15, and 20 have been calculated and are tabulated along with $F_{cr}(\frac{\pi}{2})$ in Table 4-1. L_n and M_n values listed in Table 4-1 were calculated based on the $\tilde{\sigma}_{ij}$, $\tilde{\epsilon}_{ij}$, and $\tilde{u}_i$ functions tabulated in References [79, 80] by Shih and his co-workers. To study the sensitivity of L_n and M_n on the shape of the creep zones, a creep zone shape computed per finite element method by Riedel [81] and an artificially assumed double circle creep zone for n=5 were also used to calculate L_n and M_n, and their results are shown in Table 4-2. It is seen in this table that $(L_n + M_n)$, which determines C_o, is not sensitive to the creep zone shapes tested here.

Under constant load condition, Eq. (4-18) can be further simplified as

$$C_{os}(t) = \frac{6}{n+1} F_{cr}(\tfrac{\pi}{2}) \, (L_n+M_n) \, \frac{K^4(1-\nu^2)}{E^3(n+1)\pi t} \, \frac{K'}{K} \, \left[\frac{(n+1) I_n E^n A t}{2\pi(1-\nu^2)}\right]^{2/(n-1)} \tag{4-21}$$

or

$$C_{os}(t) = \frac{6}{n+1} F_{cr}(\frac{\pi}{2}) (L_n+M_n)\frac{K^2(1-\nu^2)}{E(n+1)} \frac{K'}{K}(n-1) \dot{\epsilon}_c^o \qquad (4\text{-}22)$$

where K'=dK/da. Eqs. (4-21) and (4-22) are very similar to the asymptotic expressions derived by Saxena [63, 72], i.e. very similar to the first term of eq. (3-13). Like C_t, at small scale creep, $C_{os}(t)$ is also proportional to the rate of creep zone size growth. As discussed in Appendix E, it can be shown that, under small scale creep and constant load conditions,

$$C_t = \frac{n+1}{4} C_{os} \qquad (4\text{-}23)$$

4.4 Creep in Transition Period

For the transition period between small scale creep and steady-state creep, it is proposed that C_t is the sum of its asymptotic values at $t<<t_T$ and at $t\to\infty$, i. e.,

$$C_t(t) = \frac{n+1}{4} C_{os}(t) + C^* \qquad (4\text{-}24)$$

where C_{os} is calculated per eq. (4-18). Under constant load conditions, C_{os} can also be calculated by eqs. (4-21) or (4-22). To check the validity of eq. (4-23), the problem of a compact tension specimen under a constant force P analyzed by Bassani, et al, [63] was chosen as an example. Dimensions and material properties of this example problem are listed in Table 4-3. C^* and t_T values for this example for various n values were then calculated and summarized in Table 4-4. The resulting $C_o(t)$ values are plotted in Figures 4-2 to 4-6 for n=5, 7, 10, 15, and 20, respectively. In these figures, three curves are shown:

$(n+1)C_{os}(t)/4$, $[(n+1)C_{os}(t)/4 + C^*]$, and a reference curve $C^*[1+(\frac{t_T}{t})^{(n-3)/(n-1)}]$, which has been shown [63] to be a very good approximation of C_t for the entire time range. From these figures, it is seen that the agreement between $[(n+1)C_{os}/4 + C^*]$ and C_t are excellent for the entire time range for all n values tested.

4.5 $C_o(t)$ versus C_t

As indicated in section 4.1 and 4.2, $C_o(t)$ and C_t are similar in the following aspects:

(a) Both C_o and C_t become C^* at steady-state creep.
(b) Under small scale creep conditions, both C_o and C_t are proportional to the rate of creep zone growth.
(c) Under a constant load, both C_o and C_t behave asymptotically like $t^{-(n-3)/(n-1)}$ at very small t, which is much less than the asymptotic value of t^{-1} for C(t).
(d) C_t and C_o are related by $C_t=(n+1)C_o/4$ for small scale creep. Thus, C_o can correlate with creep crack growth data as well as C_t does.
(e) Both parameters are defined for stationary cracks.

However, there is a basic difference between C_o and C_t: C_o's definition, eqs. (4-3) and (4-4), is based on a single loading (constant load or variable load) on a single structure, while C_t's definition, eq. (3-11), is based on multiple loading (load remain constant in each single one) on multiple but identical structure bodies. However, it has been shown that, like C_o, C_t can also be computed based on a single loading for small scale creep and steady-state creep [57].

Furthermore, both C_t and C_o can be used to handle variable loading even though the existing C_t definition does not give a very clear indication on how the C_t should be calculated under variable loading conditions. To calculate C_t for a crack under variable loading, either C_o formulation in Eq. (4-3) or the C_t-$\dot{r}_c$ relationship similar to that in Eq. (4-22) should be used.

To sum up this section, an alternative way of calculating C_t has been derived. While both the existing and the newly proposed definitions of C_t are as effective and accurate in evaluating test specimens, the new C_t definition provides a more convenient way of computing C_t for analyzing structural components.

Table 4-1

Creep Fracture Constants

n	5	7	10	15	20
$F_{cr}(\pi/2)$	0.3156	0.3214	0.3262	0.3292	0.3300
L_n	0.3944	0.3980	0.4030	0.4101	0.4131
M_n	0.6177	0.6373	0.6623	0.6919	0.7131

Table 4-2

Effects of Creep Zone Shape (n=5)

	Analytical[(a)]	FEM[(b)]	Double Circles[(c)]
$F_{cr}(\pi/2)$	0.3156	0.2703	0.3156
L_n	0.3944	0.4095	0.4556
M_n	0.6177	0.5521	0.5281
L_m+M_n	1.0121	0.9616	0.9837

(a) Reference 58

(b) Reference 81

(c) $F_{cr} = 0.3156 \sin\theta$

Table 4-3

Example Material Properties

$E = 20.4 \times 10^3$ ksi

$\nu = 0.3$

$\sigma_o = 19.0$ ksi

$\dot{\epsilon}_o = 0.003444$ hr^{-1}

$F'/F = 2.912$

$w = 2$ in.

$a = 0.941$ in.

$p = 3450$ lbf

$K = 21.52$ ksi$\sqrt{\text{in}}$

Table 4-4

C^* and t_T for the Example Problem

n	5	7	10	15	20
C^* (ksi-in/hr)	6.1081	2.0540	0.4203	0.0309	0.002243
t_T (hrs)	0.5637	1.2572	4.4684	41.745	438.50

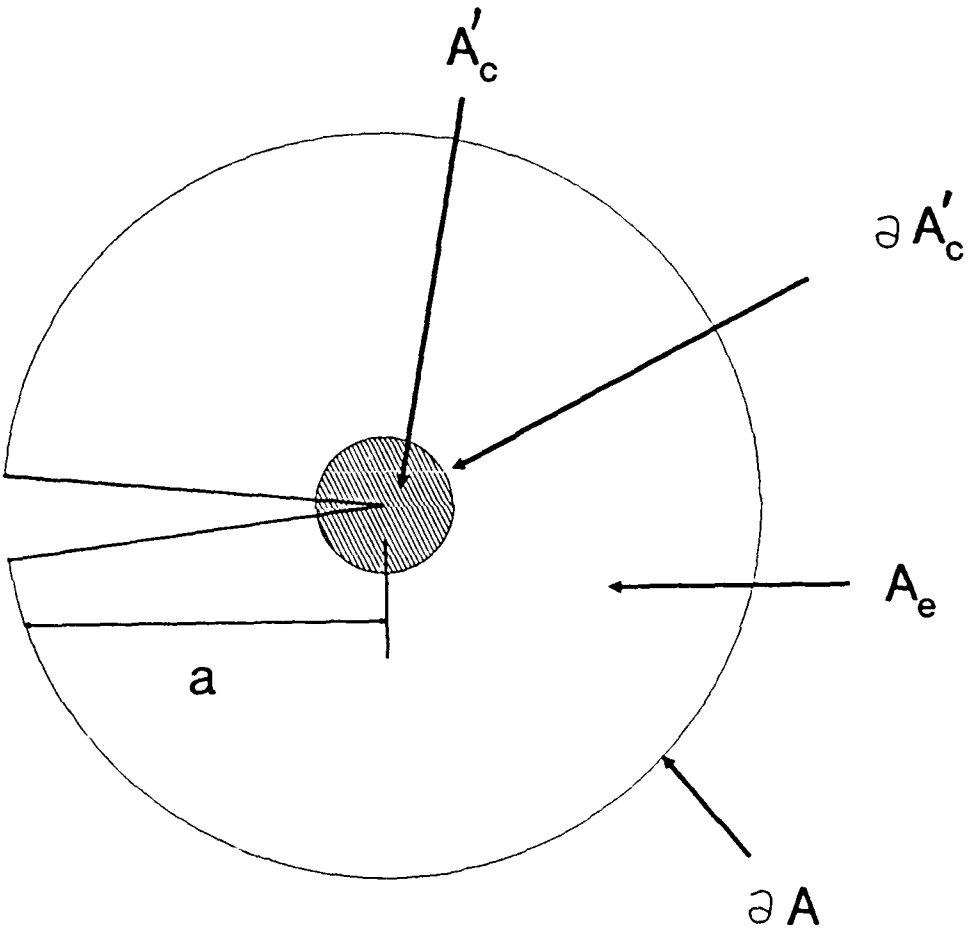

Figure 4-1. Schematic of Small Scale Creep

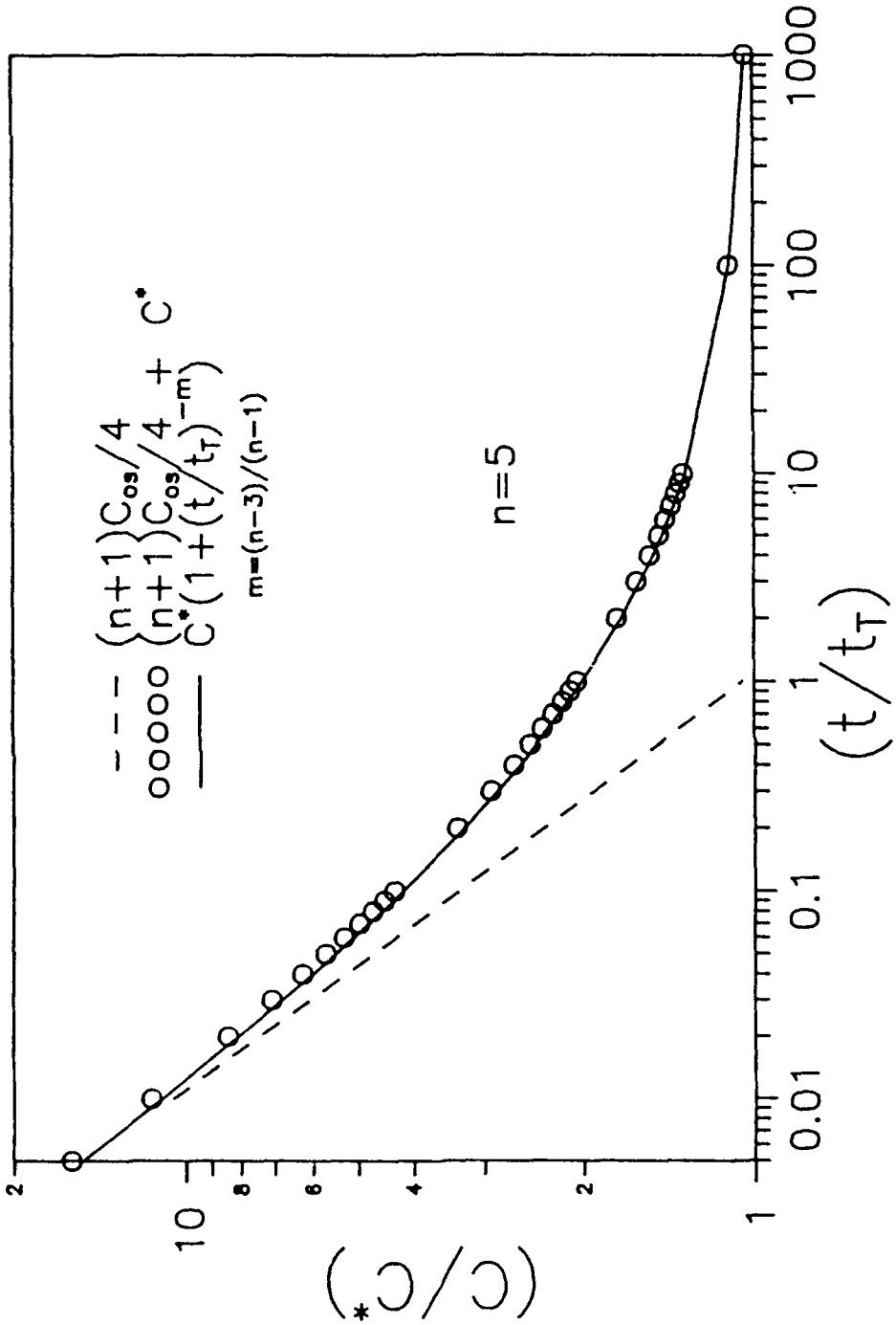

Figure 4-2. Comparison of C_0 and C_t for n=5

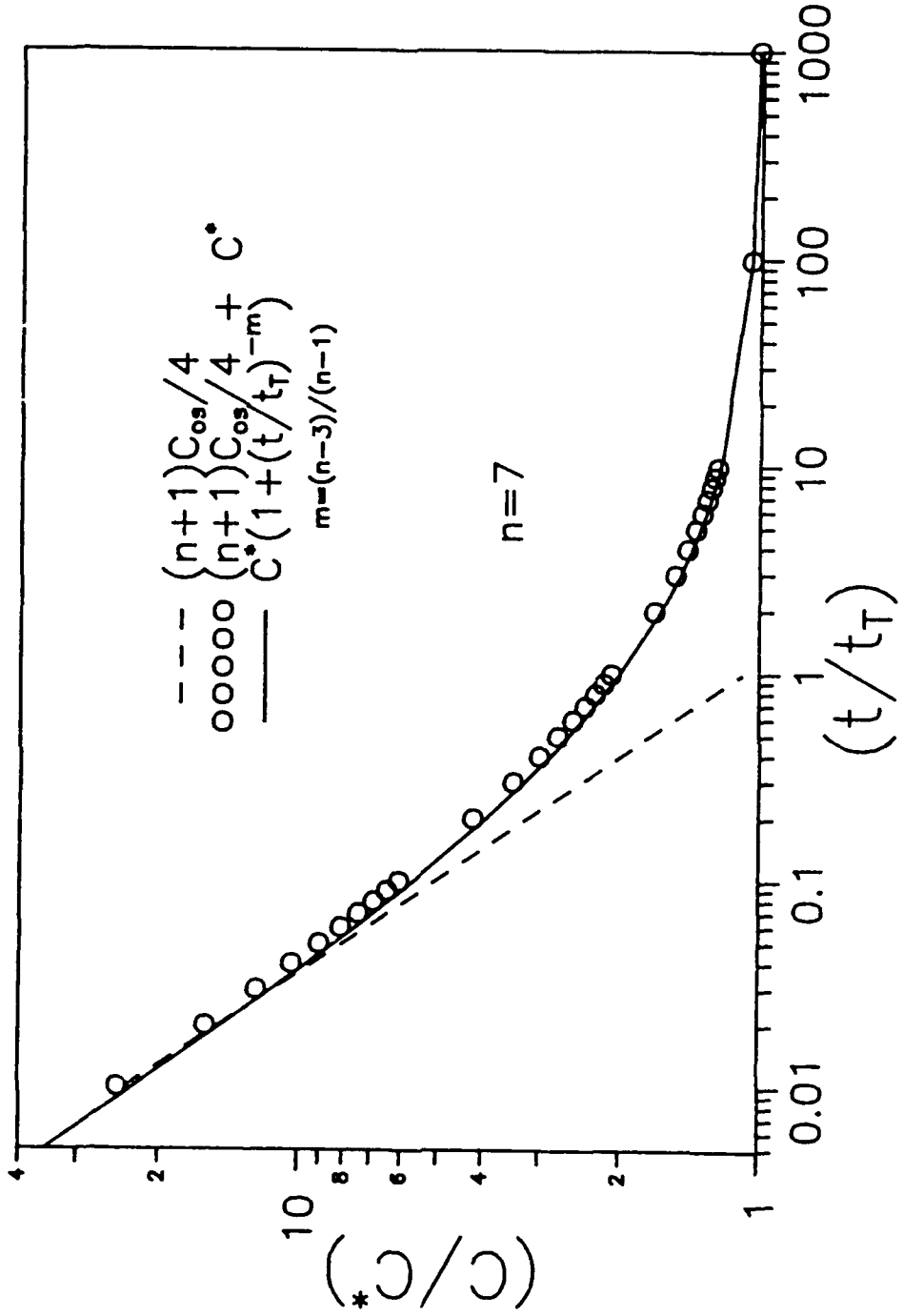

Figure 4-3. Comparison of C_0 and C_t for n=7

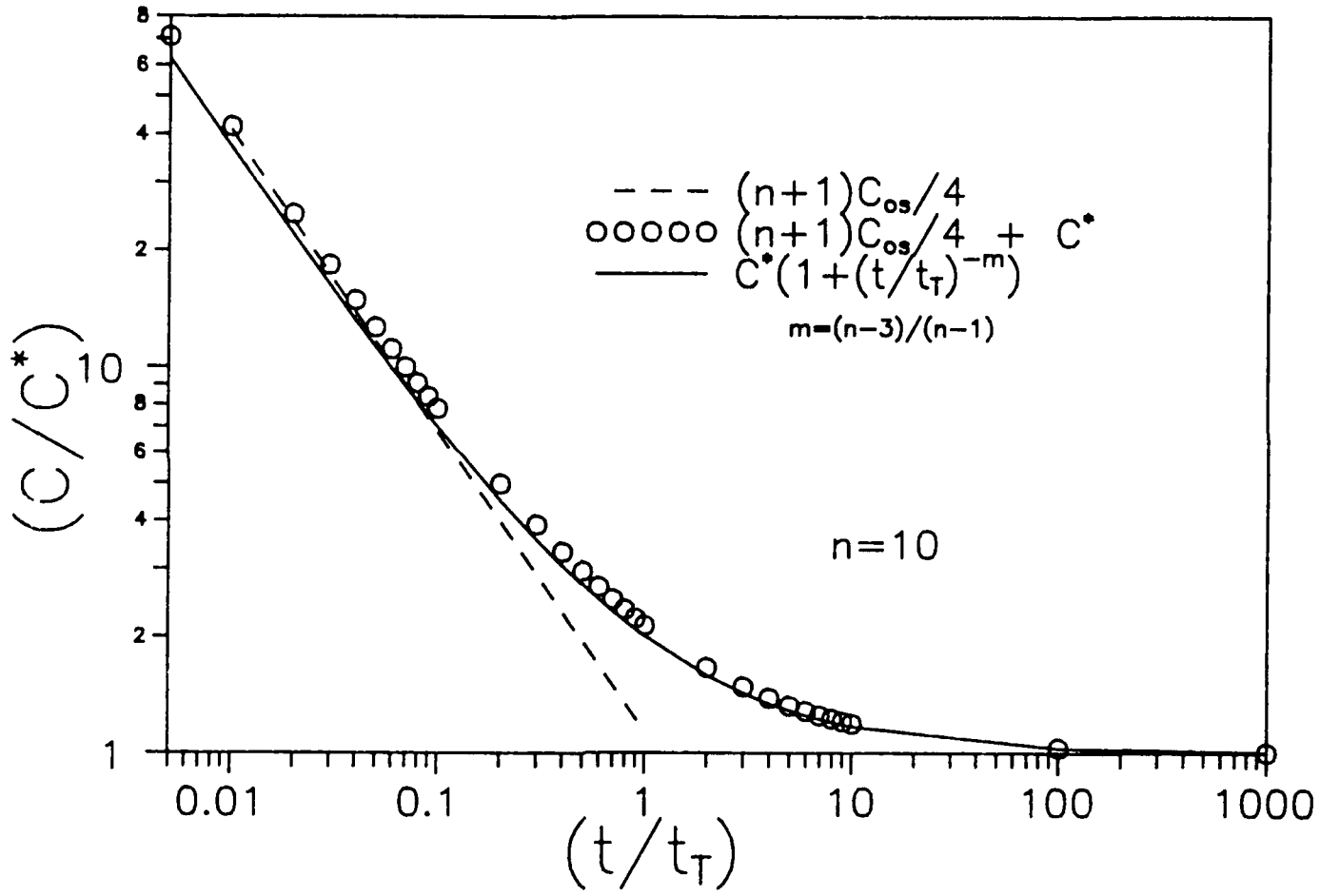

Figure 4-4. Comparison of C_o and C_t for n=10

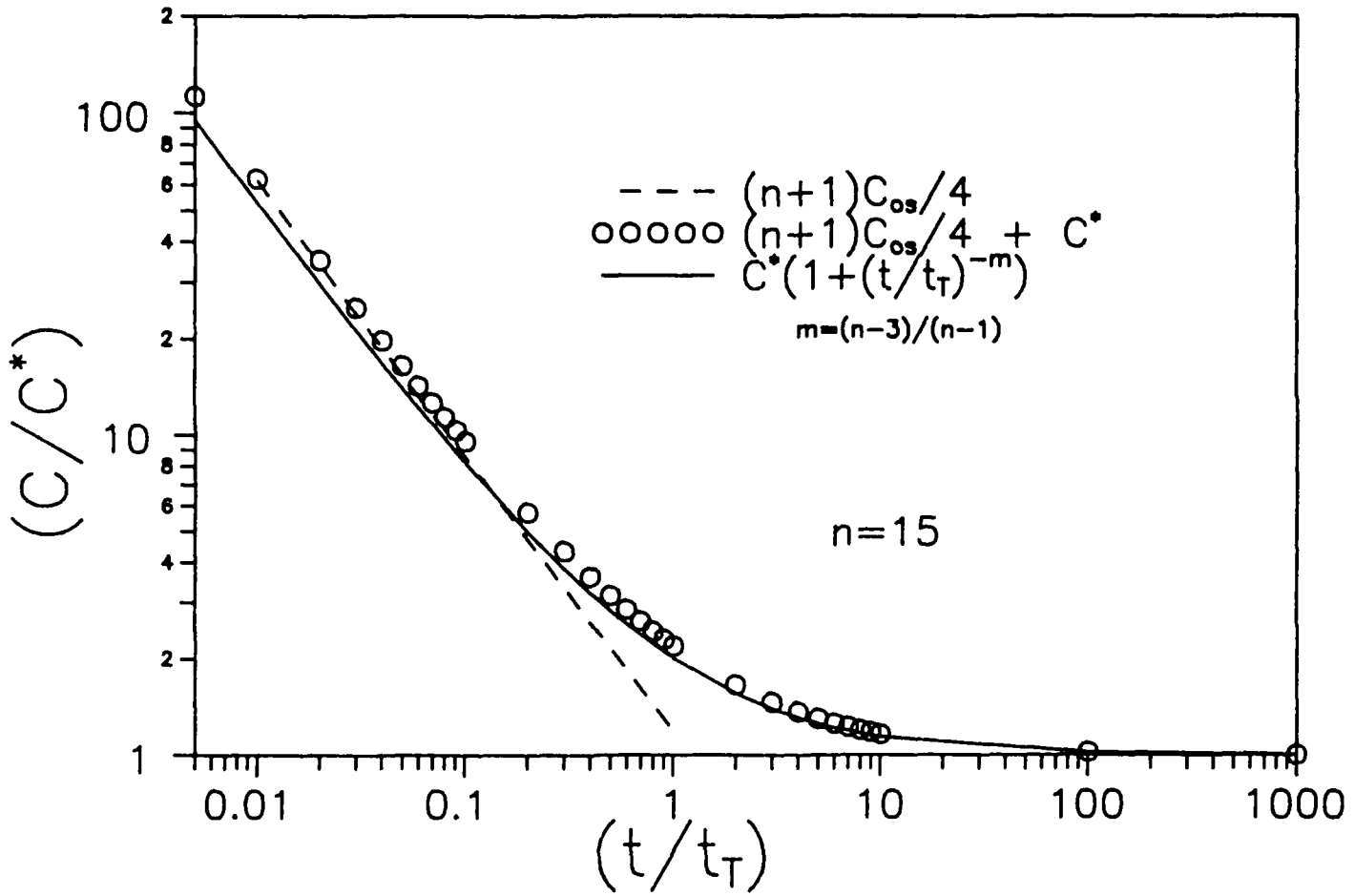

Figure 4-5. Comparison of C_o and C_t for n=15

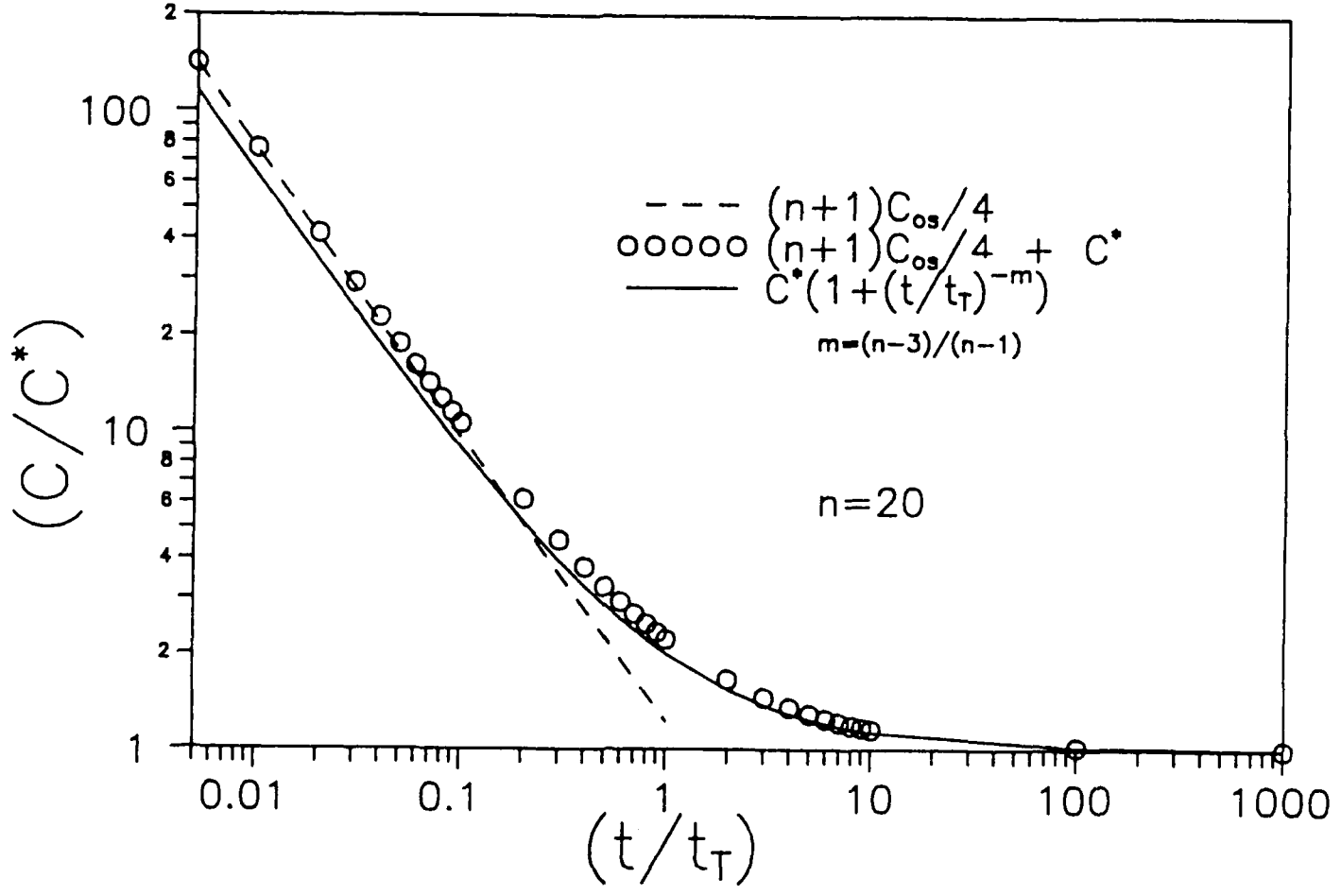

Figure 4-6. Comparison of C_o and C_t for n=20

5.0 CONCLUSION AND RECOMMENDATIONS

An extensive literature survey for creep crack growth data for titanium alloys in the high temperature environments has been conducted in this Phase I study. Creep crack growth data is found to be scarce if not non-existent in the open literature. The limited amount of data obtained in this study on Ti-24Al-11Nb alloys is expressed in terms of stress intensity factor K, which may not be an adequate parameter to characterize crack growth in the creep region. Among K, C^*, C(t), and C_t, an evaluation was then conducted in this Phase I research to see which of the four parameters is best suited for characterizing creep crack growth of titanium alloys. It is concluded, after the evaluation, that C_t may be the most promising candidate for describing creep crack growth of titanium alloys in the high temperature region. C_t can be easily measured in a test through its load line deflection history and has been found to correlate well with crack growth test data for steels in the high temperature environments. To be able to fully utilize C_t for the life prediction of a titanium alloy structure, it is important that C_t should also be computed easily and accurately for geometries and loading conditions other than those of laboratory tests. As a first step of achieving this, the definition of C_t was reexamined and another parameter $C_o(t)$ was proposed in this report. The new parameter, $C_o(t)$, can be calculated by integrating either along the outer boundary and over the entire area of the structure or along the boundary of the creep dominant zone. C_o is found to be proportional to the growth rate of the creep dominant zone at the crack tip region. C_t and C_o are closely related under constant load condition. They both approach C^* at steady-state creep. Under small scale creep conditions, they are proportional to each other, with a proportionality constant $[(n+1)/4]$. It is also found that $[(n+1)C_{os}(t)/4+C^*]$ behaves almost exactly like C_t over the entire time spectrum. However, $C_o(t)$ can be calculated for both constant and variable load conditions. Therefore, $C_o(t)$ can be

viewed as an alternative form of C_t but is easier to compute under the more general loading conditions.

It is apparent that more studies, both analytical,numerical, and experimental, are needed to fully understand creep crack growth of titanium aluminides in the high temperature environments. To name a few, it is recommended that the following studies be performed:

(a) Extensive laboratory tests should be conducted to understand the creep crack growth behavior of titanium alloys. More specifically, it is necessary to evaluate C_t as the controlling parameter for creep crack growth, to find the application range for K and C_t, to study the effects of hold time on crack growth, to obtain data on overload effects, to monitor creep zone growth, to study size effects and to have test data on both slow and fast propagating cracks.

(b) Analytically, there is a need to study the limitations on $C_o(t)$, to explore the theoretical ground of crack growth retardation and crack growth through the use of micro-mechanics models, to find a parameter for running cracks (cracks propagating in a higher speed), and to develop a way of characterizing crack growth in a temperature range where both LEFM and TDFM are important.

(c) Numerically, it is necessary to verify the concept of $C_o(t)$ proposed in this report, to study the effect of running crack, to establish a systematic way of calculating C_o and/or C_t for use in actual structural life prediction, to build a solution base (or handbook) for C_o for the geometries and loading conditions encountered the most by the Air Force, and to develop a crack growth software package such that it can cover both LEFM, TDFM, and transition between LEFM and TDFM.

6.0 REFERENCES

1. Walker, K., "The Effects of Stress Ratio During Crack propagation and Fatigue for 2024-T3 and 7075-T6 Aluminum," Effects of Environment and Complex Load History on Fatigue Life, ASTM STP 462, 1978, pp. 1-14.

2. "Fracture Mechanics Properties of Materials Used in Space Shuttle Orbiting Structures," Report SOD79-0219, Rockwell Internal, Shuttle Orbiting Division, Space System Group, Sept. 1979.

3. Yuen, A., Hopkins, S. W., Leverant, G. R., and Rau, C. A., "Correlation Between Fracture Surface Appearance and Fracture Mechanics Parameters for Stage II Fatigue Crack Propagation in Ti-6Al-4V," Metallurgical Transactions, Vol. 5, 1974, pp. 1833-1842.

4. Forman, R. G., and Hu, T., "Application of Fracture Mechanics on Space Shuttle," Damage Tolerance of Metallic Structures, ASTM STP 847, 1984, pp. 108-133.

5. Forman, R. G., et al, "Fatigue Crack Growth Computer Program -- NASA/FLAGRO," Lyndon B. Johnson Space Center JSC-22267, 1986.

6. Effects of Load Spectrum Variables on Fatigue Crack Initiation and Propagation, ASTM STP 714, 1980.

7. Wheeler, O.E., "Spectrum Loading and Crack Growth," Journal of Basic Engineering, Vol. 94, 1972, pp. 181-186.

8. Willenborg, J. D., Engle, R. M., and Wood, H. A., "A Crack Growth Retardation Model Using an Effective Stress Concept," USAF Report AFFDL-TM-71-1, Feb. 1971.

9. Saxena, A., "A Creep Crack Growth Under Non-Steady State Conditions," ASTM STP 905, 1986.

10. Khobaib, M., "An Investigation of Creep Behavior of Ti-24Al-11Nb Alloy," Presented at the 1988 Annual TMS Meeting, 25-29 September 1988, Chicago, IL.

11. Balsone, S.J., "The Effect of Elevated Temperature on the Tensile and Creep Properties of Ti-24Al-11Nb," Presented at the 1988 Titanium Aluminides Meeting, 1-3 November 1988, Stratford, CT.

12. Khobaib, M., "Creep Crack Growth Behavior of Ti-24Al-11Nb," Presented at the 1989 Annual TMS Meeting 2-5 October 1989, Indianapolis, IN.

13. Staubs, E. A., "Investigation of Crack Growth in Titanium Aluminide at Elevated Temperatures" Masters Thesis, Air Force Institute of Technology, Wright-Patterson AFB, OH.

14. Bania, P.J., "An Advanced Alloy for Elevated Temperatures", Journal of Metals, March 1988.

15. Marissen, R., Peters, M., Schulte, K., Trautmann, K. H., Mull, K., "Fatigue Properties of High Strength Titanium Alloys at Elevated Temperatures (IMI 685)", Deushe Forschurgs Versuchsanstalt Luft Raunfahr (FRG) Report No.: TB:B870-80743GAR.

16. Fujishiro, S., Matsumoto, T., "Studies on Crack Growth Rate of High Temperature Titanium Alloys," Conference: Titanium--Science and Technology, Vol. 4, Munich, FRG, 10-14 September 1984.

17. Allison, J.E., Williams, J.C., "Near-Threshold Fatigue Crack Growth Phenomena at Elevated Temperature in Titanium Alloys", Scripta Met, Vol. 19, 1985.

18. Specht, Jurgen, MTU Motoren-und Turbinen-Union Munchen GmbH. Munich, F.R.G., "Crack Propagation Behaviour of Titanium Alloys for Compressor Disks," Sixth World Conference on Titanium, France, 1988.

19. Matsumoto, T., "Studies on Fatigue on IMI 829 and Other High Temperature Ti Alloys", Conference: Titanium-Science & Technology, Vol. 4, Munich, FRG, 10-14, Sept. 1984.

20. Ruppen, J.A., McEvily, A.J., "Effect of Elevated Temperature and Environment on the Fatigue Crack Growth Characteristics of Ti-6A1-2Sn-4Zr-2Mo-0. 1Si." Univ. of conn, Storrs, Source: Fatigue of Engineering Materials and Structures v 2 n 1 1979, Pap Presented at ICM3 Ext Semin, Pt 3, Mater Behav., Univ. of Sheffield, England, August 27-29, 1979, p. 63-72.

21. Beevers, C. J., Irving, P.E., "Fatigue Crack Growth Behavior of Ti-6A1-4V in Air and vacuum at Room and Elevated Temperatures," Source: Tewksbury Symp. on Fract., 3rd., University of Melbourne, Aus. June 4-6, 1974 p. 179-193. Available from University of Melbourne, Fac. of Eng., Aust., 1974.

22. Smith, H. H., Kullen, P.S., Michel, D. J., "Fatigue Crack Propagation Behavior of titanium Alloys 642S and 5621S at Elevated Temperature," Author Affiliation: Naval Research Laboratory, Carnegie-Mellon University Metall. Trans. A 19A, (4), 881-885 Apr. 1988 ISSN: 0360-2133.

23. Chesnutt, J.C., Paton, N.E., "Hold Time Effects on Fatigue Crack Propagation in Ti-6Al and Ti-6Al-4V," Conference Title: Titanium '80, Science and Technology, Proceedings of the 4th International Conference on Titanium.

24. Neal, D.F., "Creep Fatigue Interactions in Titanium Alloys," Sixth World Conference on Titanium, France, 1988.

25. Song, Z., Hoeppner, D.W., "Dwell Time Effects on Material Fatigue Behavior-Titanium Alloys" Conference: Titanium-Science & Technology, Vol. 4, Munich, FRG 10-14, Sept. 1984.

26. Evans, W.J., Gostelow, C.R., "The Effect of Hold Time on the Fatigue Properties of a .Beta.-Processed Titanium Alloy," Location: Natl. Gas Turbine Establ., Pyestock/Farnborough/-Hants., Engl., Journal: Metall. Trans., A, 1979, Vol. 10A, No. 12, Pages 1837-46, Coden: MTTABN ISSN: 0360-2133, English.

27. Balsone, S.J., Khobaib, M., Maxwell, D.C., and Nicholas, T., "Frequency, Temperature and Environmental Effects on Fatigue Crack Growth in Ti_3Al" to be presented at the Fourth International Conference On Fatigue and Fatigue Thresholds in the Pacific Basin, to be held in Honolulu, Hawaii, July, 1990.

28. Shahinian, P., Sadananda, K., "Effects of Stress Ratio and Holt-Time on Fatigue Crack Growth in Alloy 718", Naval Research Lab., Washington, DC, Corp. Source Codes: 000927000;251950, Pub. in Journal of Engineering Materials and Technology, V101 p. 224-230 July 1979 (No copies furnished by DTIC/NTIS).

29. Lee, E. W., Chakrabortty, S.B., and Starke, Jr., E.A., "The Effect of Overload on the Fatigue Crack Propagation in Metastable Beta Ti-V Alloys", Met Trans, Vol. 15A, 1984.

30. Ral'tsevich, N.V., "Effect of cyclic Overloading on the Fatigue Strength of Two Types of Steel and a Titanium Alloy", Leningr. Korablestroit. Inst., Leningrad, USSR, Tr. Leningrad. Korablestroit. Inst., 1971, Vol. 75, Pages 113-21, Coden: TLKIAM, Russian.

31. Jones, R.E., "Fatigue Crack Growth Retardation After Single-Cycle Peak Overload in Titanium-6 Aluminum-4% Vanadium alloy", Res. Inst., Univ. Dayton, Dayton, Ohio, Eng. Fract. Mech., 1973, vol. 5, No. 3, Pages 585-604, Coden: EFMEAH, English.

32. Dubensky, R., "Overload Induced Delays in Fatigue Crack Growth in Titanium-6 Aluminum-4 Vanadium alloy", Ford Mot. Co., Dearborn, MI, Mech. Behav. Mater., Proc. Symp., 1974, Pages 195-201, Coden: 28VNAS, English, Meeting Date: 73, Soc. Mater. Sci., Kyoto, Japan.

33. Gray, T.D., Gallagher, J.P., "Predicting Fatigue Crack Retardation Following a Single Overload Using a Modified Wheeler Model", Mechanics of Crack Growth,ASTM STP-590, Philadelphia, PA, 1976, 331-334.

34. Dubensky, R.G., Morman Jr., K.N., "Predicting Fatigue Crack Retardation Under Single and Intermittent Overloading", Cracks and Fracture ASTM STP No. 601, Philadelphia, PA, 1976, 235-261.

35. Gemma, A.E., Allison, D.E., Hopkins, S. W., "New Approach to Estimate Fatigue Crack Delay Due to a Single Cycle Overload", Eng. Fract. Mech. 1977, 9, (3), 647-654.

36. Lee, E.W., Chakrabortty, S.B., "The Effect of Overload on Fatigue Crack propagation in Metastable. Beta.-Titanium-Vanadium Alloys", Fracture Fatigue Res. Lab., Georgia Inst. Technol., Atlanta, GA, USA, 1980, No. GIT-TR-80-1, Order No. AD-A093159, Pages 33, pp. Coden: D8REP4, English, Gov. Rep. Announce. Index (U.S.) 1981, 81(9), 1850 Avai: NTIS.

37. Mingda, G., Yongkui, Z. and Minggao, Y., "Evaluation of Overload Models on the Retardation Behavior in a Ti-6Al-4V Alloy," Inst. of Aeronaut Mater, Beijing, China, Fatigue of Engineering Materials and Structures v 5 n 2 1982 p. 167-176.

38. Ouyang, J., Yan, M. and Song, D., "Effect of Overload Ratios on Fatigue Crack Growth Behavior in Ti-6Al-4V Alloy", Institute of Aeronautical Materials, Beijing (China), Report No. ISTIC-TR-C-000048.

39. Jie, O.k Deyu, S. and Minggao, Y., "Effect of the Overload Ratio on Fatigue Growth Behavior in Ti-6Al-4V", Foreign Technology Div., Wright-Patterson AFB, OH, Report No. FTD-ID(RS)T-1578-83.

40. Ward-Close, C.M., Ritchie, R.O., "On the Role of Crack Closure Mechanisms in Influencing Fatigue Crack Growth Following Tensile Overloads in a Titanium Alloy: Near Threshold vs. Higher Delta K Behavior", ASTM STP-982, 1988.

41. Prokopenko, A.V., Ezhov, V.N., "Effect of Overloads on the Growth of Fatigue Cracks in Materials for Gas Turbine Blades. (Translation)", Strength Mater. (USSR) 20, (4), 471-476, April 1988 ISSN: 0039-2316.

42. Matejczyk, D.E., Jewett, R.P., Schmidt, D.W. and Hresko, G.C., "Fatigue Crack Retardation Following Overloads in Inconel 718, Ti-5Al-2.5Sn, and Haynes 188", Rockwell International, Canoga Park, CA Rocketdyne Div., Corp. Source Codes: 054566004; RY230510, In NASA, Marshall Space Flight Center, Advanced Earth-to-Orbit Propulsion Technology 1986, Vol. 2, p. 205-219.

43. Prokopenko, A.V., Exhov, V.N., "Effect of Overloads on the Growth of Fatigue Cracks in the Materials of Gas Turbine Blades", Probl. Prochn. (4), 47-52 April 1988 ISSN: 0556-171X.

44. Kobayashi, H., Nakamura, H., Hirano, A. and Nakazawa, H., "A Fraactographic Approach to the Influence of a Single-Peak Overload on Fatigue Crack Growth", Materials, Experimentation and Design in Fatigue, Warwick, University, England, 24-27 March 1981.

45. Boitcov, B.V., Petuhov, J.V., "Crack Growth Under Single and Multiple Overloads in Steel, Aluminum and Titanium Alloys", Proceedings of the 9th Congress on Material Testing, Budapest, Hung, 1986 Sept. 29 - Oct. 31.

46. Hopkins, S.W., Rau, C.A., Leverant, G.R. and Yuen, A., "Effect of Various Programmed Overloads on the Threshold for High-Frequency Fatigue Crack Growth", Fatigue Crack Growth Under Spectrum Loads, ASTM STP-595, Philadelphia, PA 1976, 125-141.

47. Ghonem, H., "Study of Probabilistic Fatigue Crack Growth and Associated Scatter Under Constant-and-Variable Amplitude Loading Spectrum", Annual Rept. 15 Jul 86-15 Jul 87, Rhode Island Univ., Kingston. Dept. of Mechanical Engineering and Applied Mechanics.

48. Mingda, G., Yongkui, Z., Minggao, Y., "Evaluation of Overload Retardation Behavior and Overload Retardation Models of Ti-6Al-4V Sheet Titanium Alloy", Foreign Technology Div., Wright-Patterson AFB, OH, Report No. FTD-ID(RS)T-1577-83.

49. Lie, O., Yan, M., Song, D., "Effect of Overload Ratios on Fatigue Crack Growth Behavior in Ti-6Al-4V Alloy (Retroactive Coverage)", ICF International Symposium on Fracture Mechanics--Proceedings, Beijing, China, 22-25 Nov. 1983.

50. Larsen, J.M., Williams, K.A., Balsone, S.J. and Stucke, M.A., "Titanium Aluminides for Aerospace Applications", 1989 TMS Fall Meeting, Oct. 1-5, 1989, to be published in High Temperature Aluminides and Intermetallics, C.T. Liu, et al editors.

51. Saxena, A., in Fracture Mechanics: Microstructure and Micromechanisms, S.V. Nair, et al editors, ASM International, 1989, pp. 283-334.

52. Riedel, H. and Detampel, V., International Journal of Fracture, Vol. 33, 1987, pp. 239-262.

53. Landes, J.D., and Begley, J.A., in Mechanics of Crack Growth, ASTM STP 590, ASTM, Philadelphia, 1976, pp. 128-145.

54. Nikbin, K.M., Webster, G.A., and Turner, C.E., in Cracks and Fracture, ASTM STP 601, ASTM ,Philadelphia, PA, 1976, pp. 47-62.

55. Saxena, A., in Fracture Mechanics: Twelfth Conference, ASTM STP 700, ASTM, Philadelphia, PA, 1980, pp. 131-151.

56. Bassani, J.L., and McClintock, F.A., International Journal of Solids and Structures, Vol. 7 ,1981, pp. 479-492.

57. Saxena, A., in Fracture Mechanics, STM STP 905, Vol. I, ASTM, Philadelphia, PA, 1986, pp. 185-201.

58. Riedel, H., and Rice, J.R., in Fracture Mechanics: Twelfth Conference, ASTM STP 700, ASTM, Philadelphia, PA, 1980, pp. 112-130.

59. Hutchinson, J. W., Journal of Mechanics and Physics of Solids, Vol. 16, 1968, pp. 13-31.

60. Rice, J.R., and Rosengren, G.F., Journal of Mechanics and Physics of Solids, Vol. 16, 1968, pp. 1-12.

61. Ehlers, R., and Riedel, H., in Advances in Fracture Research, Vol. 12, ICF-5, D. Francois, et al editors, Pergamon Press, 1981, pp. 691-698.

62. Ohji, K., Ogura, K., and Kubo, S., Japanese Society of Mechanical Eng. (Trasactions), 1979, 790-13, pp. 18-20 (in Japanese).

63. Bassani, J.L., Hawk, D.E., and Saxena, A., in Nonlinear Fracture Mechanics: Vol. I - Time Dependent Fracture, ASTM STP 995, ASTM Philadelphia, 1989, pp. 7-26.

64. Saxena, A., Han, J., and Banerji, K., Journal of Pressure Vessel Technology, Vol. 110, 1988, pp. 137-146.

65. Staley, Jr., J.T., and Saxena, A., "Mechanisms of Creep Crack Growth in 1%Sb-Cu" (in press) Acta Metallurgical, 1990.

66. Hui, C.Y., and Riedel, H., International Journal of Fracture, 1981, pp. 409-425.

67. Riedel, H., and Wagner, W., in Advances in Fracture Research, ICF-5, Pergamon Press, 1982, pp. 683-690.

68. Saxena, A., Shih, T.T., and Ernst, H. A., "Fracture Mechanics: Fifteenth Symposium, ASTM STP 833, ASTM Philadelphia, 1984, pp. 516-531.

69. Saxena, A., and Landes, J.D., in Advances in Fracture Research, ICF 6, S.R. Valluri, et al editors, Pergamon Press, 1985, pp. 3977-3988.

70. Saxena, A., Ernst, H.A., and Landes, J.D., International Journal of Fracture, Vol. 23, 1983, pp. 245-257.

71. Khobaib, M., Private Communication, 1990.

72. Saxena, A., and Liaw, P.K., "Remaining Life Estimation of Boiler Pressure Parts - Crack Growth Studies, Electric Power Research Institute, EPRI CS-4688, July, 1986, Palo Alto, CA.

73. Kumar, V., German, M.D., and Shih, C.F., An Engineering Approach to Elastic-Plastic Fracture Analysis, EPRI NP1931, Electric Power Research Institute, Palo Alto, CA, July, 1981.

74. Srawley, J.E., International Journal of Fracture, Vol. 12, June 1976, pp. 475-476.

75. Saxena, A., and Giescke, B., in High Temperature Fracture Mechanisms and Mechanics EGF6, P. Bensussan editor, Mechanical Engineering Publications, London, 1990 (in press).

76. Riedel, H., in Elastic-Plastic Fracture, Second Symposium, Vol. I, ASTM STP 803, ASTM, Philadelphia, PA 1983, pp. I-505-521.

77. Rice, J.R., "Mathematical Analysis in the Mechanics of Fracture," Chapter 3 in Fracture - Advance Treatise, Vol. II, ed. H. Liebowitz, Academic Press, New York, 1968.

78. Leung, C., McDowell, D. L., and Saxena, A, in Nonlinear Fracture Mechanics: Vol. I - Time Dependent Fracture, ASTM STP 995, ASTM Philadelphia, 1989, pp. 55-67.

79. Shih, C. F.,"Tables of Hutchinson-Rice-Rosengren Singular Field Quantities," Division of Engineering, Brown University Report, Providence, Rhode Island, 1983.

80. Symington, M, Shih,C. F., and Ortiz, M., "Tables of Plane Strain Mixed-Mode Plastic Crack Tip Fields," Brown University Report, Providence, Rhode Island, 1988.

81. Riedel, H., "Mechanics and Micromechanism of Creep Crack Growth," Proc. Advanced Seminar on Fracture Mechanics, Ispra, Italy, Oct. 1981, Applied Science Publisher, 1983.

APPENDIX A

Listing of the Computer Code

```
100 KEY OFF
110 REM this program is stored under the name udri.bas
111 CLS
115 LOCATE 5,10: INPUT "MATERIAL TYPE";M$
116 LOCATE 7,10: INPUT "SPECIMEN ID";X$
117 LOCATE 9,10: INPUT "TEST TEMPERATURE (C)";TP
120 CLS
130 INPUT "Do you want to use previously stored spec. size & material data";Y$
140 IF Y$ = "Y" GOTO 150 ELSE 200
150 OPEN "FCT" FOR INPUT AS #1
160 INPUT #1, YS,N,AA,E,BN,B,W,P
170 CLOSE #1
180 GOTO 310
200 CLS
210 LOCATE 2,10: INPUT"Yield Strength (ksi)";YS
220 LOCATE 4,10: INPUT "creep Exponent (n)";N
230 LOCATE 6,10: INPUT "Creep Coeff. (ksi^-n.hr^-1)";AA
240 LOCATE 8,10: INPUT "Elastic Modulus (ksi)";E
250 LOCATE 10,10: INPUT "Nominal Thickness (in)";BN
260 LOCATE 12,10: INPUT "Crack Plane Thickness (in)";B
270 LOCATE 14,10: INPUT "Specimen Width (in)";W
280 LOCATE 16,10: INPUT "Test Load (kips)";P
290 LOCATE 20,10: INPUT "DO YOU WANT TO EDIT THE DATA (Y/N)";Y$
300 IF Y$ = "Y" GOTO 200 ELSE 301
301 OPEN "FCT" FOR OUTPUT AS #1
302 WRITE #1, YS,N,AA,E,BN,B,W,P
303 CLOSE #1
310 CLS
320 DIM AB(50), T(50), DADT(50), CT(50), CSTAR(50), K(50),TT(50),V(50),VC(50)
321 LOCATE 5,10:INPUT "DO YOU WANT TO USE CRACK GROWTH DATA FROM FILE(Y/N)";Y$
322 IF Y$ = "Y" GOTO 323 ELSE 338
323 LOCATE 10,10:INPUT "FILE NAME";F$
330 OPEN F$ FOR INPUT AS #1
331 INPUT #1, NN
332 FOR I = 1 TO NN
333 INPUT #1, AB(I), T(I), DADT(I)
334  NEXT I
335 CLOSE #1
336 GOTO 410
338 CLS
339 LOCATE 5,10: INPUT "NUMBER OF DATA POINTS";NN
340 CLS
350 FOR I = 1 TO NN
355 LOCATE 3,10: PRINT "DATA SET NO. ";I
360 LOCATE 5,10: INPUT "CRACK SIZE(IN)";AB(I)
370 LOCATE 7,10: INPUT "TIME (HRS)";T(I)
380 LOCATE 9,10: INPUT "CRACK GROWTH RATE (IN/HR)";DADT(I)
390 CLS
400 NEXT I
410 CLS
420 PRINT "DATA SET #","  CRACK SIZE","  TIME","     DADT"
430 FOR I = 1 TO NN
440 PRINT USING "      ##.";I;
450 PRINT USING "          #.###  ";AB(I);
460 PRINT USING "   #####.##  ";T(I);
470 PRINT USING "          #.######";DADT(I)
480 NEXT I
490 LOCATE 20,10: INPUT "DO YOU WANT TO EDIT ANY OF THE DATA (Y/N)";Y$
500 IF Y$ = "Y" GOTO 510 ELSE 600
510 CLS
```

```
520 LOCATE 10,10: INPUT "WHICH POINT DO YOU WANT TO EDIT";II
530 LOCATE 12,10: INPUT "NEW CRACK SIZE";AB(II)
540 LOCATE 14,10: INPUT "NEW TIME";T(II)
550 LOCATE 16,10: INPUT "NEW DADT";DADT(II)
560 LOCATE 20,3: INPUT "NEXT DATA POINT TO BE EDITED (HIT ENTER IF EDITING COMPL
ETE)";II
570 IF II > 0 GOTO 580 ELSE 410
580 CLS
590 GOTO 530
600 CLS
610 LOCATE 10,10:INPUT "DO YOU WANT TO STORE THE DATA IN A FILE(Y/N)";Y$
620 IF Y$ = "Y" GOTO 630 ELSE 1000
630 LOCATE 12,10: INPUT "WHAT DO YOU WANT TO CALL THIS DATA FILE";F$
640 CLS
650 OPEN F$ FOR OUTPUT AS #1
655 WRITE #1, NN
660 FOR I = 1 TO NN
670 WRITE #1, AB(I), T(I), DADT(I)
680 NEXT I
690 CLOSE #1
1000 CLS
1010 REM BEGIN CALCULATIONS
1020 PI = 3.141592
1030 ALPHA2 = (.5/PI)*((N+1)^2/(2*N*.69))^(2/(N-1))
1035 AA = AA*YS^N
1040 REM SUBROUTINE FOR CALCULATING H1 VALUES
1050 GOSUB 4000
1060 FOR I = 1 TO NN
1070 AOW = AB(I)/W
1080 F = .866+4.64*AOW-13.32*AOW^2+14.72*AOW^3-5.6*AOW^4
1090 KOP = ((2+AOW)/((1-AOW)^1.5))*F/(B*W^.5)
1100 K(I) = KOP*P
1110 REM SUBROUTINE FOR INTERPOLATING H1 VALUES
1115 GOSUB 4200
1120 ALPHA1 = 2*AOW/(1-AOW)
1130 ALPHA = (ALPHA1^2 + 2*ALPHA1 +2)^.5 -ALPHA1 - 1
1140 CSTAR(I) = ((AA*H1*YS*W)/(1-AOW)^N)*(P/(YS*1.455*B*W*ALPHA))^(N+1)
1150 TT(I) = ((K(I))^2*.91)/((CSTAR(I))*(N+1)*E)
1160 RDOTC1 = ((2*ALPHA2)/(N-1))*.4*((K(I))^2)*((E*(AA/YS^N))^(2/(N-1)))
1170 RDOTC = RDOTC1*(T(I))^(-(N-3)/(N-1))
1180 FP = 4.64-26.64*AOW+44.16*AOW^2-22.4*AOW^3
1190 DFF = (1.5/(1-AOW) + 1/(2+AOW)) + FP/F
1200 CT = 2*.91*(((K(I))^2)/(W*E))*DFF*.33*RDOTC
1210 CT(I) = CT + CSTAR(I)
1220 VDOTE = ((2*(K(I))^2)/E)*DADT(I)*B/P
1230 GAMMA=2+.9717*AOW-.9756*AOW^2-.6371*AOW^3+.6352*AOW^4
1240 BETA = .2932-.7261*AOW+.4889*AOW^2+.369*AOW^3-.09324*AOW^4
1250 ETA = (1/(1-AOW))*(N/(N+1))*(GAMMA-BETA/N)
1260 VDOTSS = (CSTAR(I))*B*W/(P*ETA)
1270 VDOTSSC = (2*.91*B)/(E*P)*((K(I))^2)*.33*RDOTC
1280 VC(I) = VDOTSSC + VDOTSS
1290 V(I) = VC(I) + VDOTE
1300 NEXT I
1310 GOTO 5000
4000 REM SUBROUTINE TO CALCULATE H1 VALUES
4010 H250 = 2.58064-.3554543*N+3.498268E-02*N^2-1.574719E-03*N^3+2.938609E-05*N^
4
4020 H375 =2.633137-.5510955*N+5.561465E-02*N^2-2.754816E-03*N^3+5.176354E-05*N^
4
4030 H500 =2.355219-.5008945*N+5.437075E-02*N^2-2.870103E-03*N^3+5.632168E-05*N^
```

```
4
4040 H625 =2.089532-.3824516*N+4.028168E-02*N^2-2.102551E-03*N^3+4.072901E-05*N^
4
4050 H750 =1.993401-.3399606*N+.0384689*N^2-2.162229E-03*N^3+4.41436E-05*N^4
4060 H100 =1.677875-.1254355*N+6.621381E-03*N^2-1.493825E-04*N^3
4070 RETURN
4200 REM SUBROUTINE TO INTERPOLATE HI VALUES
4210 IF AOW < .375 GOTO 4220 ELSE 4240
4220 H1 = H250 + ((H375 -H250)/(.125))*(AOW-.25)
4230 RETURN
4240 IF AOW < .5 GOTO 4250 ELSE 4270
4250 H1 = H375 + ((H500 - H375)/(.125))*(AOW-.375)
4260 RETURN
4270 IF AOW < .625 GOTO 4280 ELSE 4300
4280 H1 = H500 +((H625 -H500)/(.125))*(AOW -.5)
4290 RETURN
4300 IF AOW <.75 GOTO 4310 ELSE 4330
4310 H1 = H625 + ((H750-H625)/(.125))*(AOW - .625)
4320 RETURN
4330 H1 = H750 + ((H100-H750)/(.125))*(AOW-.75)
4340 RETURN
5000 REM OUTPUT CODE
5010 CLS
5020 PRINT "CRACK SIZE","TIME","da/dt",;
5021 PRINT "Ct";
5022 PRINT "            K"
5030 PRINT "   in   ","hr","in/hr";
5031 PRINT "  in.lbs./in^2.hr";
5032 PRINT "   ksi.in^.5"
5040 PRINT
5050  FOR I = 1 TO NN
5060 PRINT USING "  #.###";AB(I);
5070 PRINT USING "    #####.##";T(I);
5080 PRINT USING "      #.#####  ";DADT(I);
5090 PRINT USING "######.###";(CT(I))*1000;
5100 PRINT USING "        ###.##";K(I)
5110 NEXT I
5120 LOCATE 25,10:INPUT "CONTINUE";Y$
5130 CLS
5140 PRINT "CRACK SIZE","   VCDOT","    VDOT","   TT","    CSTAR"
5150 PRINT "    (in)  "," (in/hr)"," (in/hr)"," (hr)","(in.lbs/in^2.hr)"
5160 PRINT
5165 FOR I = 1 TO NN
5170 PRINT USING "   #.###";AB(I);
5180 PRINT USING "        #.######";VC(I);
5190 PRINT USING "     #.######";V(I);
5200 PRINT USING "      #####.#";TT(I);
5210 PRINT USING "     ######.###";(CSTAR(I))*1000
5215 NEXT I
5220 LOCATE 25,10:INPUT "WOULD YOU LIKE A HARD COPY OF THE RESULTS (Y/N)";Y$
5230 IF Y$ = "Y" GOTO 5240 ELSE 5580
5240 LPRINT " MATERIAL TYPE:";M$;
5241 LPRINT "   SPECIMEN ID:";X$;
5245 LPRINT "  TEST TEMP (C):"TP
5246 LPRINT
5250 LPRINT " TEST LOAD (Kips):"P;
5260 LPRINT "   WIDTH (in):"W;
5270 LPRINT "  NOMINAL THICKNESS(in):"BN
5280 LPRINT " SIDEGROOVE (%):"((BN-B)/BN)*100
5281 LPRINT
```

```
5282 LPRINT
5290 LPRINT " CREEP EXP (n):";N;
5291 LPRINT "   CREEP COEF. (Ksi^-n.hr^-1):";AA*YS^-N
5292 LPRINT " ELAS MOD (Ksi):";E;
5293 LPRINT "    YIELD STR (Ksi):";YS
5294 LPRINT
5295 LPRINT
5310 LPRINT "CRACK SIZE","TIME","da/dt",;
5320 LPRINT "Ct";
5340 LPRINT "            K"
5350 LPRINT "   in   ","hr","in/hr";
5360 LPRINT "  in.lbs./in^2.hr";
5370 LPRINT "   ksi.in^.5"
5380 LPRINT
5390  FOR I = 1 TO NN
5400 LPRINT USING "  #.###";AB(I);
5410 LPRINT USING "    #####.##";T(I);
5420 LPRINT USING "      #.#####  ";DADT(I);
5430 LPRINT USING "######.###";(CT(I))*1000;
5450 LPRINT USING "        ###.##";K(I)
5460 NEXT I
5470 LPRINT
5475 LPRINT
5480 LPRINT "CRACK SIZE","   VCDOT","    VDOT"," TT","      CSTAR"
5490 LPRINT "    (in)  ","  (in/hr)","  (in/hr)"," (hr)","(in.lbs/in^2.hr)"
5500 LPRINT
5510 FOR I = 1 TO NN
5520 LPRINT USING "   #.###";AB(I);
5530 LPRINT USING "        #.######";VC(I);
5540 LPRINT USING "     #.######";V(I);
5550 LPRINT USING "    #####.#";TT(I);
5560 LPRINT USING "       ######.###";(CSTAR(I))*1000
5570 NEXT I
5580 CLS
5590 LOCATE 5,10:INPUT "DO YOU WANT TO STORE DATA FOR PLOTTING (Y/N)";Y$
5600 IF Y$ = "Y" GOTO 5610 ELSE END
5610 LOCATE 10,10: INPUT "FILE NAME";F$
5620 OPEN F$ FOR OUTPUT AS #1
5630 FOR I = 1 TO NN
5640 WRITE #1, (1000)*CT(I),DADT(I), K(I)
5650 NEXT I
5660 CLOSE #1
5670 END
```

APPENDIX B

Equations for Calculating $\dot{V}_c$ and $\dot{V}$ [69]

$$\dot{V}_c = \frac{2B(1-\nu^2)}{EP}\ \beta\ K^4 \alpha (EAt)^{2/n+1} + \dot{V}_{ss} \qquad \text{(B-1)}$$

where, $$\dot{V}_{ss} = \frac{BWC^*}{P\eta_1} \qquad \text{(B-2)}$$

$$\eta_1 = \frac{1}{(1-a/w)}\ \frac{n}{n+1}\ (\gamma - \alpha_1/n) \qquad \text{(B-3)}$$

$$\gamma = 2 + 0.9717\ a/w - 0.9756(a/w)^2 - 0.6371\ (a/w)^3 + 0.6352\ (a/w)^4 \qquad \text{(B-4)}$$

$$\alpha_1 = 0.2932 - C.7261(a/w) + 0.4889\ (a/w)^2 + 0.369\ (a/w)^3 - 0.09324\ (a/w)^4 \qquad \text{(B-5)}$$

All symbols have been defined previously.

$$\dot{V} = \dot{V}_c + (da/dt)\ \frac{B}{P}\left(\frac{2K^2}{E}\right) \qquad \text{(B-6)}$$

Since the true stress-strain data for these materials was not available, it was assumed that the instantaneous behavior of these specimens was linear elastic.

APPENDIX C

Results of the Analysis of Creep Crack Growth Data of Titanium Aluminides

MATERIAL TYPE:Titanium Aluminide SPECIMEN ID:88-111 TEST TEMP (C): 650

TEST LOAD (Kips): 2.142 WIDTH (in): 1.5785 NOMINAL THICKNESS(in): .3942
SIDEGROOVE (%): 0

CREEP EXP (n): 5.5 CREEP COEF. (Ksi^-n.hr^-1): 3.29E-13
ELAS MOD (Ksi): 12700 YIELD STR (Ksi): 41

CRACK SIZE in	TIME hr	da/dt in/hr	Ct in.lbs./in^2.hr	K ksi.in^.5
0.695	6.50	0.00104	0.632	34.57
0.763	17.13	0.00612	0.943	39.11
0.772	22.00	0.02710	0.995	39.83
0.840	22.85	0.47300	2.642	45.58

CRACK SIZE (in)	VCDOT (in/hr)	VDOT (in/hr)	TT (hr)	CSTAR (in.lbs/in^2.hr)
0.695	0.000064	0.000100	86.6	0.152
0.763	0.000085	0.000356	37.4	0.450
0.772	0.000087	0.001333	33.1	0.528
0.840	0.000207	0.028683	12.8	1.784

MATERIAL TYPE:Titanium Aluminide SPECIMEN ID:88-269 TEST TEMP (C): 650

TEST LOAD (Kips): .558 WIDTH (in): .8 NOMINAL THICKNESS(in): .181
SIDEGROOVE (%): 0

CREEP EXP (n): 5.5 CREEP COEF. (Ksi^-n.hr^-1): 3.29E-13
ELAS MOD (Ksi): 12700 YIELD STR (Ksi): 41

CRACK SIZE in	TIME hr	da/dt in/hr	Ct in.lbs./in^2.hr	K ksi.in^.5
0.386	4.41	0.00119	1.280	31.06
0.396	15.89	0.00072	1.131	32.30
0.406	24.46	0.00312	1.364	33.54
0.416	27.47	0.00394	1.852	34.97
0.433	29.72	0.01420	3.155	37.44
0.450	30.62	0.04677	5.804	40.36
0.466	30.89	0.06740	10.497	43.37

CRACK SIZE (in)	VCDOT (in/hr)	VDOT (in/hr)	TT (hr)	CSTAR (in.lbs/in^2.hr)
0.386	0.000105	0.000164	23.1	0.461
0.396	0.000087	0.000126	17.7	0.649
0.406	0.000101	0.000280	13.6	0.911
0.416	0.000132	0.000378	10.1	1.336
0.433	0.000212	0.001229	6.2	2.475
0.450	0.000369	0.004262	3.7	4.850
0.466	0.000635	0.007112	2.3	9.165

MATERIAL TYPE:Titanium Aluminide SPECIMEN ID:88-093 TEST TEMP (C): 700

TEST LOAD (Kips): 1.986 WIDTH (in): 1.578 NOMINAL THICKNESS(in): .3912
SIDEGROOVE (%): 0

CREEP EXP (n): 5.5 CREEP COEF. (Ksi^-n.hr^-1): 3.88E-12
ELAS MOD (Ksi): 12400 YIELD STR (Ksi): 39

CRACK SIZE in	TIME hr	da/dt in/hr	Ct in.lbs./in^2.hr	K ksi.in^.5
0.546	1.25	0.00480	1.109	25.21
0.557	3.00	0.01000	0.806	25.66
0.568	4.25	0.00800	0.757	26.13
0.579	5.50	0.01000	0.745	26.60
0.601	7.75	0.00870	0.791	27.56
0.615	9.38	0.00860	0.851	28.20
0.628	11.00	0.00800	0.931	28.84
0.646	12.50	0.01500	1.085	29.70
0.665	13.75	0.01500	1.315	30.68
0.682	14.63	0.02670	1.599	31.62
0.700	15.50	0.01500	1.966	32.60
0.715	16.50	0.01600	2.376	33.51
0.733	17.50	0.01900	2.980	34.58
0.752	18.38	0.02670	3.892	35.85
0.775	18.88	0.10000	5.397	37.40
0.805	19.13	0.14000	8.653	39.66
0.589	6.50	0.01000	0.759	27.04

CRACK SIZE (in)	VCDOT (in/hr)	VDOT (in/hr)	TT (hr)	CSTAR (in.lbs/in^2.hr)
0.546	0.000133	0.000230	46.1	0.156
0.557	0.000095	0.000305	42.4	0.175
0.568	0.000089	0.000262	39.0	0.198
0.579	0.000087	0.000311	35.8	0.223
0.601	0.000090	0.000300	29.6	0.290
0.615	0.000095	0.000313	25.4	0.354
0.628	0.000103	0.000314	21.9	0.429
0.646	0.000117	0.000537	18.0	0.554
0.665	0.000138	0.000587	14.5	0.735
0.682	0.000164	0.001012	11.8	0.957
0.700	0.000197	0.000703	9.6	1.252
0.715	0.000232	0.000803	7.9	1.595
0.733	0.000284	0.001006	6.4	2.106
0.752	0.000360	0.001450	5.0	2.889
0.775	0.000483	0.004927	3.8	4.194
0.805	0.000740	0.007734	2.5	7.085
0.589	0.000087	0.000320	33.2	0.249

MATERIAL TYPE:Titanium Aluminide SPECIMEN ID:88-268 TEST TEMP (C): 700

TEST LOAD (Kips): .435 WIDTH (in): .804 NOMINAL THICKNESS(in): .1827
SIDEGROOVE (%): 0

CREEP EXP (n): 5.5 CREEP COEF. (Ksi^-n.hr^-1): 3.88E-12
ELAS MOD (Ksi): 12400 YIELD STR (Ksi): 39

CRACK SIZE in	TIME hr	da/dt in/hr	Ct in.lbs./in^2.hr	K ksi.in^.5
0.384	1.75	0.00315	2.259	23.63
0.396	4.26	0.00720	2.307	24.66
0.407	6.35	0.00410	2.863	25.71
0.417	9.45	0.00310	3.686	26.79
0.460	14.89	0.00995	15.421	32.08

CRACK SIZE (in)	VCDOT (in/hr)	VDOT (in/hr)	TT (hr)	CSTAR (in.lbs/in^2.hr)
0.384	0.000242	0.000361	7.1	0.883
0.396	0.000233	0.000530	5.3	1.284
0.407	0.000277	0.000460	4.0	1.867
0.417	0.000342	0.000492	3.0	2.718
0.460	0.001241	0.001935	0.8	13.669

MATERIAL TYPE:Titanium Aluminide SPECIMEN ID:88-094 TEST TEMP (C): 750

TEST LOAD (Kips): 1.875 WIDTH (in): 1.575 NOMINAL THICKNESS(in): .391
SIDEGROOVE (%): 0

CREEP EXP (n): 5.5 CREEP COEF. (Ksi^-n.hr^-1): 3.61E-11
ELAS MOD (Ksi): 12000 YIELD STR (Ksi): 37

CRACK SIZE in	TIME hr	da/dt in/hr	Ct in.lbs./in^2.hr	K ksi.in^.5
0.470	23.00	0.00265	0.711	21.10
0.482	26.94	0.00281	0.767	21.51
0.495	32.40	0.00373	0.838	21.97
0.503	34.40	0.00387	0.895	22.26
0.514	36.94	0.00432	0.984	22.66
0.522	39.40	0.00481	1.053	22.96
0.531	41.39	0.00504	1.142	23.30
0.544	42.94	0.00487	1.291	23.80
0.556	45.75	0.00425	1.444	24.27
0.566	49.25	0.00391	1.584	24.67
0.576	51.25	0.00402	1.745	25.07
0.586	53.75	0.00438	1.924	25.49
0.600	56.75	0.00469	2.265	26.08
0.612	58.61	0.00505	2.643	26.61
0.623	61.25	0.00570	3.051	27.10
0.631	62.75	0.00634	3.394	27.46
0.643	64.72	0.00810	3.994	28.02
0.653	66.11	0.01027	4.586	28.50
0.666	67.22	0.01197	5.510	29.14
0.677	68.05	0.01367	6.453	29.70
0.692	69.16	0.01530	8.036	30.49
0.701	69.75	0.01614	9.187	30.98
0.723	70.75	0.01793	12.834	32.22
0.733	71.25	0.01880	14.987	32.81

CRACK SIZE (in)	VCDOT (in/hr)	VDOT (in/hr)	TT (hr)	CSTAR (in.lbs/in^2.hr)
0.470	0.000090	0.000131	11.5	0.453
0.482	0.000096	0.000141	10.5	0.513
0.495	0.000104	0.000167	9.6	0.590
0.503	0.000110	0.000177	9.0	0.642
0.514	0.000120	0.000197	8.3	0.723
0.522	0.000128	0.000216	7.8	0.788
0.531	0.000138	0.000233	7.3	0.868
0.544	0.000154	0.000250	6.6	1.000
0.556	0.000170	0.000257	6.0	1.139
0.566	0.000185	0.000267	5.6	1.271
0.576	0.000201	0.000289	5.2	1.418
0.586	0.000220	0.000319	4.8	1.582
0.600	0.000255	0.000366	4.2	1.899
0.612	0.000293	0.000418	3.7	2.252
0.623	0.000334	0.000480	3.2	2.638
0.631	0.000368	0.000535	3.0	2.962
0.643	0.000427	0.000649	2.6	3.530
0.653	0.000485	0.000775	2.3	4.092

0.666	0.000574	0.000927	2.0	4.970
0.677	0.000663	0.001082	1.8	5.870
0.692	0.000811	0.001305	1.5	7.386
0.701	0.000917	0.001455	1.3	8.492
0.723	0.001247	0.001894	1.0	12.008
0.733	0.001438	0.002141	0.9	14.093

MATERIAL TYPE:Titanium Aluminide SPECIMEN ID:88-258 TEST TEMP (C): 750

TEST LOAD (Kips): .418 WIDTH (in): .804 NOMINAL THICKNESS(in): .19
SIDEGROOVE (%): 0

CREEP EXP (n): 5.5 CREEP COEF. (Ksi^-n.hr^-1): 3.61E-11
ELAS MOD (Ksi): 12000 YIELD STR (Ksi): 37

CRACK SIZE in	TIME hr	da/dt in/hr	Ct in.lbs./in^2.hr	K ksi.in^.5
0.343	1.00	0.00950	3.334	18.91
0.355	3.00	0.00700	3.258	19.70
0.368	4.50	0.01100	4.154	20.57
0.385	5.50	0.02300	6.461	21.87
0.403	6.25	0.03280	11.075	23.44

CRACK SIZE (in)	VCDOT (in/hr)	VDOT (in/hr)	TT (hr)	CSTAR (in.lbs/in^2.hr)
0.343	0.000419	0.000676	3.0	1.386
0.355	0.000386	0.000592	2.3	1.986
0.368	0.000471	0.000824	1.7	2.915
0.385	0.000696	0.001530	1.1	4.994
0.403	0.001130	0.002495	0.7	9.189

MATERIAL TYPE:Titanium Aluminide SPECIMEN ID:88-270 TEST TEMP (C): 750

TEST LOAD (Kips): .321 WIDTH (in): .801 NOMINAL THICKNESS(in): .1758
SIDEGROOVE (%): 0

CREEP EXP (n): 5.5 CREEP COEF. (Ksi^-n.hr^-1): 3.61E-11
ELAS MOD (Ksi): 12000 YIELD STR (Ksi): 37

CRACK SIZE in	TIME hr	da/dt in/hr	Ct in.lbs./in^2.hr	K ksi.in^.5
0.384	2.50	0.00204	2.639	18.22
0.397	9.25	0.00246	3.034	19.13

CRACK SIZE (in)	VCDOT (in/hr)	VDOT (in/hr)	TT (hr)	CSTAR (in.lbs/in^2.hr)
0.384	0.000354	0.000415	2.5	1.540
0.397	0.000380	0.000462	1.8	2.367

MATERIAL TYPE:Titanium Aluminide SPECIMEN ID:88-266 TEST TEMP (C): 750

TEST LOAD (Kips): .323 WIDTH (in): .803 NOMINAL THICKNESS(in): .1758
SIDEGROOVE (%): 0

CREEP EXP (n): 5.5 CREEP COEF. (Ksi^-n.hr^-1): 3.61E-11
ELAS MOD (Ksi): 12000 YIELD STR (Ksi): 37

CRACK SIZE in	TIME hr	da/dt in/hr	Ct in.lbs./in^2.hr	K ksi.in^.5
0.389	2.11	0.00315	3.119	18.58
0.400	4.72	0.01100	3.663	19.40
0.411	5.73	0.00856	4.974	20.23
0.421	6.72	0.01130	6.744	21.04
0.432	8.18	0.00610	9.815	22.06

CRACK SIZE (in)	VCDOT (in/hr)	VDOT (in/hr)	TT (hr)	CSTAR (in.lbs/in^2.hr)
0.389	0.000413	0.000512	2.2	1.803
0.400	0.000459	0.000835	1.7	2.634
0.411	0.000601	0.000919	1.2	3.850
0.421	0.000788	0.001242	0.9	5.508
0.432	0.001104	0.001374	0.7	8.432

MATERIAL TYPE:Titanium Aluminide SPECIMEN ID:88-260 TEST TEMP (C): 750

TEST LOAD (Kips): .359 WIDTH (in): .802 NOMINAL THICKNESS(in): .18
SIDEGROOVE (%): 0

CREEP EXP (n): 5.5 CREEP COEF. (Ksi^-n.hr^-1): 3.61E-11
ELAS MOD (Ksi): 12000 YIELD STR (Ksi): 37

CRACK SIZE in	TIME hr	da/dt in/hr	Ct in.lbs./in^2.hr	K ksi.in^.5
0.367	0.59	0.00909	4.210	18.70
0.382	11.75	0.00095	3.184	19.74
0.399	22.71	0.01530	5.104	21.07
0.415	23.71	0.01760	8.606	22.39

CRACK SIZE (in)	VCDOT (in/hr)	VDOT (in/hr)	TT (hr)	CSTAR (in.lbs/in^2.hr)
0.367	0.000558	0.000824	2.6	1.583
0.382	0.000377	0.000408	1.8	2.546
0.399	0.000570	0.001138	1.1	4.506
0.415	0.000921	0.001658	0.7	7.830

MATERIAL TYPE:Titanium Aluminide SPECIMEN ID:88-254 TEST TEMP (C): 800

TEST LOAD (Kips): .252 WIDTH (in): .7978 NOMINAL THICKNESS(in): .178
SIDEGROOVE (%): 0

CREEP EXP (n): 5.5 CREEP COEF. (Ksi^-n.hr^-1): 2.7E-10
ELAS MOD (Ksi): 11700 YIELD STR (Ksi): 35

CRACK SIZE in	TIME hr	da/dt in/hr	Ct in.lbs./in^2.hr	K ksi.in^.5
0.455	1.00	0.01090	39.177	19.06
0.477	2.25	0.04480	88.160	21.15
0.499	3.00	0.02170	223.430	23.65
0.525	4.00	0.02910	723.398	27.22
0.561	4.71	0.04450	4887.374	34.29

CRACK SIZE (in)	VCDOT (in/hr)	VDOT (in/hr)	TT (hr)	CSTAR (in.lbs/in^2.hr)
0.455	0.005330	0.005808	0.1	32.483
0.477	0.011076	0.013497	0.1	81.189
0.499	0.026114	0.027579	0.0	213.388
0.525	0.077581	0.080186	0.0	706.856
0.561	0.457591	0.463908	0.0	4843.150

MATERIAL TYPE:Titanium AQluminide SPECIMEN ID:88-267 TEST TEMP (C): 800

TEST LOAD (Kips): .31 WIDTH (in): .805 NOMINAL THICKNESS(in): .1796
SIDEGROOVE (%): 0

CREEP EXP (n): 5.5 CREEP COEF. (Ksi^-n.hr^-1): 2.7E-10
ELAS MOD (Ksi): 11700 YIELD STR (Ksi): 35

CRACK SIZE in	TIME hr	da/dt in/hr	Ct in.lbs./in^2.hr	K ksi.in^.5
0.430	0.33	0.02720	51.936	20.43
0.446	1.05	0.01782	78.474	21.86
0.459	1.53	0.07520	124.186	23.15
0.472	1.65	0.17580	207.074	24.59
0.484	1.71	0.14280	331.305	26.00
0.496	1.75	0.35500	559.138	27.66
0.507	1.78	0.34100	898.003	29.26
0.521	1.80	1.49600	1672.320	31.50

CRACK SIZE (in)	VCDOT (in/hr)	VDOT (in/hr)	TT (hr)	CSTAR (in.lbs/in^2.hr)
0.430	0.006463	0.007587	0.1	36.956
0.446	0.009099	0.009942	0.1	67.737
0.459	0.013785	0.017776	0.1	112.765
0.472	0.022067	0.032598	0.0	192.504
0.484	0.034059	0.043618	0.0	312.788
0.496	0.055284	0.082178	0.0	534.690
0.507	0.085767	0.114671	0.0	866.452
0.521	0.152723	0.299743	0.0	1627.944

APPENDIX D

Derivation of $\frac{d}{da}\int_{A_c} f dA$

$$\frac{\Delta}{\Delta a}\int_{A_c} f dA = \frac{1}{\Delta A}\left[\int_{A_c+\Delta A_c} (f+\Delta f)\,dA - \int_{A_c} f dA\right]$$

$$= \int_{A_c} \frac{\Delta f}{\Delta a}\, dA + \frac{1}{\Delta a}\int_{\Delta A_c} (f+\Delta f)\,dA$$

$$= \int_{A_c} \frac{\Delta f}{\Delta a}\, dA + \frac{1}{\Delta a}\int_{\partial A_c} (f+\Delta f)\,\Delta r_c\, ds$$

$$\frac{d}{da}\int_{A_c} f dA = \int_{A_c} f_{,a}\, dA + \int_{\partial A_c} f\, r_{c,a}\, ds \qquad \text{(D-1)}$$

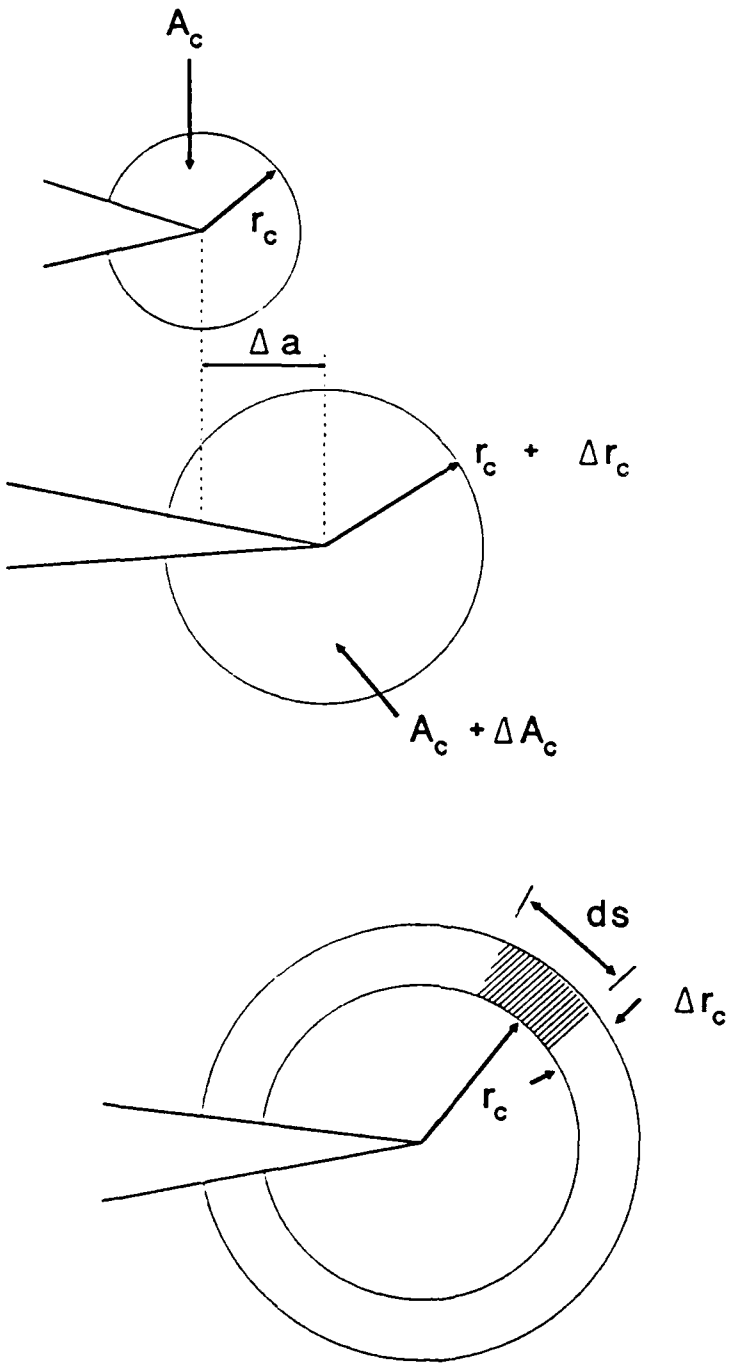

Figure D-1. Creep Zone at Two Different Crack Depths Under the Same Loading History

Appendix E
Relationship Between C_{os} and C_t

As shown in Figure E-1, C_t has been defined as [57] the area A between two P-∇ curves for crack lengths of a and a+Δa divided by Δa. The P-∇ curves are, as illustrated in Figure 15, constructed by running a series of constant load tests on specimens with crack lengths a and a+Δa. However, under small scale creep conditions, it has been shown [72] that, under constant loads, $\dot{V}_c$ is related to P by

$$\dot{V}_c = \frac{4\alpha(1-\nu^2)}{E(n-1)} \left(\frac{P^3}{B}\right)\frac{F^4}{W^2} \; t^{\frac{3-n}{n-1}} \; (EA)^{\frac{2}{n-1}} \qquad \text{(E-1)}$$

where $\alpha=0.159155[(n+1)^2/1.38n]^{2/(n-1)}$, E is Young's modulus, ν is Poisson's ratio, A and n are creep constants defined in eq. (3-2), B is plate thickness, W is plate width, P is the applied load, and F the proportional constant in calculating K (see eq. (3-13)). With eq. (E-1), it has been shown [72] that

$$C_t = \frac{P\dot{V}}{BW}\frac{F'}{F} = \frac{[\text{Area A+B}]}{\Delta a} = \frac{1}{4}\frac{[\text{Area B+C}]}{\Delta a} = \frac{1}{4} P \frac{d\dot{V}}{da} \qquad \text{(E-2)}$$

Eq. (E-2) implies that, under small scale creep conditions, C_t can be obtained based on a single constant load test at load level P instead of a series of constant load tests at several increasing load levels from zero to P.

Under small scale creep, C_o is calculated by eq. (4-10). From eq. (4-9), it can be seen that, under constant load P,

$$P\dot{V}_c = \int_{\partial A_t} T_i \dot{u}_i \, ds = \int_{\partial A_c} T_i \dot{u}_i \, ds \qquad \text{(E-3)}$$

Furthermore, by virtual work theory,

$$\int_{\partial A_c} T_i \dot{u}_i \, ds = \int_{A_c} \dot{W} \, dA = \int_{A_c} \sigma_{ij} \dot{\epsilon}_{ij} \, dA \qquad \text{(E-4)}$$

Therefore, under constant load conditions, the asymptotic solution of C_o defined in eq. (4-10) can be reduced to

$$C_{os} = \frac{1}{n+1} P \frac{d\dot{V}}{da} \qquad \text{(E-5)}$$

Eqs. (E-2) and (E-5) lead to a relationship between C_t and C_o at small scale creep conditions as

$$C_t = \frac{n+1}{4} C_{os} \quad , \; (t/t_T) << 1 \qquad \text{(E-6)}$$

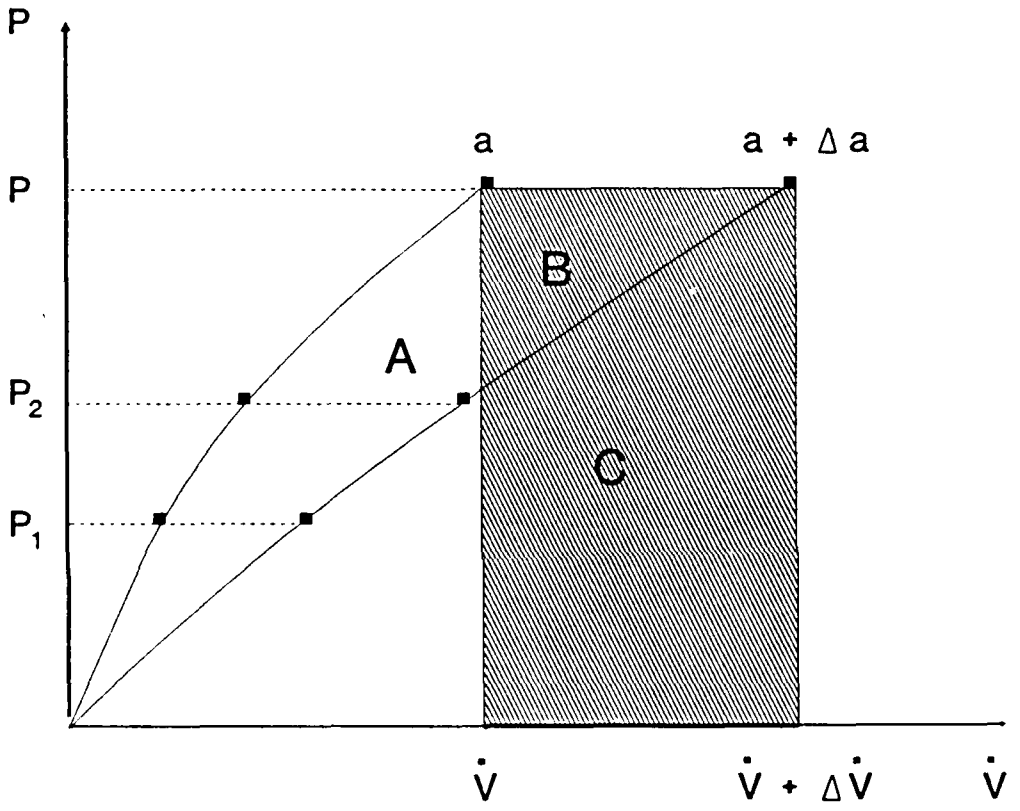

Figure E-1. Relationship between C_t and C_o at Small Scale Creep